Conception, optimization and evaluation of the performance of noncoherent MIMO schemes for future wireless systems

Ibrahim Dawi

THESE DE DOCTORAT DE

L'INSTITUT NATIONAL DES SCIENCES APPLIQUEES RENNES

ECOLE DOCTORALE N° 601
Mathématiques et Sciences et Technologies de l'Information et de la Communication
Spécialité : *Télécommunications*

Par

Ibrahim DAWI

Conception, optimization and evaluation of the performance of non-coherent MIMO schemes for future wireless systems

Thèse présentée et soutenue à Rennes, le 01/06/2021
Unité de recherche : Institut d'Electronique et des Technologies du NumeRique de Rennes
Thèse N° : 21ISAR 13 / D21 - 13

Rapporteurs avant soutenance :

Marion BERBINEAU	Directrice de Recherche, Université Gustave Eiffel
Vahid MEGHDADI	Professeur, ENSIL de Limoges

Composition du Jury :

Président :	Laurent ROS	Professeur, INP Grenoble
Examinateurs :	Ayman KHALIL	Maître de Conférences, Université Islamique de Beyrouth
	Gheorghe ZAHARIA	Maître de Conférences, INSA Rennes
Dir. de thèse :	Jean-François HELARD	Professeur, INSA Rennes

Invité(s)

Youssef NASSER	Enseignant-Chercheur, Université Américaine de Beyrouth

"However difficult life may seem, there is always something you can do, and succeed at. It matters that you just don't give up"

Stephen Hawking

Abstract

In current wireless communication systems, the knowledge of the instantaneous channel coefficients or the so-called Channel State Information (Channel State Information (CSI)) is required in order to adapt the transmitter and receiver to the current channel conditions. It is usually carried out through the transmission of pilot/training symbols to the receiver side for a reliable channel estimation. Nevertheless, CSI acquisition is not free of charge, and achieving accurate CSI estimation is a challenging task in practice. This is due to two major obstacles, i.e.,. fast variation of the channel conditions causing impaired channel estimation, and significant overhead in training sequence with the increase of the number of antennas in a Multiple-input Multiple-output (Multiple-Input Multiple-Output (MIMO)) system, which takes up a large portion of the available spectral and power resources. In this context, non-coherent systems, which do not require channel knowledge at neither transmitter nor receiver become an attractive solution for the above mentioned issues. Differential schemes are commonly used for non-coherent systems ; among those are differential space-time modulation (DSTM) schemes.

It is within this context that this thesis aims to explore the possibilities of enhancing the performance of DSTM systems in terms of spectral efficiency and error performance through a thorough analysis of different constellations used for this scheme. The first part of the thesis introduces non-coherent systems, the advantages they offer and the challenges they face. More specifically, it surveys systems based on differential modulation and how the research community participated in studying and enhancing existing solutions.

The contributions of this thesis are divided into three parts. In the first part, the thesis investigates differential group codes and the use of the the multiplicative Weyl

group of unitary matrices in a DSTM MIMO system having two transmit antennas. In the efforts of enhancing the error performance of the mentioned system, and given that the distance between the information matrices is used as a performance metric, the thesis thoroughly studies the distance spectrum of the information matrices employed, and a selection algorithm is proposed. In addition, optimal mapping based on the distance between selected information matrices and the Hamming distance between binary data vectors is proposed. Moreover, in the aim of increasing the maximum achievable spectral efficiency of the proposed DSTM system, a simple and double extension of the Weyl group are proposed and their performance is studied.

The second part handles the expansion of the DSTM MIMO system from two transmit antennas to four and eight transmit antennas through the use of the Kronecker product of matrices of the Weyl group. This is followed by the performance study of the DSTM system in a more realistic continuously fading channel model.

The final part of the thesis studies the performance of the two transmit antennas DSTM system analytically, and proposes the pairwise error probability as a new metric for the selection of the optimal matrices, which then leads to the conception of an optimal matrix selection algorithm and an optimal mapping strategy based on PEP and Hamming distance.

Résumé en Français

Aujourd'hui les techniques multi-antennaires MIMO (Multiple Input Multiple Output) et Massive MIMO sont très présentes dans les différents systèmes de communications sans fils. Cependant, ces schémas nécessitent de disposer en réception d'une estimation de la réponse de chaque canal entre chaque antenne d'émission et de réception, ce qui, dans beaucoup de cas, peut diminuer fortement l'efficacité spectrale finale de ces systèmes. Cette thèse a pour but d'explorer une solution alternative reposant sur l'utilisation de schémas de modulation différentielle espace-temps (DSTM) pour ces systèmes MIMO non cohérents ne nécessitant pas de disposer d'une estimation de la réponse du canal en réception.

Dans cette thèse, nous nous concentrons sur les performances des systèmes non cohérents, plus spécifiquement, nous étudions les schémas de modulation différentielle espace-temps (Differential Space-Time Modulation (DSTM)) pour les systèmes MIMO.

Le groupe multiplicatif de Weyl se presente comme un ensemble approprié pour être employé par le schéma DSTM, étant donné la nature unitaire des matrices qui le composent. Nous décrivons d'abord l'utilisation du groupe de Weyl dans le schéma DSTM pour les systèmes MIMO ayant deux antennes d'émission. Ensuite, afin de résoudre le problème de l'efficacité spectrale limitée réalisable que ce groupe offre, nous proposons d'utiliser une extension simple et double en appliquant des rotations sur l'ensemble des matrices du groupe considéré. Les groupes générés sont ensuite analysés en profondeur, et un algorithme de recherche est conçu, sélectionnant les matrices d' information à employer en fonction de la métrique de distance entre les matrices candidates, et une stratégie de mapping optimale basée sur la distance entre les matrices d'informations et la distance de Hamming des vecteurs binaires

qui est suivie d'une analyse des performances d'erreur du système étudié.

Par la suite, nous avons cherché à augmenter le nombre d'antennes d'émission du système DSTM MIMO afin d'augmenter la robustesse du système. Pour ce faire, on a conçu d'autres matrices unitaires, de taille 4×4 ou 8×8 en appliquant le produit Kronecker, ce qui a permis de produire des matrices adaptées aux schémas DSTM à quatre et huit antennes de transmission. Néanmoins, l'augmentation du nombre d'antennes d'émission a réduit l'efficacité spectrale maximale réalisable du système DSTM. Nous abordons ce problème en appliquant les extensions simples et doubles sur les groupes nouvellement générés. L'algorithme de recherche est utilisé pour sélectionner les matrices d'information des groupes nouvellement générés et la performance d'erreur du système est analysée.

Dans la suite, le système DSTM pour deux, quatre et huit antennes d'émission est étudié dans un modèle de canal à évanouissement continu, plus réaliste, plutôt que dans le modèle de canal pas à pas classique, utilisé dans la littérature et les études précédentes sur les performances d'erreur. Le modèle de canal décrit un scénario de cas réel, où le canal varie légèrement avec chaque colonne de la matrice transmise (durée du symbole). L'effet de la variation de la matrice de canal et du temps de cohérence sur les performances du système est analysé.

Au final, nous utilisons les résultats analytiques d'une précédente étude sur les systèmes DSTM, afin d'évaluer la probabilité d'erreur exacte par paire (Pair-Wise Error Probability (PEP)) et la limite supérieure de la PEP. Les résultats de simulation produits sont validés par l'étude analytique. Cela a conduit à la conception d'un algorithme de sélection optimale de matrices, ayant comme mesure de performance la valeur exacte de la PEP entre les couples de matrices. Les performances d'erreur du système MIMO DSTM dans le cadre du nouvel algorithme de sélection sont supérieures aux résultats obtenus avec la méthode de sélection précédente.

Le résumé en français présente une synthèse des principaux résultats obtenus par chacun des chapitres.

Chapitre 1 : Etat de l'art

Les systèmes MIMO sont apparus comme une technologie susceptible d'améliorer considérablement les taux d'erreur réalisables par un système "Single-Input Single-Output" Single-Input Single-Output (SISO), et des travaux approfondis sur cette technologie ont commencé à la fin des années 1990 avec des efforts pour développer des techniques de codage et de traitement du signal pouvant s'approcher de la capacité des canaux MIMO. Cependant, ces éléments nécessitent de disposer en réception voire à l'émission d'une estimation de la réponse de chaque canal entre chaque antenne d'émission et chaque antenne de réception pour la mise en oeuvre de la démodulation cohérente. Le nombre de séquences pilotes devant dans ce cas être insérées pour l'estimation du canal est proportionnel au nombre d'antennes utilisées à l'émission, ce qui diminue fortement l'efficacité spectrale finale du système. Une solution alternative repose sur l'utilisation de schémas MIMO différentiels. Toutefois, lorsque ces conditions s'avèrent difficiles à estimer, le système peut effectuer une détection non cohérente.

Nous nous concentrons sur une famille de codes inspirés des DSTM (Differential Space-Time Modulation), appelés groupes de codes différentiels (DGC). Les schémas DGC sont basés sur des matrices de signaux qui forment un groupe mathématique sous l'opération de multiplication. Au cours des dernières années, les schemas differentieles ont a été intégrés aux schémas de modulation spatiale afin de tenter de réduire les complexités excessives rencontrées dans les DGC et les "Differential Linear Dispersion Codes" DLDC. De plus, le concept de transmission différentielle a été intégré dans la modulation spatiale qui a été développée pour inclure une constellation de signaux "Quadrature Amplitude Modulation" QAM. Ensuite, afin d'obtenir une diversité de transmission bénéfique, un schéma de "Differential Spatial Modulation" DSM en "Radio Frequency" RF unique est conçu.

Chapitre 2 : DSTM utilisant des extensions du groupe Weyl

Dans ce chapitre, nous développons l'utilisation du groupe de Weyl multiplicatif de matrices unitaires de 2×2 pour le système DSTM.

Génération du groupe Weyl

Le groupe de Weyl est composé de 192 matrices unitaires qui forment le groupe sous operation de multiplication. Le groupe multiplicatif de Weyl est désigné par $\mathcal{G}_{w2}$ et comporte 12 cosets $\{C_0, C_2 \ldots, C_{11}\}$, chacun contenant 16 matrices unitaires (donc inversibles).

Pour un groupe $\mathcal{P}$ donné, l'efficacité spectrale maximale est donnée par :

$$R_{max} = (1/M)\lfloor log_2|\mathcal{P}|\rfloor \quad bps/Hz \tag{1}$$

où $|\mathcal{P}|$ désigne la cardinalité du groupe. Ainsi le groupe Weyl atteint une efficacité spectrale maximale de 3.5 bps/Hz.

Extension simple

Dans le but d'augmenter l'efficacité spectrale maximale, nous proposons de générer un nouveau groupe multiplicatif, que nous appelons $\mathcal{G}_{we2}$. Nous effectuons une rotation *optimale* des matrices du groupe $\mathcal{G}_{w2}$ en les multipliant par $e^{\frac{j\pi}{8}}$. Le groupe de Weyl étendu $\mathcal{G}_{we2}$ améliore l'efficacité spectrale maximale à 4 bps/Hz pour un système MIMO avec 2 antennes d'émission :

$$\mathcal{G}_{we2} = \mathcal{G}_{w2} \cup \mathcal{G}_{w2} e^{\frac{j\pi}{8}} \tag{2}$$

Double extension

En suivant la même méthode et afin d'augmenter encore l'efficacité spectrale maximale réalisable, nous proposons une double extension du groupe de Weyl en

multipliant $\mathcal{G}_{we2}$ par $e^{\frac{j\pi}{16}}$ qui correspond à la constellation 32-PSK. Ainsi, l'efficacité spectrale maximale devient égale à 4,5 bps/Hz pour un système MIMO avec 2 antennes d'émission :

$$\mathcal{G}_{wee2} = \mathcal{G}_{we2} \cup \mathcal{G}_{we2} e^{\frac{j\pi}{16}} \tag{3}$$

Algorithme de sélection matricielle

Dans ce travail, un algorithme de sélection des matrices est proposé, maximisant les distances entre les matrices sélectionnées afin d'obtenir le meilleur sous-ensemble $\mathcal{S}$ à utiliser pour une efficacité spectrale donnée où nous devons utiliser $K = 2^n$ matrices sélectionnées dans le groupe P (n étant la longueur du vecteur d'information binaire). L'algorithme de sélection des matrices est le suivant :

1. La première matrice M_1 du groupe $\mathcal{P}$, qui est en fait la matrice d'identité I_M (ici $M = 2$), est insérée dans l'ensemble $\mathcal{S}$ comme référence ($S_1 = M_1$) où $S_1 \in \mathcal{S}$. $\mathcal{S}$ est de taille K qui est déterminée par l'efficacité spectrale souhaitée.

2. La distance $D(M_1, M_i)$ est calculée pour toutes les matrices $M_i \in \mathcal{P} \setminus \{M_1\}$, puis $D_{max} = maxD(M_1, M_i)$. S_2 est inséré dans $\mathcal{S}$ comme la matrice avec $D(M_1, M_i) = D_{max}$. Si plusieurs matrices M_i ont la même distance maximale D_{max} avec M_1, alors on en choisit une au hasard pour l'insérer dans $\mathcal{S}$ comme S_2.

3. Pour chaque matrice non sélectionnée $M_i \in \mathcal{P} \setminus \{\mathcal{S}\}$, on calcule le vecteur $D_{M_i} = [D(M_i, S_1) \dots D(M_i, S_k)]$, où k est le nombre de matrices déjà sélectionnées pour l'ensemble $\mathcal{S}$.

4. Les valeurs du vecteur D_{M_i} sont triées par ordre croissant.

5. Nous retenons les vecteurs D_{M_i} qui ont la valeur minimale maximale. Si un seul vecteur D_{M_i} est retenu, alors M_i est ajouté à $\mathcal{S}$. Si plusieurs vecteurs D_{M_i} sont retenus, alors les secondes valeurs des vecteurs retenus sont comparées et celles ayant la seconde valeur la plus élevée sont retenues. Si un seul vecteur D_{M_i} est retenu, alors M_i est ajouté à $\mathcal{S}$. Si plusieurs vecteurs D_{M_i}

sont retenus, alors les troisièmes valeurs des vecteurs retenus sont comparées. Cette comparaison peut se poursuivre jusqu'aux dernières valeurs des vecteurs D_{M_i}. Si, au final, toutes les valeurs des vecteurs D_{M_i} sont identiques, on en choisit une au hasard. Enfin, un nouveau vecteur M_i est ajouté à $\mathcal{S}$.

6. Les étapes 3 à 5 sont itérées pour obtenir l'ensemble $\mathcal{S}$ ayant des matrices K sélectionnées dans le groupe $\mathcal{P}$.

Le processus d'extension et l'algorithme de recherche appliqués permettent, pour une efficacité spectrale similaire, de sélectionner des matrices plus performantes en termes de distance dans les nouveaux groupes. Cela est évident lorsque l'on examine dans figure 1 les performances du système 2×2 DSTM pour la même efficacité spectrale de 3.5 bps/Hz mais pour des différents groupes.

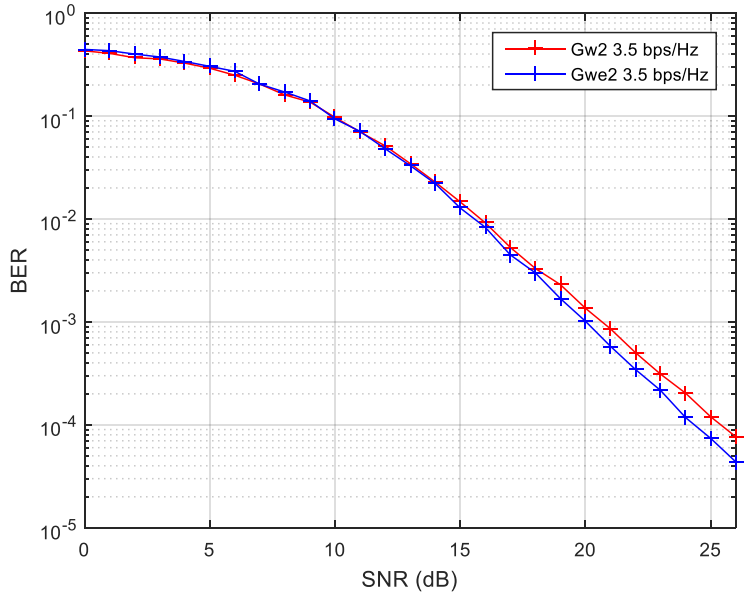

FIGURE 1 – Performance of the selected sets of matrices for $\mathcal{G}_{w2}$ and $\mathcal{G}_{we2}$ (or $\mathcal{G}_{wee2}$) for 3.5 bps/Hz

Résultats de la simulation

Le taux d'erreur binaire (TEB) en fonction du rapport signal/bruit (SNR) du système MIMO DSTM utilisant des antennes d'émission $M = 2$ et des antennes de

réception $N = 2$ pour les efficacités spectrales 1, 2, 3, 4, 4,5 bps/Hz et utilisant $\mathcal{G}_{wee2}$ est présenté sur la figure 2.

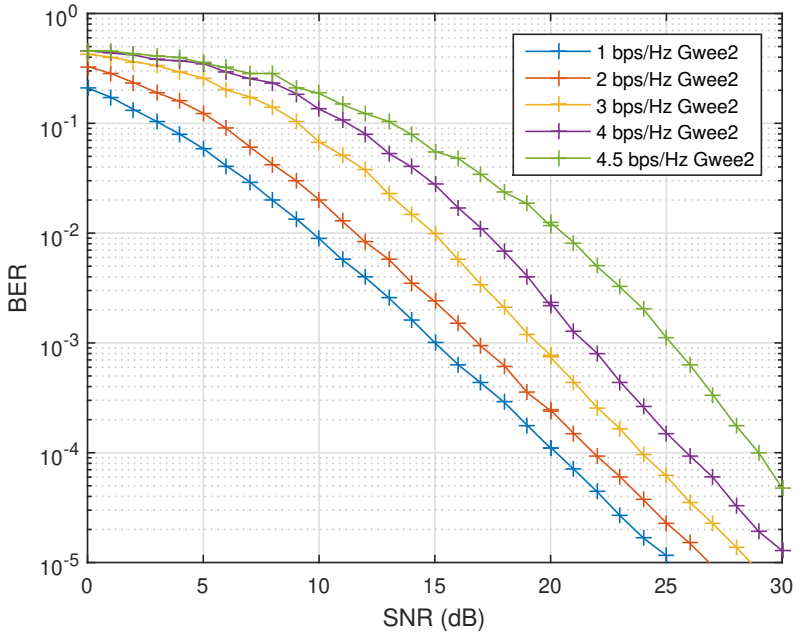

FIGURE 2 – Performances BER du système DSTM MIMO 2×2 pour différentes efficacités spectrales

Chapitre 3 : Systèmes DSTM utilisant 4 et 8 antennes

Dans ce chapitre, nous étendons le système DSTM MIMO de 2×2 à 4×4 et 8×8 grâce à l'utilisation du produit Kronecker sur le groupe Weyl. De plus, nous appliquons des extensions aux groupes multiplicatifs de matrices unitaires nouvellement générés de 4×4 et 8×8 dans le but d'augmenter leur efficacité spectrale maximale réalisable.

Système DSTM utilisant 4 antennes de transmission

Afin d'étendre notre système DSTM MIMO à 4 antennes de transmission, l'opération du produit Kronecker est appliquée sur $\mathcal{G}_{w2}$.

Expansion de $\mathcal{G}_{w2}$ à $\mathcal{G}_{w4}$

Pour un système MIMO utilisant 4 antennes d'émission et avec l'hypothèse $M = T$ en place, nous devons utiliser des matrices d'émission de taille 4×4. Lorsque le produit Kronecker est appliqué à $\mathcal{G}_{w2}$, un groupe de matrices unitaires de 4×4 $\mathcal{G}_{w4} = \mathcal{G}_{w2} \otimes \mathcal{G}_{w2}$ est obtenu. Ainsi, pour un système MIMO de 4 antennes d'émission, l'efficacité spectrale maximale est réduite à $R_{max} = \frac{1}{4}\lfloor log_2 4608 \rfloor = 3\, bps/Hz$.

Simple extension de $\mathcal{G}_{w4}$

En effet, cette diminution de l'efficacité spectrale devient plus sévère avec une augmentation supplémentaire du nombre d'antennes de transmission. C'est pourquoi il devient important d'étendre le groupe $\mathcal{G}_{w4}$ dans le but d'augmenter l'efficacité spectrale maximale réalisable. Nous proposons d'utiliser une extension du groupe $\mathcal{G}_{w4}$ en utilisant :

$$\mathcal{G}_{we4} = \mathcal{G}_{w4} \cup \mathcal{G}_{w4} e^{\frac{j\pi}{8}} \tag{4}$$

$\mathcal{G}_{we4}$ est capable d'améliorer l'efficacité spectrale maximale à 3,25 bps/Hz par rapport à l'efficacité spectrale maximale de 3 bps/Hz pour $\mathcal{G}_{w4}$.

Double extension de $\mathcal{G}_{w4}$

En essayant d'augmenter encore l'efficacité spectrale réalisable, nous appliquons la double extension à travers :

$$\mathcal{G}_{wee4} = \mathcal{G}_{we4} \cup \mathcal{G}_{we4} e^{\frac{j\pi}{16}} \tag{5}$$

Ce qui porte l'efficacité spectrale maximale réalisable à 3,5 bps/Hz.

Analyse des performances d'erreur

La figure 3 montre les simulations de taux d'erreur binaire par rapport aux SNR des systèmes 4×4 utilisant Gwee4 pour différentes efficacités spectrales.

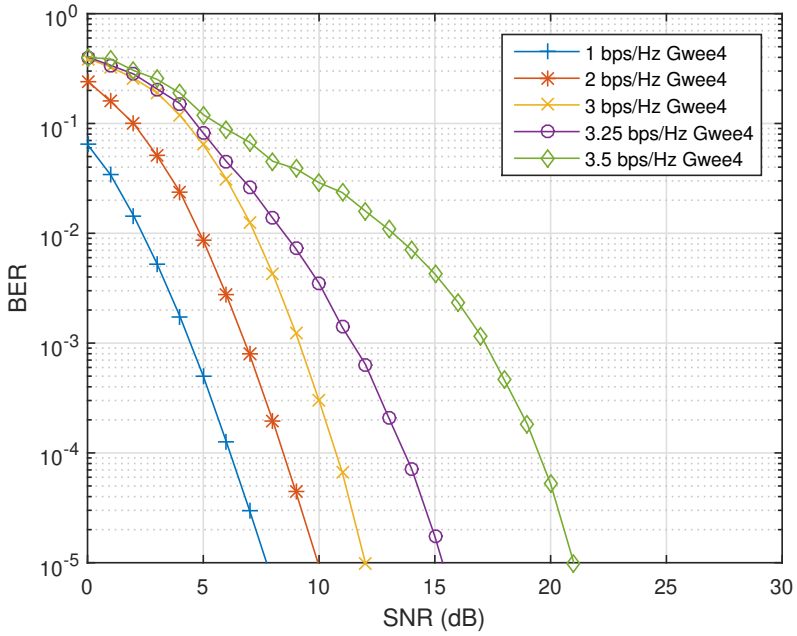

FIGURE 3 – BER performance of DSTM MIMO 4×4 system for different spectral efficiencies

Système DSTM utilisant 8 antennes de transmission

En adoptant la même méthode que celle utilisée pour générer les matrices unitaires 4×4, nous appliquons le produit Kronecker entre $\mathcal{G}_{w2}$ et $\mathcal{G}_{w4}$ afin de produire des matrices de taille 8×8 adaptées aux systèmes MIMO employant 8 antennes d'émission. Le groupe généré $\mathcal{G}_{w8} = \mathcal{G}_{w4} \otimes \mathcal{G}_{w2}$ a son efficacité spectrale maximale encore plus réduite à $R_{max} = \frac{1}{8}\lfloor log_2 110592 \rfloor = 2\, bps/Hz$.

Simple et double extension de $\mathcal{G}_{w8}$

Pour un système à 8 antennes d'émission, l'efficacité spectrale maximale est réduite de 3,5 bps/Hz en employant le groupe $\mathcal{G}_{w2}$ dans les systèmes à 2 antennes d'émission à 2 bps/Hz. Dans le but de résoudre la question d'une diminution importante de l'efficacité spectrale, et de manière similaire aux extensions précédemment effectuées, nous étendons le $\mathcal{G}_{w8}$ à travers :

$$\mathcal{G}_{we8} = \mathcal{G}_{w8} \cup \mathcal{G}_{w8} e^{\frac{j\pi}{8}} \tag{6}$$

puis

$$\mathcal{G}_{wee8} = \mathcal{G}_{we8} \cup \mathcal{G}_{we8} e^{\frac{j\pi}{16}} \tag{7}$$

permettant une augmentation à 2,25 bps/Hz pour $\mathcal{G}_{wee8}$.

Analyse des performances d'erreur du système DSTM à 8 antennes de transmission

La figure 4 présente ensuite la simulation du TEB par rapport au SNR pour les systèmes MIMO DSTM ayant $M = 8$ et $N = 8$ et utilisant les matrices du groupe $\mathcal{G}_{wee8}$ et intervalle de cohérence normalisé $L = 120$ pour les efficacités spectrales 0,5, 1, 2 bps/Hz.

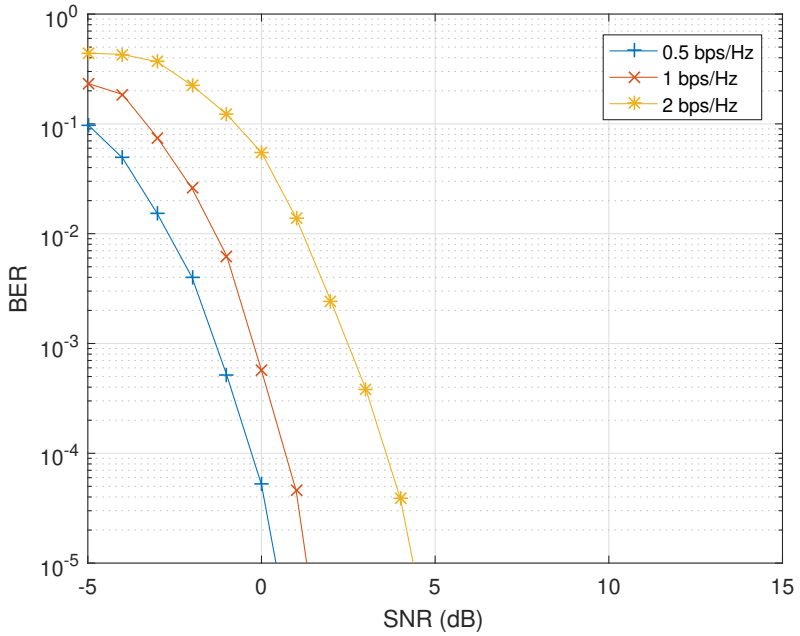

FIGURE 4 – Performance TEB du système DSTM MIMO 8×8 pour différentes efficacités spectrales utilisant $\mathcal{G}_{wee8}$

Chapitre 4 : Performances des systèmes DSTM dans un canal variant dans le temps

Dans ce chapitre, plutôt que d'utiliser le modèle classique "step channel", où le canal reste constant durant la transmission d'une trame et change aléatoirement d'une trame à l'autre, nous proposons un nouveau modèle de canal sélectif dans le temps pour lequel nous étudions les performances du système DSTM. Le nouveau modèle de canal représente un scénario de cas réel.

Modèle de canal sélectif dans le temps

D'après le théorème d'échantillonnage de Nyquist, on sait que si le canal est échantillonné avec une fréquence au moins égale au double de la composante de fréquence maximale du signal, la réponse impulsionnelle du canal peut être reconstruite par les points échantillonnés. Cette méthode est utilisée dans le modèle de canal conçu.

Description du modèle

On considère un système MIMO $M \times N$, transmettant une matrice $T \times M$, où T est le nombre de symboles dans une matrice transmise par chaque antenne et $T = M$ est supposé. On considère que L est le temps de cohérence normalisé, ce qui signifie que $N_m = \frac{L}{M}$ symboles sont transmis pendant l'intervalle de cohérence. Ensuite, les $L-1$ matrices de canaux, $H(1), H(2), \ldots, H(L-1)$ sont interpolées entre 2 matrices successives générées de façon aléatoire $R(K)$ et $R(K+1)$ au lieu de considérer une matrice constante $R(K)$. Le processus est décrit comme suit :

1. $2K$ de matrices distribuées de Rayleigh sont générées, c'est-à-dire, $R(1), R(2), \ldots, R(2K)$.
2. En utilisant la formule de Nyquist, $L-1$ matrices de canal sont générées.

Les matrices aléatoires de Rayleigh $R(K)$ agissent comme les échantillons d'une matrice de canal continu H séparés par le temps de cohérence de cohérence $T_0 = T_c = L \times T_s$. Avec les matrices générées aléatoirement $2K$, on obtient par interpolation

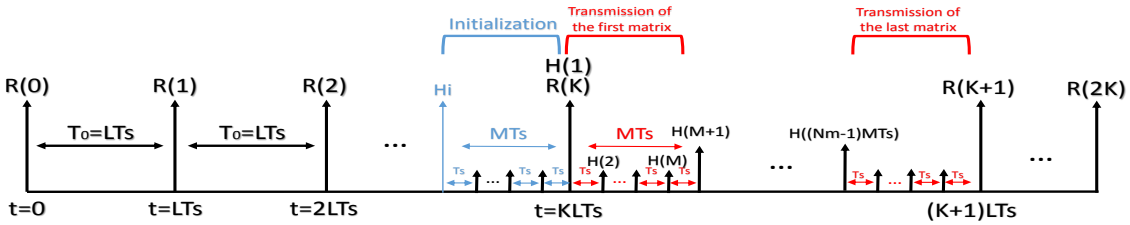

FIGURE 5 – Modèle de canal Rayleigh continu

$L-1$ matrices de canal entre $R(K)$ et $R(K+1)$:

$$\begin{aligned} H(1) &= R(K) \\ H(i+1) &= \sum_{k=1}^{2K} R(k) \frac{sin\pi(f_0 t - k)}{\pi(f_0 t - k)} \\ &= \sum_{k=1}^{2K} R(k) \frac{sin\pi(K + \frac{i}{L} - k)}{\pi(K + \frac{i}{L} - k))} \end{aligned} \tag{8}$$

où,

$$f_0 t(i) = K + \frac{i}{L} \tag{9}$$

Dans ce modèle, les matrices $H_i(l)$, où $l = \overline{1, M}$, sont utilisées pour initialiser le processus différentiel (émission de la matrice identité) . Les matrices H_i sont multipliées avec la colonne l de la matrice identité., et sont obtenues comme suit :

$$\begin{aligned} H_i(l) &= \sum_{k=1}^{2K} R(k) \frac{sin\pi(K - \frac{(M+1)-l}{L} - k)}{\pi(K - \frac{(M+1)-l}{L} - k))} \\ l &= \overline{1, M} \end{aligned} \tag{10}$$

Cette procédure est illustrée dans la figure 5.

Analyse des performances

Analyse des performances des systèmes à 2, 4 et 8 antennes d'émission

La figure 6 présente les résultats des simulations du TEB en fonction du rapport signal/bruit (SNR) du système DSTM pour les systèmes comportant 2, 4 et 8

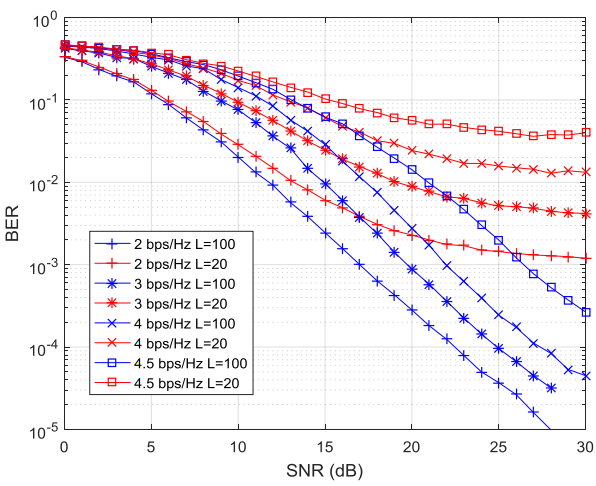

(a) 2 antennes d'émission

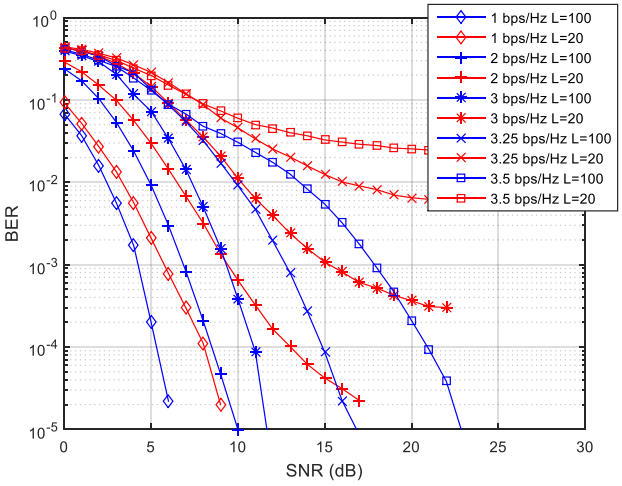

(b) 4 antennes d'émission

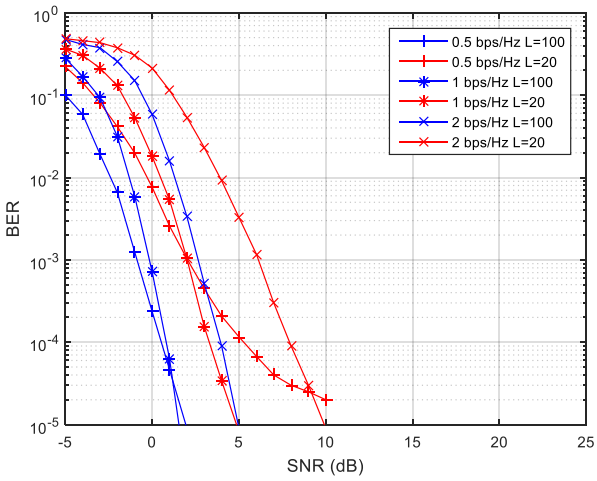

(c) 8 antennes d'émission

FIGURE 6 – Performances TEB des systèmes DSTM MIMO 2×2, 4×4 et 8×8 en fonction du temps de cohérence normalisé

antennes d'émission pour différents valeurs du temps de cohérence normalisé noté L.

Chapitre 5 : Analyse du système DSTM avec une nouvelle métrique d'optimisation

Dans ce chapitre, inspirés du travail analytique réalisé en [1], nous menons une analyse analytique des matrices du groupe de Weyl afin de produire des expressions de la limite supérieure et exacte de la probabilité d'erreur par paire (PEP). Les résultats théoriques sont ensuite comparés aux résultats de simulation pour validation. Par conséquent, la PEP exacte est utilisée comme nouveau critère d'optimisation dans la sélection optimale des matrices d'information, ce qui conduit à des améliorations des performances d'erreur du système DSTM.

D'après [1], l'expression pour la PEP exacte du DSTM dans des canaux à évanouissements rapides (les coefficients de canal changent avec chaque matrice transmise) spatialement indépendants est donnée par :

$$
\begin{aligned}
P(\mathbf{S}_i, \mathbf{S}_j) &= \frac{1}{\pi} \int_0^{\frac{\pi}{2}} \sum_{l=1}^{L} \sum_{p=1}^{\mu_l} c_{p,l} \big(\frac{sin^2\theta}{sin^2\theta + \frac{1}{2}\gamma\lambda_l}\big)^p d\theta \\
&= \frac{1}{2}\Big\{ \sum_{l=1}^{L} \sum_{p=1}^{\mu_l} c_{p,l} \\
&- \sum_{l=1}^{L} \sum_{p=1}^{\mu_l} c_{p,l} \sqrt{\frac{\gamma\lambda_l}{2+\gamma\lambda_l}} \sum_{q=0}^{p-1} \binom{2q}{q} \big(\frac{1}{4+2\gamma\lambda_l}\big)^q \Big\} \\
&= \frac{1}{2} - \frac{1}{2} \sum_{l=1}^{L} \sqrt{\frac{\gamma\lambda_l}{2+\gamma\lambda_l}} \sum_{p=1}^{\mu_l} c_{p,l} \sum_{q=0}^{p-1} \binom{2q}{q} \big(\frac{1}{4+2\gamma\lambda_l}\big)^q
\end{aligned} \tag{11}
$$

Canaux à évanouissements lents spatialement indépendants

Les canaux à évanouissement lent spatialement indépendants peuvent être considérés comme un cas particulier des canaux à évanouissements rapides spatialement indépendants où le taux d'évanouissement $f_D T_B = 0$ où f_D est la fréquence Doppler maximale et T_B est la durée pour transmettre une matrice. Dans ce cas d'évanouis-

sement lent, $\mathbf{A} = \mathbf{I}_{MN}$, $\mathbf{G} = 0_{MN}$, et $\mathcal{Z}_{k-1} = \mathbf{I}_{MN}$. Par conséquent, la PEP exacte est toujours donnée par (11) avec γ se réduit maintenant à

$$\gamma = \frac{E_s^2}{2\sigma_v^2(2E_s + \sigma_v^2)} \tag{12}$$

Borne supérieure de la PEP

Il est à noter que la borne de Chernoff peut être dérivée de cette approche basée sur le "Moment Generting Function" MGF. En substituant l'expression susmentionnée de γ et en fixant $\theta = \frac{\pi}{2}$, on peut observer que la PEP dans des canaux à évanouissements lents spatialement indépendants peut être limitée par

$$P(\mathbf{S}_i, \mathbf{S}_j) \leq \frac{1}{2} \prod_{l=1}^{L} \Big(\frac{1}{1 + \frac{E_s^2}{4\sigma_v^2(2E_s+\sigma_v^2)}\lambda_l}\Big)^{\mu_l} \tag{13}$$

Cas particulier

En dérivant la PEP exacte du couple de matrices du groupe de Weyl et de ses extensions, nous étudions la condition des valeurs propres de leur matrice de distance : si pour la matrice de distance, il y a une seule valeur propre, on utilise le cas particulier dans (14). Et sur cette base, nous dérivons la PEP soit selon le cas particulier dans (14), soit selon le cas général dans (11) où il y a plusieurs valeurs propres pour la matrice de distance.

$$P(\mathbf{S}_i \to \mathbf{S}_j) = \frac{1}{2}\Big\{1 - \sqrt{\frac{\gamma\lambda}{2+\gamma\lambda}} \sum_{q=0}^{\mu-1} \binom{2q}{q} \Big(\frac{1}{4+2\gamma\lambda}\Big)^q\Big\} \tag{14}$$

Interprétation des résultats théoriques de la PEP

Afin de valider les expressions de PEP énoncées dans la section précédente, nous produisons les valeurs théoriques (limite exacte et limite supérieure de la PEP) pour les couples de matrices appartenant au groupe de Weyl. Ensuite, nous produisons les résultats de simulation de la PEP exacte et de la limite supérieure des couples de ces matrices dans le but de comparer les résultats théoriques et les résultats de simulation. L'analyse des performances est donnée dans la figure 7.

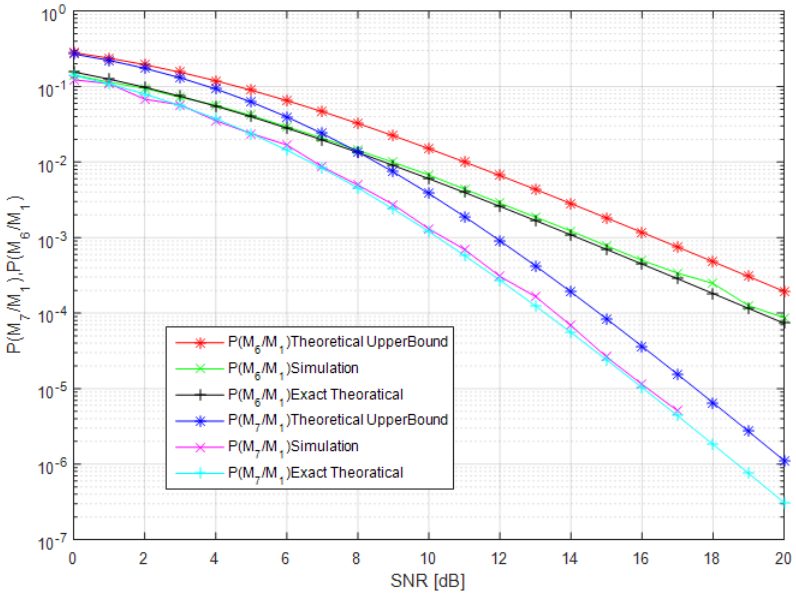

FIGURE 7 – Résultats théoriques et de simulation de la borne exacte et supérieure sur PEP du couple de matrices (M_6, M_1) et (M_7, M_1) qui ont des distances similaires

Nouvel algorithme de recherche optimal basé sur la valeur exacte de la PEP

Au lieu d'utiliser la distance entre les couples de matrices dans notre recherche des matrices d'information optimales à employer dans le système DSTM, nous produisons toutes les valeurs PEP exactes entre les couples de matrices d'un groupe donné selon les expressions de formes fermées conçues précédemment. Ensuite, en utilisant les valeurs PEP générées, nous appliquons un algorithme de recherche optimal pour sélectionner les meilleures matrices possibles dans le but d'améliorer les performances d'erreur du système.

L'algorithme de recherche optimal est le suivant : Soit P le groupe de matrices candidates à la recherche, et S l'ensemble de matrices optimales à sélectionner.

1. La première matrice V_1 de P est ajoutée à S comme première entrée (S_1).
2. La deuxième matrice V_{x2_i} à sélectionner $(V_{2_i} \in P, V_{2_i} \notin S)$ a la plus petite valeur exacte de PEP (calculées pour une valeur SNR donnée) vers S_1 : $Min(PEP(V_{2_i} \rightarrow S_1))$. S'il existe plusieurs matrices ayant la plus petite

valeur exacte de PEP, nous invoquons la recherche par arbre décrite dans l'étape 6.

3. Pour la matrice suivante à ajouter à l'ensemble optimal S, nous produisons l'ensemble $\mathcal{P}$ de valeurs PEP : $\mathcal{P}_{3_i} = [PEP(V_{3_i} \rightarrow S_1), PEP(V_{3_i} \rightarrow S_2)]$, où $V_{3_i} \in P, V_{3_i} \notin S$. Ce qui signifie qu'un ensemble $\mathcal{P}_{3_i}$ est créé pour chaque matrice V_{3_i}. $(\mathcal{P}_3 = [\mathcal{P}_{3_1}, \mathcal{P}_{3_2}, \dots])$.

4. Les ensembles $\mathcal{P}_{3_i}$ sont triés par ordre décroissant, dans le but de sélectionner la matrice appartenant à l'ensemble $\mathcal{P}_{3_i}$ ayant les valeurs maximales de PEP les plus basses. Pour le faire, on compare les valeurs de PEP après avoir trié l'ensemble par ordre croissant et choisi la première valeur la plus petite de l'ensemble. Si les premières valeurs sont identiques, la deuxième valeur PEP est vérifiée, et ainsi de suite jusqu'à la fin de l'ensemble.

5. Dans le cas où il reste un ensemble $\mathcal{P}_{3_i}$ (ayant un ensemble unique de PEPs correspondant au *"critère maximal le plus bas"*), on choisit la matrice V_{3_i} qui lui est associée.

6. Sinon, si plusieurs $\mathcal{P}_{3_i}$ ont le *"critère maximal le plus bas"*, nous utilisons une recherche par arbre.

   (a) Supposons que les deux ensembles $\mathcal{P}_{3_1}$ et $\mathcal{P}_{3_2}$ correspondent au *"critère maximal le plus bas"* et correspondent effectivement

   (b) Nous effectuons une recherche optimale selon un "Tree Search" en ajoutant les matrices V_{3_1} (associées à $\mathcal{P}_{3_1}$) et V_{3_2} (associées à $\mathcal{P}_{3_2}$) à deux ensembles optimaux temporaires S_α et S_β respectivement.

   (c) Nous exécutons l'algorithme de recherche de l'étape 3 dans les deux ensembles optimaux temporaires, pour chaque matrice ajoutée à chaque ensemble, nous comparons à la fois S_α et S_β de la même manière que l'étape 4.

   (d) Nous sélectionnons l'ensemble auquel la meilleure matrice a été ajoutée (en termes de *"critère maximal le plus bas"*), nous voyons à quel ensemble $\mathcal{P}_{3_1}$ ou $\mathcal{P}_{3_2}$ est lié et nous passons à l'étape 5.

(e) Si pour les deux matrices ajoutées, les ensembles S_α et S_β correspondent toujours, nous continuons en relançant la recherche à partir de l'étape 3, et ainsi de suite. Cette opération est répétée jusqu'à ce que nous atteignions la taille requise de l'ensemble optimal. Dans ce cas, et si les ensembles S_α et S_β continuent de correspondre, nous en sélectionnons un au hasard et nous poursuivons à partir de l'étape 5.

7. La matrice V_{3_i} est ensuite ajoutée à l'ensemble S, et nous répétons la recherche à partir de l'étape 3 jusqu'à ce que nous atteignions la taille requise en fonction de l'efficacité spectrale choisie.

Comparaison métrique de distance et métrique PEP pour différentes efficacités spectrales

Sur la figure 8, on peut remarques que les performances observées avec la métrique PEP sont bien meilleures que celle obtenue précédemment en utilisant la métrique de distance. Si pour les efficacités spectrales de 3 et 3.5 bps/Hz la différence est faible, elle devient bien plus intéressante pour les schémas à faible efficacité spectrale de 1 et 2 bps/Hz.

Conclusion

Dans notre travail, le groupe de Weyl multiplicatif de matrices unitaires 2×2 $\mathcal{G}_{w2}$ est utilisé comme constellation codée espace-temps du schéma DSTM. Dans un premier temps, la taille de $\mathcal{G}_{w2}$ est étendue par rotation optimale, produisant ainsi le nouveau groupe multiplicatif de matrices unitaires $\mathcal{G}_{we2}$. Cette opération a pour but d'augmenter l'efficacité spectrale maximale réalisable de $\mathcal{G}_{w2}$ de 3,5 bps/Hz à 4 bps/Hz. Dans le même but, le premier groupe étendu $\mathcal{G}_{we2}$ est encore étendu par rotation optimale au groupe multiplicatif de matrices unitaires $\mathcal{G}_{wee2}$, augmentant ainsi encore l'efficacité spectrale maximale réalisable à 4,5 bps/Hz. Dans cette partie, nous avons utilisé la distance entre les couples de matrices comme mesure de performance et un algorithme de sélection des matrices d'information ainsi qu'un

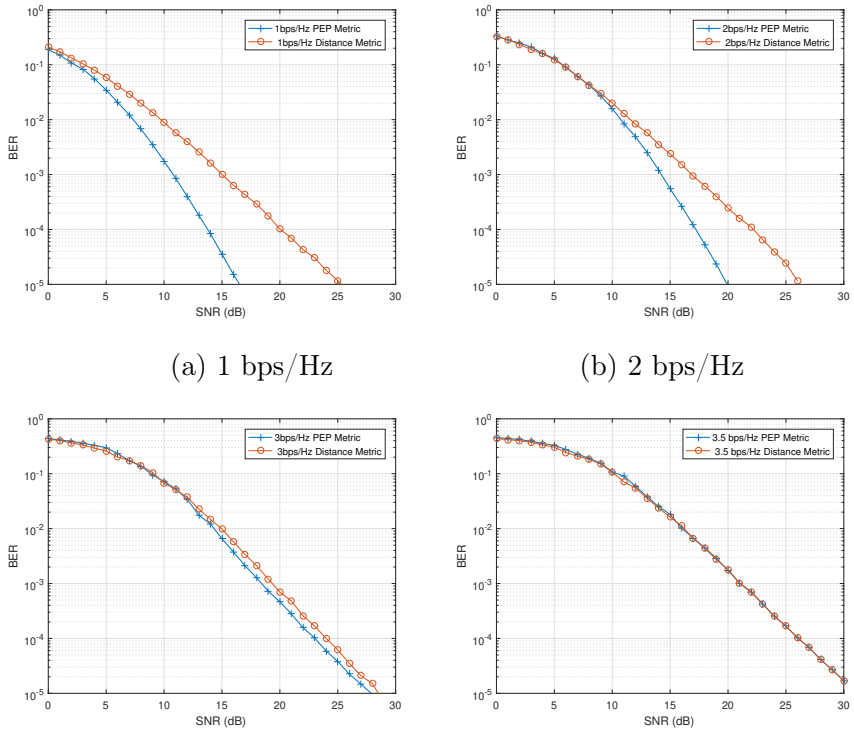

(a) 1 bps/Hz (b) 2 bps/Hz

(c) 3 bps/Hz (d) 3.5 bps/Hz

FIGURE 8 – Comparaison entre la métrique de la distance et la métrique PEP pour différentes efficacités spectrales en $\mathcal{G}_{w2}$.

mappage optimal sont produits dans le but d'améliorer la performance d'erreur du système qui est analysé par des résultats de simulation.

Dans un deuxième temps, $\mathcal{G}_{w2}$ est étendu par l'utilisation de l'opérateur de produit de Kronecker, produisant le groupe multiplicatif $\mathcal{G}_{w4}$ de matrices unitaires de 4×4. Ce groupe, comme précédemment, est étendu à $\mathcal{G}_{we4}$ et $\mathcal{G}_{wee4}$, augmentant ainsi l'efficacité spectrale maximale réalisable de 3 bps/Hz à 3,25 bps/Hz et 3,5 bps/Hz respectivement. Le spectre de distance des groupes générés est étudié, ce qui conduit à une analyse des performances de leurs résultats de simulation. En outre, le groupe $\mathcal{G}_{w8}$ de matrices unitaires 8×8 est produit par l'utilisation du produit de Kronecker de manière similaire, ce qui est suivi par la génération de ses extensions $\mathcal{G}_{we8}$ et $\mathcal{G}_{wee8}$ qui augmentent encore l'efficacité spectrale maximale réalisable de 2 bps/Hz à 2,125 bps/Hz et 2,25 bps/Hz respectivement. Ces schémas sont ensuite étudiés dans un modèle de canal à évanouissement continu plus réaliste.

Ce travail de thèse se termine en utilisant le travail analytique de [1] pour déterminer la performance des schémas DSTM proposés en utilisant des expressions de probabilité d'erreur par paire (PEP). Ceci a conduit à un nouvel algorithme optimal de sélection des matrices d'information, ayant comme mesure de performance la valeur exacte de la PEP entre des matrices. En particulier, il est montré que la performance de la probabilité d'erreur des systèmes MIMO DSTM ainsi obtenus est supérieure aux résultats obtenus avec les schémas précédents qui utilisent la distance entre les matrices comme mesure de performance, et offre donc des perspectives intéressantes.

Contents

List of Figures

List of Tables

List of Symbols

$(.)^*$ the complex conjugate

$(.)^H$ the conjugate transpose

$(.)^T$ the transpose

$\lambda(\mathbf{X})$ eigenvalue of $\mathbf{X}$

$\mathcal{A}$ the set $\mathcal{A}$

$\mathcal{R}(.), \mathcal{I}(,)$ the real and imaginary parts

μ multiplicity of eigenvalue

$\otimes$ the Kronecker product

$\mathbf{A}$ the matrix $\mathbf{A}$

$\mathbf{a}$ the vector $\mathbf{a}$

$\mathbf{A}_k, l$ the (k, l)th element of $\mathbf{A}$

$\mathbf{I}_N$ the identity matrix of dimension $N \times N$

$\mathbf{x} \sim N(\mu, Q)$ $\mathbf{x}$ is real-valued Gaussian with mean μ and covariance Q

$\mathbf{x} \sim NC(\mu, Q)$ $\mathbf{x}$ is circularly symmetric Gaussian with mean μ and covariance Q

a the scalar a

$E_{\mathbf{x}}[.]$ statistical expectation over $\mathbf{x}$

i the imaginary unit $(i = \sqrt{-1})$

$J_0(.)$ zero-order Bessel function of the first kind

$log(x)$ the natural logarithm of x

$log_2(x)$ the base-2 logarithm of x

$M_\Gamma(.)$ Moment Generating Function of Γ

$P(\mathbf{X}_1) \rightarrow \mathbf{X}_2)$ pairwise error probability of mistaking $\mathbf{X}_1$ with $\mathbf{X}_2$

$Q(.)$ the Gaussian Q-function

$rank(.)$ the rank of a matrix

$Tr(.)$ the trace of a matrix

$vec(\mathbf{X})$ the vector obtained by stacking the columns of $\mathbf{X}$ on top of each other

Acronyms

1G First Generation of Wireless Cellular Technology. 4

2G Second Generation of Wireless Cellular Technology. 4

3G Third Generation of Wireless Cellular Technology. 4, 17

3GPP 3rd Generation Partnership Project. 17

4G Fourth Generation of Wireless Cellular Technology. 4

5G-NR Fifth Generation New Radio. 4, 17, 109

AWGN Additive White Gaussian Noise. 15, 18, 23–25

BER Bit Error Rate. 15, 48, 52, 53, 55, 68, 70, 75, 82–85, 104

BLAST Bell Laboratories Layer Space-Time. 16, 17

BPSK Binary Phase Shift Keying. 28

BS Base Station. 14, 17

CDD Conventional Differential Detection. 23, 24

CDMA Code-Division Multiple Access. 4, 17

CIR Channel Impulse Response. 20

CSI Channel State Information. iii, 4–6, 11, 20–22, 24, 29

DAPSK Differential Amplitude Phase Shift Keying. 26

DFDD Decision-Feedback Differential Detection. 25, 26

DGC Differential Group Codes. 27–29

DLDC Differential Linear Dispersion Code. 28

DPSK Differential Phase Shift Keying. 23, 24, 26

DQAM Differential Quadrature Amplitude Modulation. 24

DSTM Differential Space-Time Modulation. v, vi, viii, x, xi, xiv–xvi, xviii, xx, xxii, xxiv, 6–9, 11, 27, 29, 31, 43, 45, 50, 52, 53, 55, 63, 67, 68, 75, 77, 81–85, 87, 88, 91, 94–96, 100, 106–110

DSTSK Differential Space-Time Shift Keying. 28

GSM The Global System for Mobile Communications. 4, 14

IAI Inter-Antenna Interference. 16

IM Index Modulation. 17

LDC Linear Dispersion Codes. 17

LOS Line-of-Sight. 13, 19

LTE Long-Term Evolution. 4, 17

MIMO Multiple-Input Multiple-Output. iii–xv, xxiv, xxvi, xxvii, xxix–xxxi, 5–9, 11, 14–21, 27, 28, 31, 32, 40, 43, 50, 52, 53, 55, 57, 68–71, 75–77, 81–85, 97, 107–109

ML Maximum Likelihood. 16

MLSE Maximum Likelihood Sequence Estimation. 22–24

MMSE Minimum Mean Square Error. 16

MPSK M-Ary Phase Shift Keying. 23, 24

MSDD Multiple-Symbol Differential Detection. 24–26

MSDSD Multiple-Symbol Differential Sphere Detection. 26

NLOS Non-Line-of-Sight. 14

O-STBC Orthogonal Space-Time Block Codes. 16

OFDM Orthogonal Frequency-Division Multiplexing. 4, 21, 22

PEP Pair-Wise Error Probability. vi, xviii–xxi, xxiv, xxix, 7–9, 87, 88, 91, 92, 94–97, 99–102, 104, 106, 108, 109

QAM Quadrature Amplitude Modulation. 17, 26–28

QO-STBC Quasi-Orthogonal Space-Time Block Codes. 16

RF Radio Frequency. 17

SD Sphere Detection. 26

SISO Single-Input Single-Output. vii, 5, 15

SMS Short Message Service. 4

STBC Space-Time Block Codes. 16, 17, 27, 29

STSK Space-Time Shift Keying. 17

UE User Equipment. 17

Introduction

In this chapter, an overview of the thesis is presented through an explanation of the context of the work achieved and a detailed interpretation of the motivation behind this work, along with the contributions made to the subject. This part ends with the thesis organization and a list of the publications.

Context

All animal species have perfected a system of communication, but humans are the only species capable of spoken language. Effective communication is essential for a variety of reasons. It serves to inform, motivate, establish authority and control, and allows for emotive expression. For humans in particular, communication is also vital for creating a sense of social cohesion. Just as mankind has evolved over the centuries, our means of communication have followed suit. What began as primitive cave paintings and signed language has morphed into an endless variety of ways to express oneself to other humans.

The history of wireless communication began with the understanding of magnetic and electric properties, which was laid out by the work of James C. Maxwell in 1864, as he formulated the classical theory of electromagnetic radiation, bringing together electricity, magnetism and light as different manifestations of the same phenomenon, which was then demonstrated by Heinrich Hertz in 1880 and 1887. Basically, the theory demonstrates the potential to transfer information using electromagnetic waves and the help of electronic devices at the transmitter and receiver sides. This work laid the foundation for Guglielmo Marconi to invent the first means of radio communication through radiotelegraphy in 1895. Following the development

of integrated circuits, electromagnetic wireless communication grew enormously as radio and television broadcasting became widespread worldwide. The iconic work of Claude Shannon in 1948 paved the way for the evolution from analog signal transmission to digital signal transmission using bits. Mobile wireless systems have been evolving from one generation to the next nearly every decade since the 1980s, each generation featuring new regulations and technologies. Following the first generation (First Generation of Wireless Cellular Technology (1G)) analog communication systems featuring only basic phone calling and fax services at high prices, the second generation (Second Generation of Wireless Cellular Technology (2G)), which was based on Global System of Mobile Communication (The Global System for Mobile Communications (GSM)), was launched in the early 1990s in Europe and offered improved phone calls, short messaging service (Short Message Service (SMS)) and low rate data services such as email. The third generation (Third Generation of Wireless Cellular Technology (3G)) was introduced in the 2000s after the advances offered in Code Division Multiple Access (Code-Division Multiple Access (CDMA)), providing higher-rate data services such as video conferencing, TV streaming following the spread of smart phones with applications demanding ever increasing internet access. The spectral-efficient Orthogonal Frequency Division Multiplexing (Orthogonal Frequency-Division Multiplexing (OFDM)) was the key enabler of Fourth Generation of Wireless Cellular Technology (4G) Long-Term evolution (Long-Term Evolution (LTE)) in the 2010s, which achieved a high speed in both downlink and uplink, and facilitates a wide range of services. The fifth generation New Radio Fifth Generation New Radio (5G-NR) has been under development since the early 2010s following recent digital and analog circuit breakthroughs in processing massive-bandwidth millimeter Wave (mm-Wave) signals.

Current wireless standards rely on the knowledge of the instantaneous channel coefficients or (CSI), which enables a reliable communication link through adapting the transmitter and the receiver to the current channel conditions. The CSI is obtained through training/pilot symbol sequences transmission between transmitter and receiver, which take a non-negligible amount of resources, specially with the increase of the number of transmit antennas, creating channel impairments. As a

consequence, non-coherent systems, where the CSI is not known at either the transmitter or receiver have been proposed in literature as a solution for the occurring problems in coherent systems.

Motivation and objectives

Coherent communication relies on the knowledge of CSI in order to perform adequately. In practice, because the channel matrix is random and fades over time and frequency, its value is not given a priori and must be measured. Typically, channel estimation is carried out by sending reference symbol sequences, so-called pilot symbol sequences, known to the receiver. The receiver then estimates the channel using the known pilots symbol sequences, then inter/extrapolates them to infer the channel gains of the remaining channel uses within the coherence time. The estimates of the channel gain are used in the reception process of the remaining channel uses of the coherence time in what is called coherent communication. The cost of channel estimation and channel estimation error must be taken into account for a proper analysis of system performance.

Pilot symbol sequences do not carry any information to the receiver, rather they occupy a large portion of the spectral (time/frequency) resources with the increasing number of antennas. In a MIMO channel with M transmit antennas and N receive antennas, $M \times N$ Single-Input Single-Output SISO channels need to be estimated. In a highly mobile environment where the channel state changes rapidly, the coherence time is short, and the fraction of pilot symbol sequences transmission can be disproportionate to data transmission, especially if the number of antennas is large.

Channel error estimation has a negative effect on the efficiency of both channel throughput and error. On one hand, if one treats the channel estimate as the true channel and disregard any inaccuracy, the optimal detector under this assumption is a mismatched detector for the channel with channel estimation error, and the channel throughput is determined by the mismatched rate. On the other hand, even if the statistics of the channel estimation error is taken into account, this residual

error imposes a secondary noise which increases the total noise power and reduces the channel capacity for a given signal power.

When the cost of channel estimation becomes inconvenient/impossible, it might be beneficial to refrain from doing it by using a communication scheme that does not rely on the knowledge of CSI. Non-coherent communication accounts for such a scheme.

In this thesis, we focus on the performance of non-coherent systems. More specifically, we investigate Differential Space-Time Modulation (DSTM) schemes for MIMO systems.

Contributions

In this thesis, we first provide a detailed survey on differential detection schemes, as a proposed solution in the face of channel estimation challenges. These schemes are first described for the single antenna environment. Then we identify the significant schemes conceived for the multiple antennas environment. More specifically, we focus on DSTM schemes for MIMO systems. The advantages of these schemes are discussed to identify the opportunities they provide, along with the challenges they face.

The multiplicative Weyl group is shown to provide a suitable set to be employed by DSTM schemes, given the unitary nature of the matrices therein. We first describe the use of the Weyl group in the DSTM scheme for MIMO systems having two transmit antennas. Then, in order to solve the issue of the limited achievable spectral efficiency this group offers, we propose to use a simple and double extension through applying rotations on the studied group. The groups generated are then analyzed thoroughly, and a search algorithm is conceived, selecting the information matrices to be employed based on the distance metric between the candidate matrices, which is followed by an error performance analysis of the system studied.

Subsequently, we aimed at increasing the number of transmit antennas of the DSTM MIMO system. This was achieved through generating new matrices by applying the Kronecker product, thus producing matrices suitable for four and eight

transmit antenna DSTM schemes. Nonetheless, the increase of the number of transmit antennas decreased the achievable maximum spectral efficiency of the DSTM system. We address this issue through applying the simple and double extensions on the newly generated groups. The search algorithm is used to select the information matrices from the newly generated groups and the system error performance is analyzed.

Thereafter, the DSTM systems for two, four and eight transmit antennas is studied in a more realistic continuously fading channel model, rather than the conventional step channel model used in literature and previous error performance studies. The channel model depicts a real case scenario, where the channel varies slightly with each column of the transmitted matrix (symbol duration). The effect of the channel model on the error performance of the studied system is then analyzed.

Finally, we study the performance of the DSTM system analytically inspired by the work done in [1], leading to closed form expressions evaluating the exact Pair-Wise Error Probability (PEP) and the upper bound on PEP. The produced simulation results are validated by the analytical study. This led to the conception of an optimal matrix selection algorithm, having the exact PEP value between two matrices as the performance metric. Moreover, and for the sake of making an optimal choice of matrices, a tree search is integrated within the new selection algorithm. The error performance of DSTM MIMO system under the new selection algorithm outperforms the results under previous selection metrics.

Thesis organization

The thesis is organized in 5 chapters excluding this introduction and the conclusion.

In chapter 1, notions of wireless propagation and MIMO systems are addressed. First we investigate the key elements in MIMO technology, and how they make a corner stone in all current and future wireless systems, along with the challenges they face. Then we discuss the concept of coherent communication systems, the advantages they offer, and the cost behind them, which leads us to the alternative,

non-coherent systems. The most popular standards of these methods, the challenges and pitfalls of each are presented, with the solution proposed by the research community, with focus on differential space-time modulation systems.

In Chapter 2, the multiplicative Weyl group of 2×2 unitary matrices is described to be used in DSTM MIMO systems of 2 transmit antennas. Additionally, new simple and double extensions of the Weyl group are performed based on optimal rotations of the matrices of the group, thus increasing the maximum achievable spectral efficiency of the DSTM scheme. The distance spectrum of the matrices of the generated groups is studied, and an information matrices selection algorithm is proposed based on the distance metric aiming at improving error performance. This is followed by an optimal mapping strategy between binary vectors and information matrices. Finally, the performance of the DSTM system employing the newly generated extensions is simulated and analyzed.

In Chapter 3, the multiplicative Weyl group is enlarged using the Kronecker product. This is done in the aims of employing DSTM MIMO schemes having 4 and 8 transmit antennas. Additionally, extensions of the 4×4 and 8×8 newly generated groups are performed through optimal rotations with the same aim of increasing the maximum achievable spectral efficiency. Distance spectrum analysis of the newly generated groups is performed, followed by the search algorithm from the previous chapter, which is used to select the information matrices. Finally, the system error performance is analyzed through simulation results.

In Chapter 4, a comparative analysis is conducted on the DSTM MIMO scheme employing 2, 4, and 8 transmit antennas in two channel model scenarios. The first case is the conventional step channel model used in literature and previous error performance studies. The second model is a more realistic continuously fading channel model, depicting a real case scenario. In the new continuously fading channel model, the channel varies slightly with each column of the transmitted matrix (symbol duration). The effect of the channel model on the error performance of the studied system is then analyzed.

In Chapter 5, a new error performance metric is introduced, which is the PEP. An analytical study is conducted based on [1], producing closed form expressions

of the exact PEP and upper-bound on PEP. Furthermore, the simulation results are validated through the analytical study. This has led to the conception of a new optimal information matrix selection algorithm based on the exact PEP value as a metric rather then the distance between the matrices. The error performance of DSTM MIMO system under the new selection algorithm is compared to the results under the previous selection metric.

Finally, in the conclusion, the main contributions of the thesis are summarized and future perspectives are proposed.

Publications

Conferences

— **I. Dawi**, G. Zaharia, J.F. Hélard, Y. Nasser, A. Khalil, "Performance Of DSTM MIMO System with 2, 4 and 8 Transmit Antennas Using Extensions of the Mathematical Weyl Group", 14th International Conference on Signal Processing and Communication Systems (ICSPCS 2020), Adelaide, Australia, 2020.

— **I. Dawi**, G. Zaharia, Y. Nasser, A. Khalil, J.F. Hélard, "Increase of DSTM Spectral Efficiency by the Extension of the Mathematical Weyl Group with Application to Differential MIMO System", 26th International Conference on Telecommunications (ICT 2019), Hanoi, 2019.

— **I. Dawi**, G. Zaharia, J.F. Hélard, A. Khalil, Y. Nasser, "Performance of DSTM MIMO Systems Using a Double Extension of the Weyl Group in Time-Varying Rayleigh Channel", the 14-th International Symposium on Signals, Circuits and Systems (ISSCS 2019), Iasi, Romania, 2019.

Chapter 1

State of the art review

1.1 Introduction

The ever increasing demand for data throughput and reliability in wireless communication has made MIMO technology a corner stone in most current wireless communication systems, and will most probably be present in most future systems as well. This is due to the ability of MIMO systems to achieve impressive increases in overall system performance. MIMO systems can be regrouped into two categories: coherent systems, which require the instantaneous channel knowledge in order to operate, and non-coherent systems, which do not need the CSI neither at transmitter nor receiver. Due to channel impairments between transmitter and receiver in fast fading scenarios, and since MIMO systems experience pilot overhead with the increase of the number of transmitting and receiving antennas, non-coherent systems become an attractive solution for the mentioned issues. In this chapter we present background notions of wireless propagation and key elements of the MIMO technology along with the challenges faced to achieve its potential. We then survey recent scientific advances in non-coherent schemes with focus on DSTM systems.

1.2 Wireless propagation

In this section, we start with background material on signal transmission and the channel characteristics.

1.2.1 Signal propagation

An electromagnetic wave is emitted by an antenna at the transmitter side. The wireless radio channel where this electromagnetic wave propagates does not present itself as a reliable medium for high speed communication, rather it faces multiple challenges, among which are noise, interference and other channel impairments challenges which also vary in time due to user movement and changes in environment. The variation of the received signal power over distance is characterized by *path loss*. Path loss is caused by dissipation of the power radiated by the transmitter as well as effects of the propagation channel, and occurs over very large distances. Whereas shadowing is related to the attenuation of the signal due to obstacles present in the environment, through absorption, reflection, scattering and diffraction and occurs over distances proportional to the length of the obstructing object.

For analytical simplicity, the propagation channel is modeled using a complex frequency response i.e., real modulated and demodulated signals are often represented as the real part of a complex signal to facilitate analysis. This gives rise to the complex baseband representation of bandpass signals.

The transmitted signal is modeled as [2]:

$$\begin{aligned} s(t) &= \Re\{u(t)e^{j2\pi f_c t}\} \\ &= \Re\{u(t)\}cos(2\pi f_c t) - \Im\{u(t)\}sin(2\pi f_c t) \\ &= x(t)cos(f_c t) - y(t)sin(2\pi f_c t) \end{aligned} \tag{1.1}$$

where $u(t) = x(t) + jy(t)$ is a complex baseband signal with in-phase component $x(t) = \Re\{u(t)\}$, quadrature component $y(t) = \Im\{u(t)\}$, bandwidth B_u, and power P_u. The signal $u(t)$ is called complex envelope or complex low pass equivalent signal of $s(t)$. This is a standard representation for bandpass signals with bandwidth $B << f_c$, as it allows signal manipulation via $u(t)$ irrespective of the carrier frequency. The power of the transmitted signal $s(t)$ is $P_t = P_u/2$. And the form of the received signal is as follows:

$$r(t) = \Re\left\{v(t)e^{j2\pi f_c t}\right\} \tag{1.2}$$

where the complex baseband signal $v(t)$ will depend on the channel through which $s(t)$ propagates.

1.2.2 Statistical multipath fading channel

As mentioned in section 1.2.1, in the case of the multipath channel, the receiver antenna receives a superposition of the various multipaths. Thus, a pulse transmitted over a multipath channel is received as multile replicas of the trasnmitted signal. Each pulse in the train corresponding either to the Line-of-Sight (Line-of-Sight (LOS)) component, or to a distinct multipath associated with a distinct scatterer. This phenomenon is called *time delay spread* and is described as the time delay between reception of the first signal component (LOS component) and the last received signal component (multipath component).

1.2.2.1 Time-varying channel impulse response

We consider the transmitted signal as in equation 1.1:

$$s(t) = \Re\{u(t)\}cos(f_c t) - \Im\{u(t)\}sin(2\pi f_c t) \tag{1.3}$$

where $u(t)$ is the complex envelop of $s(t)$ with bandwidth B_u and f_c is its carrier frequency. In the case of a time-varying channel impulse response, the received signal would amount to the sum of the LOS component and all the resolvable multipath components [2]:

$$r(t) = \Re\left\{\sum_{n=0}^{N(t)} \alpha_n(t)u(t-\tau_n(t))e^{j(2\pi f_c(t-\tau_n(t))+\phi_{D_n})}\right\} \tag{1.4}$$

where $\alpha_n(t)$ is the complex channel gain of path n at a time t. $n = 1$ corresponds to the LOS component, and $N(t)$ corresponds to the number of resolvable multipath components. $\tau_n(t)$ is the delay of the n-th path at time t and ϕ_{D_n} the Doppler phase shift. The received signal can also be expressed as:

$$r(t) = \Re\left\{\left(\int_{-\infty}^{\infty} c(\tau,t)u(t-\tau)d\tau\right)e^{j2\pi f_c t}\right\} \tag{1.5}$$

where,

$$c(t,\tau) = \sum_{n=0}^{N(t)} \alpha_n(t)e^{-j\phi_n(t)}\delta(\tau-\tau_n(t)) \tag{1.6}$$

is the channel impulse response at a time t and delay τ, i.e., the response of the channel at a time t to an impulse transmitted at $t-\tau$. And

$$\phi_n(t) = 2\pi f_c \tau_n(t) - \phi_{D_n} \tag{1.7}$$

is used in order to simplify $r(t)$.

Since the environment is random in nature, channel gain $\alpha_n(t)$, the delay $\tau_n(t)$, and the number of paths $N(t)$ are random. And in the case of non LOS (Non-Line-of-Sight (NLOS)) environment, the channel impulse response $c(t, \tau)$ is modeled as realization of a complex random variable (which has uniformly distributed phase and a Rayleigh distributed magnitude) when the number of multipath components $N_p(t)$ is large, by evoking the central limit theorem [3]. In such situation, the channel is said to be *Rayleigh fading*.

1.3 Multiple antenna systems

MIMO systems emerged as a result of the increasing demand for capacity in cellular and wireless local area networks. The feasibility of implementing MIMO systems and their associated signal processing algorithms was possible because of the increase in computational power of integrated circuits.

1.3.1 Receive diversity

As mentioned in 1.2.2, the propagation environment varies with time, the channel gain can sometimes be so small that the channel becomes useless. In order to resolve this problem, *diversity* was employed, which comes to transmitting the same information over multiple channels which fade independently of each other. Types of diversity include *time diversity* and *frequency diversity*, which amounts to transmitting the same information either in different time instances or different frequencies. *Antenna diversity* exploits the fact that the fading is (partly) independent between different points in space. An efficient way of exploiting *antenna diversity* is equipping the receiver with multiple antennas, which yields considerable gain in performance, mainly in terms of co-channel interference. This is due to the diversity gain created at the receiver, because of the independent fading of the signal received by multiple receive antennas. An example of the use of receive diversity was in (GSM) [4] where the (Base Station (BS)) is equipped with two receive antennas, improving the quality of the *uplink* (from the mobile to the base station). Receive

diversity is characterized by the number of independent fading branches or paths, which are also known as diversity order and are equal to the number of receive antennas. The overall receive Signal-to-Noise Ratio (SNR), is increased through proper combination of the received replicas of the transmitted signals, which also mitigates destructive fading. The combination methods at the receiver included selection combining, switching combining and equal combining [5, 6]

1.3.2 Transmit diversity and MIMO technology

After the gains achieved with receive diversity, it was only logical to next try to reproduce these gains in *transmit diversity*, through the employment of multiple transmit antennas at the transmitter side. This interest and development in transmit diversity started in the 1990's and since then have grown rapidly. This is because at the mobile end for instance, a performance enhancement is possible without adding extra antennas, power consumption or complexity. In fact this increase in error performance and data rates offered by transmit diversity and MIMO technology has made it a corner stone in most future wireless communication systems.

It is generally known that there exists a trade-off between bit rate and Bit Error Rate (Bit Error Rate (BER)) performance. The channel capacity is defined as the maximum possible transmission rate such that the probability of error can be made small by appropriate encoding and decoding. The pioneering work of Shannon [7] demonstrated that the capacity of a SISO perturbed by Additive White Gaussian Noise (Additive White Gaussian Noise (AWGN)) is a function of the average received SNR and the bandwidth.

MIMO systems emerged as a technology that could offer significant improvement to the achievable rates by a SISO system, and extensive work on this technology began in the late 1990's with efforts to develop coding and signal processing techniques that can approach the MIMO channel capacity.

1.3.3 MIMO trade-offs

In general there exists three MIMO design trade-offs that arise throughout the conception of MIMO techniques. The use of MIMO codes in order to increase the data rate through multiplexing was presented mainly with the work of Foschini in Bell Laboratories Layer Space-Time (Bell Laboratories Layer Space-Time (BLAST)) techniques [8] in 1996 and later with [9, 10]. These techniques use M transmit antennas to transmit M independent data streams, which leads to a linear increase in capacity rather than a logarithmic increase, with the number of antennas. Although, the simultaneous transmission of multi-stream signals imposes inter-antenna interference (Inter-Antenna Interference (IAI)), resulting in Maximum-Likelihood (Maximum Likelihood (ML)) detection complexity growing exponentially with the number of transmit antennas. In order to solve the previously mentioned issue, BLAST detectors are conceived to strike a **performance/complexity** trade-off, either with the work in [11, 12] imposing an excessive complexity ML scheme, or with Sphere Decoders (SD) in [13, 14], or with the popular Minimum Mean Square Error (Minimum Mean Square Error (MMSE)) arrangement in [15–17] , and finally with the decision feedback techniques [18, 19].

A second class of MIMO codes aims at enhancing the quality of link, represented mainly by Alamouti's Space-Time Block Codes (Space-Time Block Codes (STBC)) [20] conceived in 1998. The spacial resources of multiple transmit antennas have been exploited for the sake of achieving diversity gain, giving rise to a **multiplexing/diversity** trade-off between BLAST schemes and STBC schemes. Indeed, multiple replicas of the modulated symbols are transmitted by multiple transmit antennas over multiple symbol periods as in Orthogonal STBC's (Orthogonal Space-Time Block Codes (O-STBC)) in [20],[21–24]. Owing to the orthogonality of these designs, the multiple data streams may be decoupled at the receiver, eliminating the IAI. On the other hand, because of replica transmission, the MIMO bandwidth efficiency is undermined by the STBC design. To solve this issue and improve the throughput, the family of Quasi-Orthogonal STBC's (Quasi-Orthogonal Space-Time Block Codes (QO-STBC)) [25–31], has been conceived, only to face the problem of IAI again because of the compromise on the orthogonality.

It was shown in [32] that it is possible to obtain both diversity and multiplexing gain in a single scheme, which inspired the conception of Linear Dispersion Codes (Linear Dispersion Codes (LDC)) [33, 34]. These codes can achieve the full BLAST throughput (multiplexing gain), and the full STBC diversity (diversity gain). In fact, according to [34], the MIMO signals transmitted by M transmit antennas over T symbol periods are modeled as $S = \sum_{q=1}^{Q} S_q A_q$, where Q modulated symbols are dispersed by Q dispersion matrices $\{A_q\}_{q=1}^{Q}$ of size $(T \times M)$.

A third MIMO design trade-off arises with the increase of the number of transmit antennas that occurs at both the BS and the User Equipment (UE). Indeed, it becomes more complex to assign a dedicated RF chain to all antenna elements, as in BLAST, STBC and LDC. A solution to this problem is Index Modulation (Index Modulation (IM)) techniques, proposing a variety of single-RF and reduced-RF MIMO schemes [35–46]. Spatial-Modulation (SM) is a single RF scheme proposed in [37] that has attracted a lot of research attention, since it's advantages were shown in [39]. More specifically, in an SM scheme, two blocks of source bits are separately assigned for modulating a M-PSK/Quadrature Amplitude Modulation (QAM) symbol and an activation index. By doing so, one out of M transmit antennas is activated. In addition, Space-Time Shift Keying (Space-Time Shift Keying (STSK)) [47] is a technique proposed for achieving diversity gain, where the IM bits are assigned to activate a single one out of Q LDC dispersion matrices. Indeed, these techniques reduce power consumption through the use of a single Radio Frequency (RF)-chain, regardless of the number of transmit antennas used. The problem lies with the spectral efficiency of SM and STSK schemes not being able to reach that of BLAST and LDC [48]. Some solutions to solve this issue were the use of reduced-RF Generalized SM and Generalized STSK [42],[49–52], striking the third trade-off being the **full/reduced/single-RF trad off** of MIMO systems.

Since their conception, MIMO systems have become a part of wireless communication technologies, such as 3G with Code Division Multiple Access (CDMA) using Alamouti's diversity scheme [53], the IEEE 802.11n Wireless Local Area Network (WLAN)[54], 802.20 (mobile broadband wireless access system), the 3rd Generation Partnership Project (3GPP) LTE in wide band CDMA [55] and recently in 5G-NR,

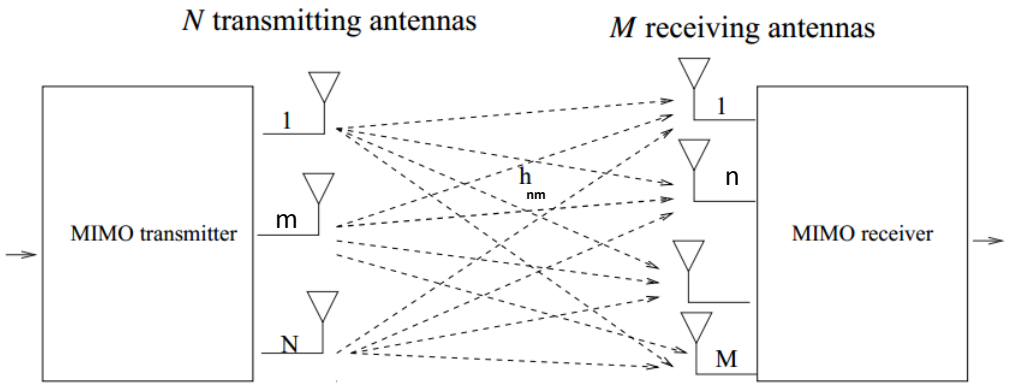

Figure 1.1 – A MIMO channel with M transmit and N receive antennas

where MIMO systems are required to support the diverse requirements of the NR platform.

1.3.4 MIMO system model

We consider MIMO systems having M transmit antennas and N receive antennas. At a time t, the antenna n receives the symbol:

$$y_n = \sum_{m=1}^{M} h_{n,m} x_m + w_{n,m} \tag{1.8}$$

where $h_{n,m}$ is the path gain of the channel from transmit antenna m to receive antenna n, which are independent and identically distributed (iid), complex Gaussian distributed. It is common for practical purposes to model the channel as frequency flat whenever the bandwidth of the signal is smaller than the inverse delay spread of the channel. x_m is the signal transmitted from antenna m at a time t, and $w_{n,m}$ is the noise term, which is spatially white circular Gaussian random variable with zero mean and variance σ^2:

$$w_{n,m} \sim \mathcal{CN}(0, \sigma^2) \tag{1.9}$$

which is AWGN. This system model is shown in Fig.1.1.

The equation 1.8 can be expressed in a matrix framework. Let $\mathbf{x}$ of size M and $\mathbf{y}$ of size N, be the vectors containing the transmitted and received symbols,

respectively. The channel gain matrix is defined as the $N \times M$:

$$\mathbf{H} = \begin{bmatrix} h_{1,1} & \dots & h_{1,M} \\ \vdots & & \vdots \\ h_{N,1} & \dots & h_{N,M} \end{bmatrix} \tag{1.10}$$

which amounts to

$$\mathbf{y} = \mathbf{H}\mathbf{x} + \mathbf{w} \tag{1.11}$$

where $\mathbf{w} = [w_1 \dots w_N]^T$ is a vector of noise samples. The matrix form of equation (1.8) is:

$$Y_\tau = H_\tau X_\tau + W_\tau \tag{1.12}$$

where X_τ is the $M \times T$ transmission matrix, H_τ is the channel matrix of size $N \times M$ and Y_τ is the $N \times T$ received matrix. W_τ is the additive white Gaussian noise of size $N \times T$. T denotes the number of columns of the transmitted matrix and $T \leq L$.
Here, the elements of the channel matrix $\mathbf{H}$ are complex Gaussian random variables with zero mean. This assumption is normally used in an environment with local scatterers and no LOS components. Consequently the magnitudes of the channel gains $|h_{m,n}|$ have a Rayleigh distribution.
For each receive antenna, the Signal to Noise Ration (SNR), is defined as:

$$SNR = \frac{\mathbb{E}[|y_{nt} - w_{nt}|^2]}{\mathbb{E}[|w_{nt}|^2]} \tag{1.13}$$

1.3.5 Capacity of MIMO Systems

The MIMO systems can be studied by the evaluation of the information-theoretic (Shannon) capacity. Considering the MIMO system in Fig. 1.1, the capacity of such a system for a flat fading channel is given by

$$C = log_2 \left[det \left(I + \frac{P}{N_0} \mathbf{H}\mathbf{Q}\mathbf{H}^H \right) \right] \tag{1.14}$$

where $\mathbf{Q} \in \mathbb{C}^{M \times M} = \mathbb{E}\{\mathbf{x}\mathbf{x}^H\}$, $\mathbb{E}\{\}$ is the expectation and . P is the total transmitter power, I is $N \times N$ identity matrix, and N_0 is the noise spectral density. The analysis of MIMO systems in step Rayleigh-fading channels is presented in [56], and

a Gaussian approximation to the capacity distribution is studied in [57]. These analysis show that MIMO systems can potentially provide enormous Shannon capacities in uncorrelated Rayleigh fading channels.

1.3.6 Challenges in channel estimation

As previously mentioned, a signal received at the output of a wireless communication channel is conventionally a faded and noise contaminated replica of the transmitted signal.

In this context, a receiver is referred to as being **coherent**, when the CSI is estimated prior to detection at the receiver. This requirement led to the development of channel estimation techniques such as [11, 58, 59].

Coherence bandwidth and coherence time

Factors that may determine the *capacity* and *integrity* of the wireless communication link are the specific distribution of the multipath fading and the Doppler frequency, which is proportional to the carrier frequency, as well as the vehicular speed. Which in their turn affect the length and shape of the channel impulse response (Channel Impulse Response (CIR)).

— When all the diffracted and reflected multipath components arrive almost simultaneously within a *symbol period*, **non-dispersive fading** is encountered, represented by a dirac-delta CIR, leading to near constant frequency-domain channel transfer function across the signal bandwidth.

— When the time-domain delay-spread of the multipath components exceeds the symbol period, the system is faced with inter-symbol interference, leading to a frequency-dependent channel transfer function.

The **coherence-bandwidth** defines the range of frequency over which the frequency-domain channel transfer function is near-constant, which in its turn is inversely proportional to the delay spread.

Coherence-time is a concept used to quantify the Doppler effect, which in its turn describes the change in the channel. Coherence-time is inversely proportional

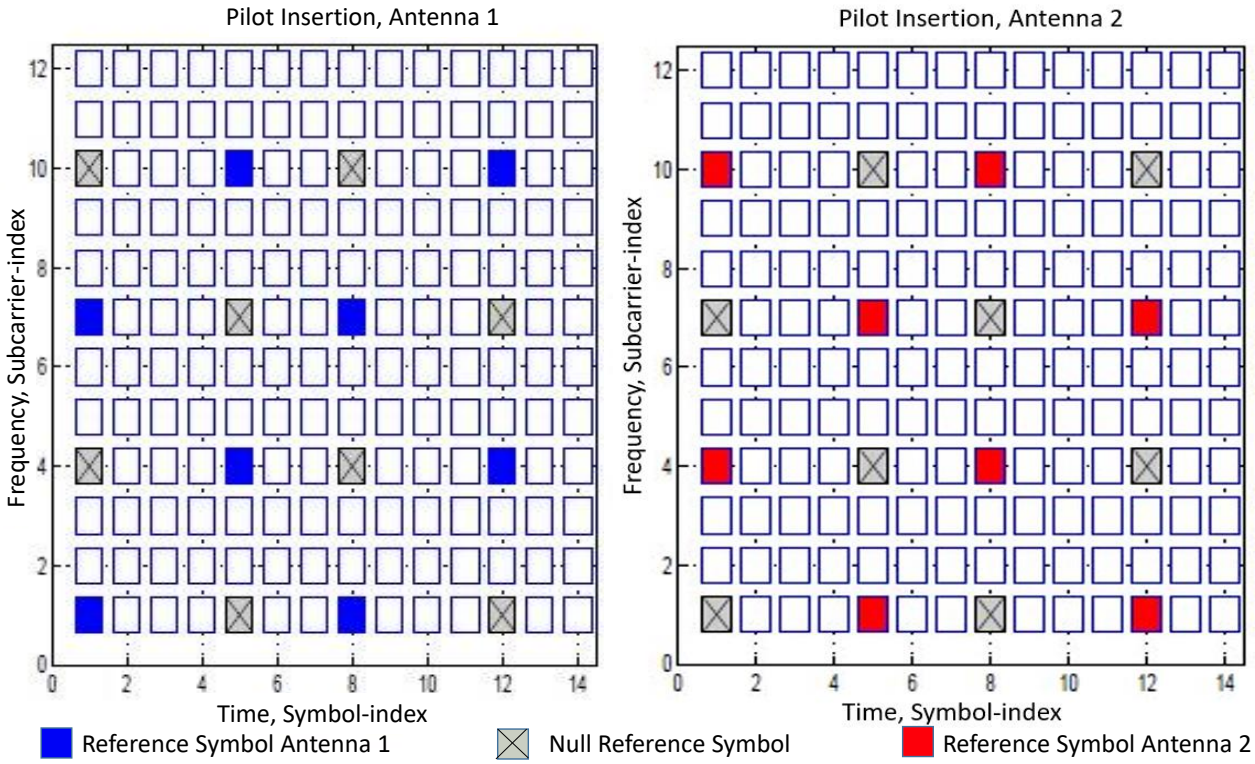

Figure 1.2 – Insertion of pilot symbol sequences in data frame

to the Doppler frequency, and it characterizes the time over which fading channel envelope may be deemed near constant.

When long coherence-time with reference to symbol duration are encountered, the channel gains remains constant over a set of symbol transmissions. If so, CSI estimation could be carried out by transmitting training symbol sequences that are known to the receiver at the beginning of the signal frame. On the other hand, if the vehicular speed (outdoor case) or the movements of people (indoor case) is increased , coherence time is reduced and the fading changes more rapidly over time, leading to more frequent insertion of pilot symbols in the data frame.

The scheme shown in Fig. 1.2 is a time and frequency domain pilot-based estimation technique in the case of OFDM frame for MIMO system having two antennas. When applying coherent demodulation in fading channels, information about the channel frequency response for any sub-carrier of any OFDM symbol is required and has to be estimated by the receiver. The basic principle of pilot symbol aided channel estimation is to multiplex reference symbols, so-called pilot symbols into the

data stream in order to sample the channel frequency directions. The pilot symbols are then scattered in time and frequency on OFDM frames.

In [60], the authors observed that the use of training is optimal for obtaining accurate CSI estimation for the high SNR values in the case of a long coherence time, although if these simulations are done in low SNR region, estimates become less reliable. Which confirms that the use of training for channel estimation is challenging when the noise power is high i.e. SNR is low.

The cost of acquiring CSI

Since pilot symbol sequences are already known at the receiver side, they do not carry any user information, rather they occupy the available time/spectral resources. In a fast fading channel environment, the coherence interval becomes short, which leads to disproportionate transmission of pilot symbols with respect to data symbols.

1.4 Overview of non-coherent techniques

In this section we review the non-coherent techniques conceived in literature, for single-antenna systems as well as multiple-antenna systems. The use of these techniques is also explored for modern communication systems.

1.4.1 Non-coherent receivers history

As was mentioned in section 1.3.6, CSI estimation could become extremely challenging in high mobility scenarios, which require insertion of a prohibitive number of pilot symbols for accurate channel estimation. On the other hand, when the receiver does not have knowledge of the CSI, *non-coherent* reception is encountered. These methods rely on blind CSI estimation techniques, that take advantage of the correlation between the consecutively received signals. This correlation is in fact imposed by the channel memory.

One of the most well-known optimization criterion firstly conceived is presented by the Maximum Likelihood Sequence Estimation (Maximum Likelihood Sequence

Estimation (MLSE)), which is a technique capable of performing channel estimation and data detection jointly, and was conceived by Kailath dating back to 1960 [61]. Channel estimation is performed on each possible combination of the data carrying sequence. This method faced an exponential increase in complexity with the increase of the message length, this is why it was proposed by Forney to invoke the Viterbi algorithm with MLSE in 1972 [62]. In this case, the number of trellis states that determined the MLSE complexity increased exponentially with the channel's memory rather than the message length. In 1979, Morely and Snider [63] demonstrated that MLSE is capable of tackling any form of channel memory, regardless whether the memory is imposed by frequency-selective or time-selective channels such as correlated Rayleigh, Rician and log-normal fading.

Differential receivers

In analogy to the channel memory concept, the philosophy of "modulation with memory" was first explored by Lawton [64, 65] in 1960, with the classic Differential Phase Shift Keying (DPSK). At the DPSK transmitter, the data-carrying M-Ary Phase Shift Keying (MPSK) symbol x_{n-1} is mapped onto the difference between the consecutive transmitted symbols as $s_n = x_{n-1}s_{n-1}$. In the presence of a AWGN channel or in a non-dispersive slow fading channel, the received symbol would amount to

$$y_n = s_n h_n + v_n \tag{1.15}$$

where h_n refers to the channel gain, and v_n refers to the AWGN. Through the use of DPSK, the need for channel estimation is eliminated, and a simple correlation operation is used as in

$$z_{n-1} = y_n y_{n-1}^* \tag{1.16}$$

z_{n-1} may be directly demapped to bits using and M-PSK demapper as in Fig. 1.3 which portrays the DPSK transceiver. This low complexity non-coherent detection at the receiver side is termed as Conventional Differential Detection (CDD). In fact, CDD is a special case of MLSE, where the channel memory is truncated to a window length of $N_w = 2$.

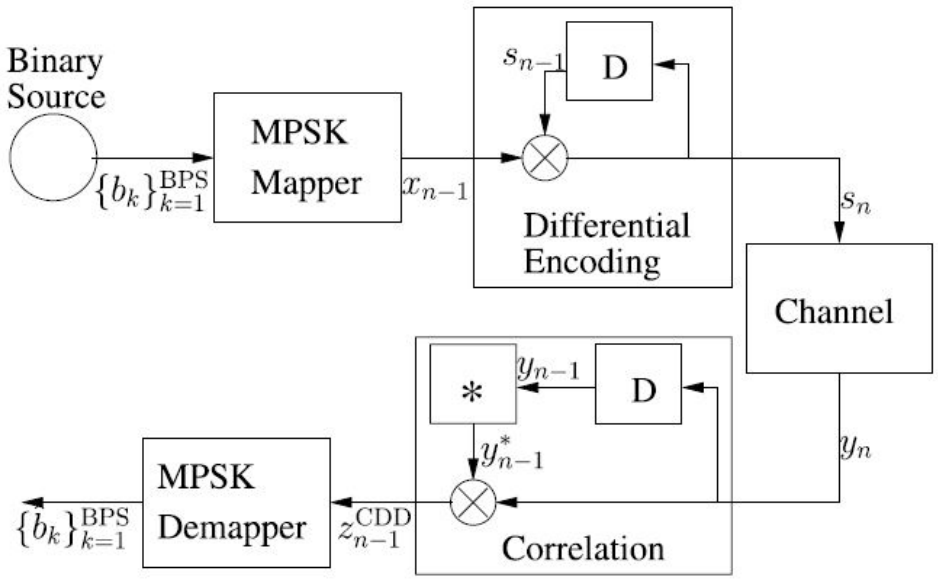

Figure 1.3 – DPSK transceiver

It was demonstrated by Cahn in [66] that CDD aided DPSK scheme suffers from a 3 dB performance penalty compared to its coherent MPSK counterpart (having perfect CSI). In addition, an irreducible error floor is encountered when the fading channel fluctuates rapidly [67].

With the aim of reaching the optimal performance of the MLSE, the groundbreaking Multiple-Symbol Differential Detection (MSDD) is conceived for DPSK operating in AWGN channels by Wilson *et al.* in [68]. As an attempt to improve the performance of CDD, the MSDD extends the CDD's observation window from $N_w = 2$ to $N_w \geq 2$ observations, where a total number of $(N_w - 1)$ data carrying symbols are jointly detected, which is portrayed in Fig. 1.4. This MSDD design that was conceived for DPSK was extended to operate in Rayleigh fading channels in [69]. In addition, the MSDD techniques conceived for DPSK and Differential Quadrature Amplitude Modulation (DQAM), operating both in AWGN and Rayleigh fading channels were shown to be able to reduce the performance penalty imposed by the use of CDD [70] and also attenuate the error floor experienced in fast fading channels [69, 70].

The issue faced with the use of MSDD was that the complexity increased exponentially with the length of N_w. For an M-Level DPSK scheme the complexity order is given for the detection of a single symbol by $O[M^{N_w-1}/(N_w - 1)]$. Attempts to

resolve this complexity issue were conceived by [71], where an efficient algorithm was created for MSDD in AWGN with a detection complexity of $O(logN_w)$ by detecting a single symbol through tracking the phase changes over the N_w samples.

In fact, the MSDD's complexity problem is the result of jointly detecting $N_w - 1$ data symbols. In the aim of separately detecting the data symbols, decision-feedback is introduced, and is called Decision-Feedback Differential Detection (DFDD) [72, 73], where a total of $N_w - 2$ data carrying symbols are detected from the previous detection windows, while only a single data symbol has to be detected in the current detection window, which is described in figure 1.5.

Since only a single data symbol is detected in a detection window, the complexity of DFDD is given simply by $O(M)$. Nevertheless, the imperfect decision feedback given by DFDD results in a performance loss compared to MSDD. With the aim

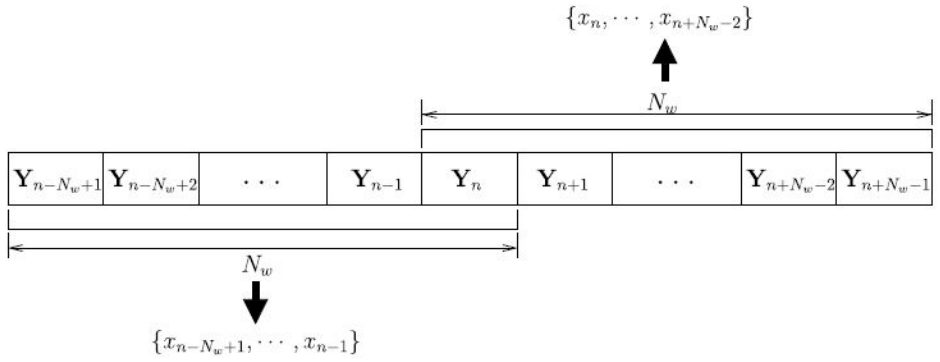

Figure 1.4 – MSDD non-coherent detection schematic

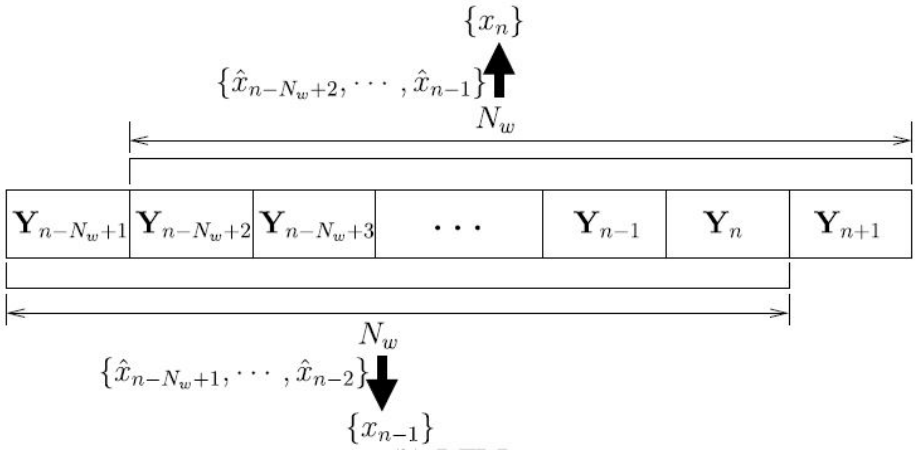

Figure 1.5 – DFDD non-coherent detection schematic

of resolving this issue, Multiple-Symbol Differential Sphere Detection (MSDSD) is conceived by Lampe *et al.* in [74] for DPSK operating in Rayleigh fading channels. This technique is based on transforming the problem of optimizing the MSDD decision metric into a shortest vector search problem, so that Sphere Detection (SD) may be described for MSDSD as follows:

1. SD radius is set to be sufficiently large.
2. Initial SD index is set to be $v = 1$.
3. M M-PSK candidates are examined for detecting a single symbol for each SD index v.
4. The SD index v is increased when the best candidate is chosen.
5. The search is repeated until $v = N_w$ is reached where a valid MSDSD output is found and the SD's radius may be updated accordingly.
6. Afterwards, the SD index v is reduced so that the next best candidate may be examined.
7. In the case where no more valid candidates can be found within the SD radius, v is reduced until reaching 1. In which case the SD process is terminated.

The MSDSD complexity order imposed by detecting a single symbol is then lower-bounded by $O(M)$.

Following this, Pauli *et al.* proposed the soft-decision-aided MSDSD for DPSK communicating in Rayleigh fading channels in 2006 [75], so that MSDSD may be invoked in turbo detection. In 2012, Wang and Hanzo [42] proposed to invoke MSDD and MSDSD for detecting the Differential Amplitude Phase Shift Keying (DAPSK) amplitudes and phases. The use of both techniques leads to the exchange of decisions amongst them, in order to achieve a near-optimum MSDD performance in coded systems. More recently Xu *et al.* proposed dynamic MSDSD/DFDD algorithms in [76, 77], that facilitate the estimation of the QAM-amplitude dependent channel correlation matrix with hard and soft decision MSDSD solutions achieving the optimal MSDD performance at reduced complexities.

1.4.2 MIMO detection techniques

It has been shown in [60] that the increase in the number of antennas used is responsible for a pilot overhead in coherent detection for MIMO schemes. This is why it was inevitable that non coherent detection schemes would extend to MIMO systems.
One of these schemes are the family of DSTM that are capable of ridding themselves from the prohibitive process of channel estimation, which is why it attracted a lot of research interest.

1.4.2.1 Differential Space-Time Modulation Schemes

One of the first schemes proposed in DSTM, was in fact an extension of the famous Alamouti STBC scheme in [20], and was called Differential STBC (DSTBC) [78], which employed the same signal structure as Alamouti's scheme. DSTBC was further extended to be able to function using multiple transmit antennas [24, 79], and star/square QAM constellations [80–82]. More explicitly, the DSTM schemes operate based on the matrix-based differential encoding process portrayed by:

$$\mathbf{X}_\tau = V_{l(\tau)}\mathbf{X}_{\tau-1} \tag{1.17}$$

where $\mathbf{X}_\tau$ is the $(M\times T)$-element signal matrix, and $V_{l(\tau)}$ is the $(M\times M)$-element data signal matrix carrying the source information. For any coherence interval T and any fixed number of receiver antennas, the capacity obtained with $M > T$ transmitter antennas equals the capacity obtained with $M = T$ transmitter antennas [83]. In order for the transmitted signal matrix $\mathbf{X}_\tau$ to retain orthogonal columns, and in the aim of conserving an average signal power over differential encoding in the time domain, the authors of [83, 84] proved that $V_{l(\tau)}$ should be designed to be unitary i.e. $V_{l(\tau)}^H V_{l(\tau)} = V_{l(\tau)} V_{l(\tau)}^H = I$, where H denotes the conjugate transpose and I the identity matrix.

1.4.2.2 Differential Group Codes

Throughout this thesis work, we focus on a family of codes inspired from the DSTM philosophy, called Differential Group Codes (DGC), which were originally

proposed in [83, 84]. DGC schemes are based on signal matrices that form a multiplicative group under the multiplication operation. Indeed, a group $\mathcal{X}$ is a set of matrices $X^i \in \mathcal{X}$, meaning that the matrices of this group must satisfy the following conditions:

1. If $X_i, X_j \in \mathcal{X}$, $X_i X_j \in \mathcal{X}$.
2. If $X_i, X_j, X_k \in \mathcal{X}$, $(X_i X_j)X_k = X_i(X_j X_k)$.
3. $I \in \mathcal{X}$
4. If $X_i \in \mathcal{X}$, $(X_i)^{-1} \in \mathcal{X}$

The class of group codes includes poly-phase codes [85], permutation codes [86], block-circulant unitary codes [87] and all binary linear codes with Binary Phase Shift Keying (BPSK) modulation [88],[89]. This means that group codes can be constructed for any number of transmit antennas and any constellation $\mathcal{C}$.

Spatial modulation using differential transmission

In recent years, the differential transmission philosophy was integrated with spatial modulation schemes in an attempt to diminish the excessive complexities encountered in DGCs and Differential Linear Dispersion Code (DLDC)s. More explicitly, Suguira *et. al* conceived the Differential Space-Time Shift Keying (DSTSK) in [47], which was further extended to QAM constellations in [90] and the DLDC's Cayley transform was eliminated in [91] since the DSTSK's dispersion matrices $\{A_{q=1}^{Q}\}$ are directly generated to be unitary, which is due to the absence of DLDC's matrix summation. Moreover, Bian *et. al* integrated the differential transmission concept in spatial modulation [92, 93] which was developed to include a star QAM constellation in [94, 95]. Furthermore, in order to achieve a beneficial transmit diversity, a single-RF DSM scheme is conceived in [96, 97]. Recently, in 2017, Rajashekar *et al.* [97] proposed Field Extension based Differential Spatial Modulation (FE-DSM) as a diversity aided DSM scheme (operating using single-RF). Ishikawa *et al.* [98] proposed a rectangular DSM scheme for open-loop massive MIMO scenarios which was later extended in [99] to support an arbitrary number of activated RF-chains. This led to the design of Differential Generalized Spatial Modulation scheme used

in high mobility millimeter wave communications.

1.5 Conclusion

Adaptivity in modern wireless communication systems is of high importance. Which means that a system should be able to adapt to different channel conditions and remain capable of providing reliable communication. If the conditions for a non-prohibitive channel estimation process are met, the system is called coherent and perform channel estimation accordingly. Although, when these conditions prove to be difficult for channel statistics acquisition, the system could perform non-coherent detection. Modern techniques to provide blind CSI-estimates are proposed in the research community recently in the aim of solving channel estimation issues, among which are DSTM schemes that range from differential STBC schemes, DGCs, and differential spatial modulation techniques. In our work we focus on DGCs and how we can improve their throughput while maintaining their performance.

Chapter 2

DSTM Using Extensions of the Weyl Group

In this chapter, we use the multiplicative Weyl group of 2×2 unitary matrices for DSTM system. More explicitly, we study the composition and the method of generation of the Weyl group and propose extensions to it, in order to improve the throughput of the DSTM system employing the obtained groups of larger size. We propose a selection algorithm of the sets of information matrices to be used for a given value of the spectral efficiency along with an optimal mapping strategy between binary vectors and information matrices. This aims at improving the overall error performance of the system, which is evident in simulation results produced and analyzed for MIMO systems having 2 transmit antennas employing the Weyl group and its extensions.

2.1 The general model of the DSTM scheme

The differential MIMO system model is based on the model portrayed in section 1.3.4 in the first chapter and the encoding process is described in relation (1.17). In fact, a differential space-time modulation scheme maps a vector of information bits onto a matrix V that belongs to a candidate group P according to a specific mapping rule that maximises error performance. The differential encoding process is described next and the nature of the candidate group used by the DSTM scheme

is described later in this chapter.

The transmission matrix X is of dimension $M \times T$, M being the number of transmit antennas and T the number of symbols for one transmitted matrix. For simplicity, we set $T = M$, since according to [56], having $T < M$ or $T = M$ would not modify the capacity of a non-coherent system. Naturally this scheme can be extended to MIMO systems with $T > M$ or $T < M$. This extension introduces some complications since the groups used in this work are multiplicative and thus have $T = M$. Consequently this extension will not be addressed here.

2.1.1 Differential encoding process

The differential encoding process for the multi-antenna communication system is very similar to the standard single-antenna DPSK as previously mentioned. Since signals are transmitted set-by-set, it is convenient to use $\tau = 0, 1, \ldots$ to denote the indexes of the transmitted matrices.

Let us denote the $M \times M$ matrix transmitted over M antennas as X. At the start of the transmission, the transmitter sends a reference matrix $X_0 = V_0$ during τ_0, which is usually the identity matrix $X_0 = I_M$. Thereafter, data are differentially encoded according to

$$\mathbf{X}_\tau = V_{l(\tau)}\mathbf{X}_{\tau-1} \tag{2.1}$$

where $V_{l(\tau)}$, with $l(\tau) \in \{0, 1, \ldots, K-1\}$, is the $M \times M$ data matrix at time τ which is selected from a set $\mathcal{S}$ of size K. $\mathcal{S}$ is a set of matrices chosen from a multiplicative group of unitary matrices $\mathcal{P}$, i.e., $V_{l(\tau)} \in \mathcal{S}$. Therefore, each matrix V_l verifies the relation$\{V_l | V_l^H V_l = V_l V_l^H = I_M, l = 0, 1, \ldots, K-1\}$. Indeed, the first vector of the information bits is mapped onto the information matrix $V_{l(1)}$ and the second vector is mapped onto $V_{l(2)}$. Therefore, at the transmitter end, the sequence of transmitted

matrices is:

$$\begin{aligned} X_0 &= V_0 \\ X_1 &= X_0 V_{l(1)} = V_0 V_{l(1)} \\ &\vdots \\ X_\tau &= X_{\tau-1} V_{l(\tau)} = V_0 V_{l(1)} V_{l(2)} \dots V_{l(\tau)} \\ &\vdots \end{aligned} \tag{2.2}$$

At the receiver side, the N antennas receive a stream of matrices of the form $Y_0, \dots, Y_\tau, Y_{\tau+1}$, obtained with the following relations:

$$Y_\tau = HX_\tau + W_\tau \tag{2.3}$$

for the signal obtained with matrix time τ, and

$$Y_{\tau+1} = HX_{\tau+1} + W_{\tau+1} \tag{2.4}$$

for the matrix received afterwards.

The differential equation (2.2) is used to produce:

$$\begin{aligned} Y_{\tau+1} &= HX_{\tau+1} + W_{\tau+1} \\ &= Y_\tau V_{l(\tau+1)} + W'_{\tau+1} \end{aligned} \tag{2.5}$$

where $W'_{\tau+1} = W_{\tau+1} - W_\tau V_{i(\tau+1)}$.

2.1.2 Differential demodulation

Given that the receiver has knowledge of the received matrices at times τ and $\tau + 1$, it would then be simple to use the maximum likelihood decoder to retrieve the transmitted information matrix:

$$\begin{aligned} \hat{V}_{i_{(\tau+1)}} &= argmin_{V \in \mathcal{S}} ||Y_{\tau+1} - Y_\tau V|| \\ &= argmin_{V \in \mathcal{S}} Tr\{(Y_{\tau+1} - Y_\tau V)^H (Y_{\tau+1} - Y_\tau V)\} \\ &= argmax_{V \in \mathcal{S}} Tr\{Re(Y_{\tau+1}^H Y_\tau V\} \end{aligned} \tag{2.6}$$

Once the information matrix is obtained, the binary vector is acquired through the inverse mapping rule, thus recovering the information bits.

2.2 Constellation design for MIMO systems with 2 transmit antennas

For a given group $\mathcal{P}$, the maximum spectral efficiency is given by:

$$R_{max} = (1/M)\lfloor log_2|\mathcal{P}|\rfloor \quad bps/Hz \tag{2.7}$$

where $|\mathcal{P}|$ denotes the cardinality of the group.

As the information matrices are selected from the multiplicative group $\mathcal{P}$, each transmitted matrix also belongs to $\mathcal{P}$. For L_v bits, each transmitter antenna sends M symbols. The corresponding spectral efficiency is:

$$R = L_v/M$$

In our scheme, the information matrices are selected from the mathematical Weyl group [100].

2.2.1 Weyl Group Generation

The Weyl group is composed of unitary (hence invertible) matrices that form the group under multiplication. The multiplicative group of Weyl is denoted by $\mathcal{G}_{w2}$ and has 12 cosets $\{C_0, C_2 \ldots, C_{11}\}$, each one containing 16 matrices. The first coset C_0 is defined as:

$$C_0 = \left\{ \alpha \begin{bmatrix} 1 & 0 \\ 0 & \pm 1 \end{bmatrix} \ , \ \alpha \begin{bmatrix} 0 & 1 \\ \pm 1 & 0 \end{bmatrix} \right\}$$

with $\alpha \in \{+1, -1, +i, -i\}$. All the 12 cosets are derived from C_0 as follows:

$$C_k = A_k C_0 \ \forall k = 0, 1, \ldots, 11$$

where A_k can be grouped into two sets, the first one being $\{A_0, A_1, \ldots, A_5\}$ where:

$$A_0 = \begin{bmatrix} 1 & 0 \\ 0 & 1 \end{bmatrix} \ A_1 = \begin{bmatrix} 1 & 0 \\ 0 & i \end{bmatrix} \ A_2 = \frac{1}{\sqrt{2}} \begin{bmatrix} 1 & 1 \\ 1 & -1 \end{bmatrix}$$

$$A_3 = \frac{1}{\sqrt{2}} \begin{bmatrix} 1 & 1 \\ i & -i \end{bmatrix} \ A_4 = \frac{1}{\sqrt{2}} \begin{bmatrix} 1 & i \\ 1 & -i \end{bmatrix} \ A_5 = \frac{1}{\sqrt{2}} \begin{bmatrix} 1 & i \\ i & 1 \end{bmatrix}$$

The second set $\{A_6, A_7, \ldots A_{11}\}$ is given by:
$A_{k+6} = \eta A_k$, with $\eta = (1+i)/\sqrt{2}$ $\forall k = 0, 1, \ldots, 5$, leading to a total of 192 unitary matrices numbered as $M_0, M_1, \ldots, M_{191}$. The matrices of the Weyl group can be seen as points distributed on the complex matrices sphere and the distance between two matrices M_a and M_b is given by:

$$D(M_a, M_b) = \|M_a - M_b\| \tag{2.8}$$

Here, the norm used is the Frobenius norm, because it is induced by a natural matrix inner product:

$$\langle A, B\rangle = tr(A^T B) = \sum_i \sum_j A_{ij} B_{ij} \tag{2.9}$$

that is,

$$\|A\| = \sqrt{\langle A, A\rangle} = \sqrt{\sum_i \sum_j A_{ij}^2} \tag{2.10}$$

This is directly analogous to how the dot product:

$$\langle x, y\rangle = x^T y = \sum_i x_i y_i \tag{2.11}$$

induces the Euclidean norm:

$$\|x\| = \sqrt{x^T x} = \sqrt{\sum_i x_i^2} \tag{2.12}$$

In fact, the Frobenius norm is precisely the Euclidean norm applied to the vectorized version of a matrix (where all the rows or columns of the matrix are concatenated to produce a single vector).
In addition, $D(M_a, M_b) = D(M_b, M_a)$, meaning that there are $191 \times \frac{192}{2} = 18336$ values $D(M_a, M_b)$ with $0 \leq a < b \leq 191$. The 191 values of $D(M_a, M_b)$ for a fixed a where $b \neq a$, is the same for any a, which is shown in Table 2.1.

Regarding the distance spectrum of each coset of G_{w2} individually, if A is an $n \times n$ unitary matrix, i.e., $A^H A = AA^H = I_n$, the Frobenius norm of A is

$$\|A\| = \sqrt{Tr(AA^H)} = \sqrt{Tr(A^H A)} = \sqrt{n} \tag{2.13}$$

In addition, $\forall M_a, M_b \in C_0$,

$$\|M_a - M_b\| = \sqrt{Tr[(M_a - M_b)^H (M_a - M_b)]} \tag{2.14}$$

Table 2.1 – Distance values $D(M_a, M_b)$ for a given matrix M_a in $\mathcal{G}_{w2}$

Distance	Occurrence
$\sqrt{4-2\sqrt{2}}$	8
$\sqrt{2}$	20
$\sqrt{4-\sqrt{2}}$	16
2	102
$\sqrt{4+\sqrt{2}}$	16
$\sqrt{6}$	20
$\sqrt{4+2\sqrt{2}}$	8
$2\sqrt{2}$	1
Total	191

Since all the cosets are generated from C_0 by multiplying special unitary matrices A_k, the distance between A_kM_a and A_kM_b is

$$\begin{aligned} \|A_kM_b - A_kM_b\| &= \sqrt{Tr[(M_a - M_b)^H A_k^H A_k (M_a - Mb)]} \\ &= \sqrt{Tr[(M_a - M_b)^H (M_a - M_b)]} \\ &= \|M_a - M_b\| \end{aligned} \tag{2.15}$$

which means that the distance spectrum of each coset of the Weyl group is exactly the same as the spectrum of C_0 in Fig. 2.1. The distance spectrum of the whole group $\mathcal{G}_{w2}$ is shown in Figure 2.2

2.3 Extensions of the Weyl group

In studying the construction of the Weyl group, we found that it presents an interesting symmetry: if a matrix $M \in \mathcal{G}_{w2}$, then $e^{\frac{jk\pi}{4}}M \in \mathcal{G}_{w2}$ for $k = 0, 1, ..., 7$. This property is shown in the construction of C_0 (a sub-group of $\mathcal{G}_{w2}$):

$$C_0 = P \cup e^{\frac{j\pi}{2}}P \cup e^{\frac{j2\pi}{2}}P \cup e^{\frac{j3\pi}{2}}P \tag{2.16}$$

where P is the set of 4 real matrices $\begin{bmatrix} 1 & 0 \\ 0 & \pm 1 \end{bmatrix}, \begin{bmatrix} 0 & 1 \\ \pm 1 & 0 \end{bmatrix}$ mentioned in section 2.2.1. The elements of the matrices of C_0, are the constellation points of $4PSK \cup \{0\}$, as

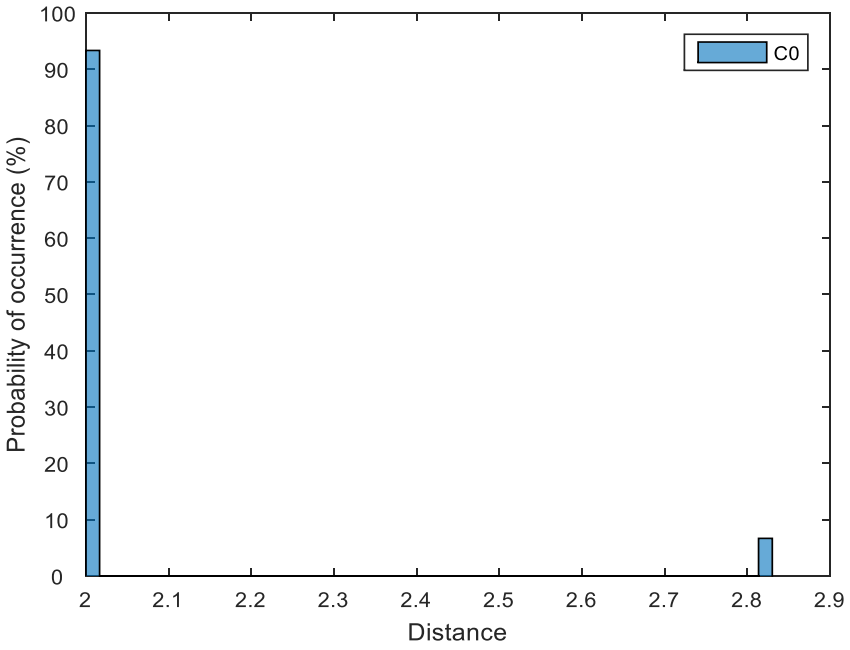

Figure 2.1 – C_0 distance spectrum

shown in Fig. 2.3a . The first 6 cosets of the Weyl group form a set E of 96 matrices which satisfy a similar relation to (2.16):

$$E = Q \cup e^{\frac{j\pi}{2}} Q \cup e^{\frac{j2\pi}{2}} Q \cup e^{\frac{j3\pi}{2}} Q, \tag{2.17}$$

where the set Q is:

$$Q = \bigcup_{k=0}^{5} A_k P \tag{2.18}$$

and A_k, $\forall k = 0, 1, \ldots, 5$, is the set of matrices mentioned in 2.2.1. The elements of the matrices in E are shown in Fig. 2.3b. And thus, the remainder of the Weyl group is constructed by multiplying the set E by $e^{\frac{jk\pi}{4}}$ which belongs to $8PSK$ constellation:

$$\begin{aligned} \mathcal{G}_{w2} &= E \cup e^{\frac{j\pi}{4}} E \\ &= \bigcup_{k=0}^{7} e^{\frac{jk\pi}{4}} Q \end{aligned} \tag{2.19}$$

The elements of the matrices in $\mathcal{G}_{w2}$ are shown in Fig. 2.3c.

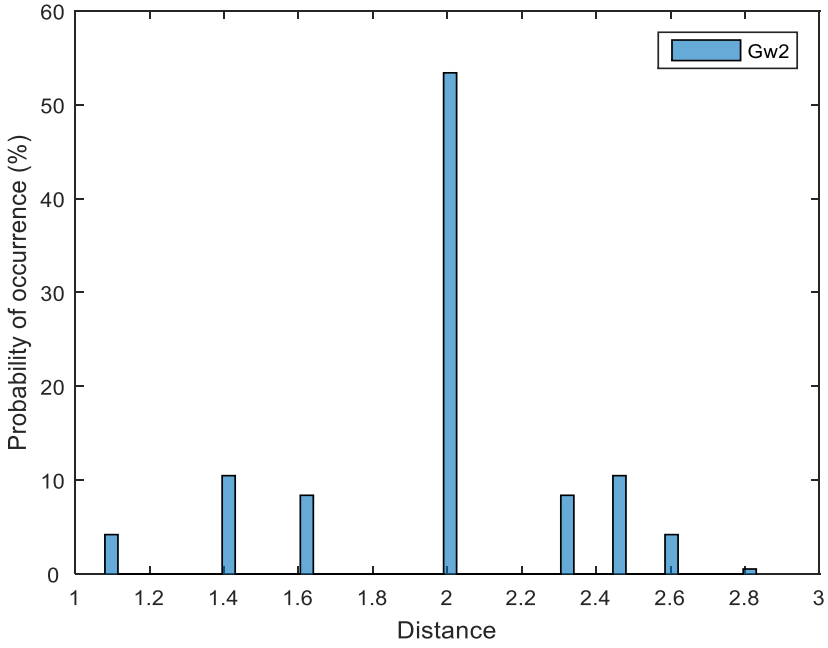

Figure 2.2 – Distance spectrum of $\mathcal{G}_{w2}$

2.3.1 Simple extension

Using two transmit antennas ($M = 2$), a matrix is transmitted during two symbol durations suiting the size of the matrices of the Weyl group. According to (2.7), $\mathcal{G}_{w2}$ achieves 3.5 bps/Hz maximum spectral efficiency using $2^{R_{max} \times M} = 2^{3.5 \times 2} = 128$ matrices:

$$\begin{aligned} R_{max} &= \frac{1}{M} \lfloor \log_2 K \rfloor \\ &= \frac{1}{2} \lfloor \log_2 192 \rfloor = 3.5 \, bps/Hz \end{aligned} \tag{2.20}$$

With the aim of increasing the maximum achievable spectral efficiency, we propose to generate a new multiplicative group, which we call $\mathcal{G}_{we2}$. The generation is inspired by the relation (2.19), where we perform an *optimal* rotation of the matrices in $\mathcal{G}_{w2}$ through multiplying it with $e^{\frac{j\pi}{8}}$:

$$\mathcal{G}_{we2} = \mathcal{G}_{w2} \cup \mathcal{G}_{w2} e^{\frac{j\pi}{8}} \tag{2.21}$$

The non-nul elements of the matrices in the newly generated group belong to a 16-PSK constellation. The extended Weyl group $\mathcal{G}_{we2}$, composed of 384 distinct unitary matrices, obeys the power constraint (having unitary matrices) and upgrades

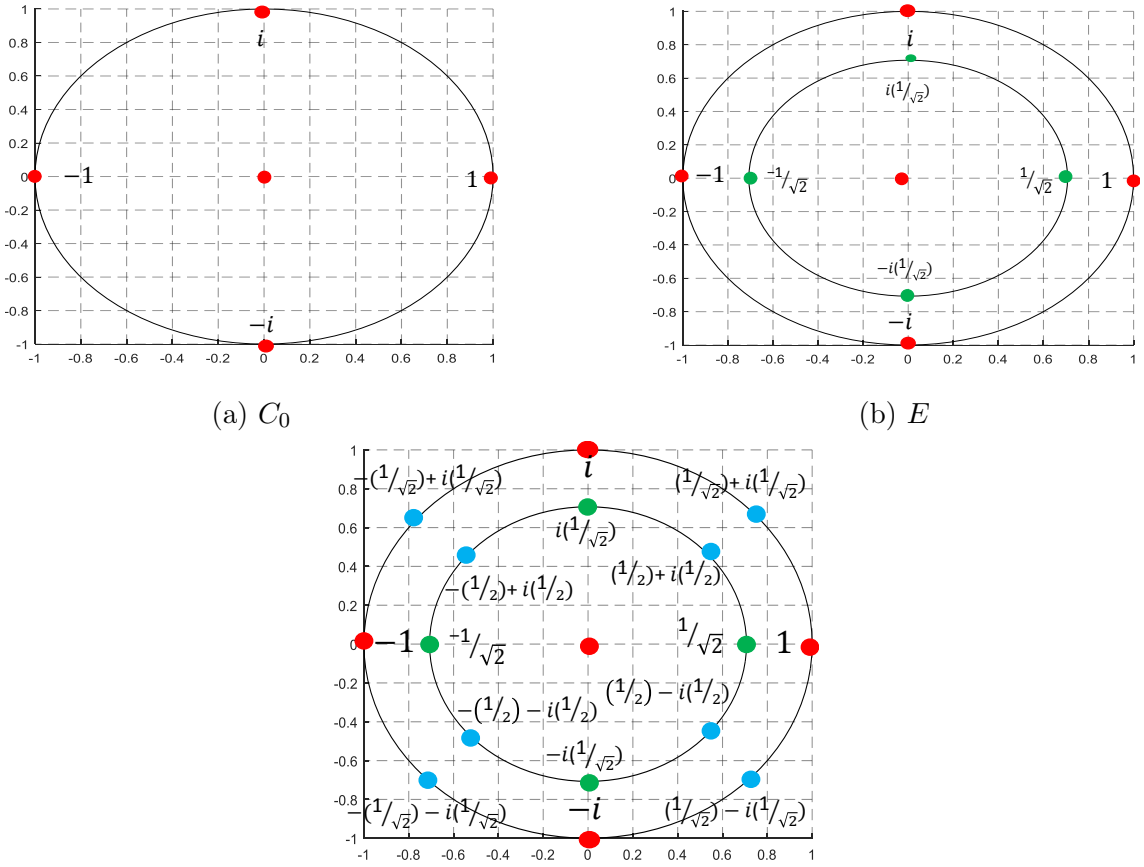

(a) C_0

(b) E

(c) $\mathcal{G}_{w2}$

Figure 2.3 – Elements of matrices sets from $\mathcal{G}_{w2}$ represented on constellation diagram

the maximum spectral efficiency to 4 bps/Hz for a MIMO system with 2 transmit antennas.

2.3.1.1 Optimal rotation

The relation in 2.21 can be rewritten in the form of:

$$\begin{aligned}\mathcal{G}_{we2} &= \mathcal{G}_{w2} \cup \mathcal{G}_{w2} e^{\frac{j\pi}{8}} \\ &= \bigcup_{k=0}^{15} e^{\frac{jk\pi}{8}} Q \\ &= \left\{ \bigcup_{k=0}^{7} e^{\frac{jk\pi}{4}} Q \right\} \cup \left\{ \bigcup_{l} e^{\frac{jl\pi}{8}} Q,\ l = 1,3,5,7,9,11,13,15 \right\} \\ &= \mathcal{G}_{w2} \cup \left\{ \bigcup_{l} e^{\frac{jl\pi}{8}} Q,\ l = 1,3,5,7,9,11,13,15 \right\} \end{aligned} \tag{2.22}$$

An optimal rotation means that the newly generated matrices have elements that are inserted within an equal footing of the already existing matrices elements. This is evidently performed in the generation of $\mathcal{G}_{we2}$, where the elements of the matrices newly added belong to a $16PSK$ constellation thus of equal footing to the already existing elements belonging to $8PSK$ as in relation 2.22. An illustration of the newly added elements are shown in Fig. 2.4.

The distance spectrum of $\mathcal{G}_{we2}$ is presented in Fig. 2.5 showing clearly how the additional number of matrices provides larger scope of search for matrices along with higher distances amongst them. In fact, $D(M_a, M_b) = D(M_b, M_a)$, which means that there are $383 \times \frac{384}{2} = 73586$ values $D(M_a, M_b)$ with $0 \leq a < b \leq 383$.

2.3.1.2 Group properties

It is important that the newly generated set $\mathcal{G}_{we2}$ is a group under the multiplication operation. The group property ensures that the transmitted matrices after differential encoding will still belong to the group, thus are unitary. This means that the total transmit power will remain constant, which ensures a good functioning of the RF (Radio Frequency) amplifiers, avoiding non-linearity issues.
Indeed, the Weyl group $\mathcal{G}_{w2}$ is not commutative under multiplication, though it satisfies all other group properties mentioned in section 1.4.2.2:

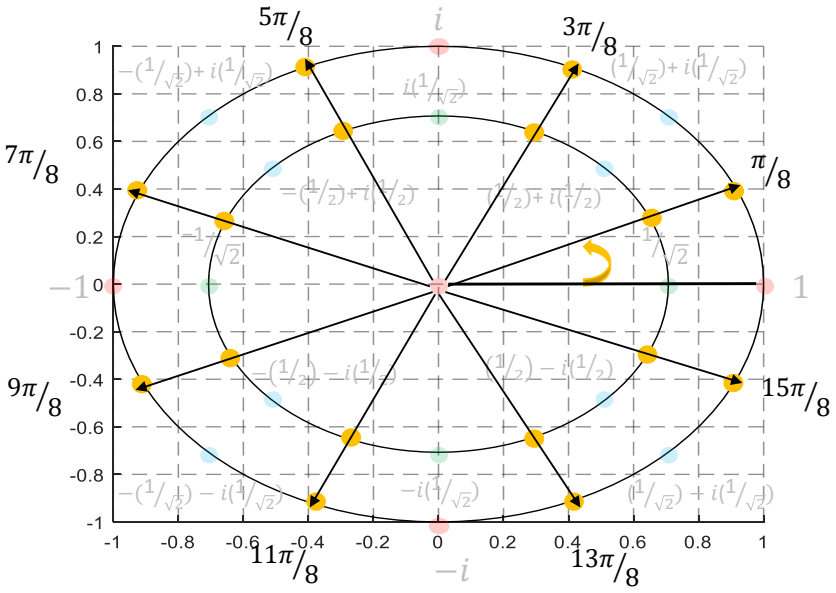

Figure 2.4 – $\mathcal{G}_{we2}$ matrices elements, showing new elements inserted with equal distance from already existing elements of $\mathcal{G}_{w2}$

1. If $M_a, M_b \in \mathcal{G}_{w2},\ M_a M_b \in \mathcal{G}_{w2}$.
2. If $M_a, M_b, M_c \in \mathcal{G}_{w2},\ (M_a M_b)M_c = M_a(M_b M_c)$
3. $I \in \mathcal{G}_{w2}$
4. If $M_a \in \mathcal{G}_{w2},\ (M_a)^{-1} \in \mathcal{G}_{w2}$

In fact, $\mathcal{G}_{we2}$ satisfies these conditions as well:

1. The identity element is indeed in $\mathcal{G}_{we2}$ since:

$$I \in \mathcal{G}_{w2},\ \mathcal{G}_{we2} = \mathcal{G}_{w2} \cup \mathcal{G}_{w2} e^{\frac{j\pi}{8}} \tag{2.23}$$

2. $\mathcal{G}_{we2}$ is indeed a closed group under multiplication:
   — The multiplication of two matrices $M_a, M_b \in \mathcal{G}_{w2}$:

$$M_a M_b \in \mathcal{G}_{w2} \implies M_a M_b \in \mathcal{G}_{we2} \tag{2.24}$$

   — The multiplication of a matrix $M_a \in \mathcal{G}_{w2}$ with a matrix $M_i \in \mathcal{G}_{w2} e^{\frac{j\pi}{8}}$:

$$\begin{aligned} M_a M_i &= M_a(M_b e^{\frac{j\pi}{8}}),\ M_b \in \mathcal{G}_{w2} \\ &= (M_a M_b) e^{\frac{j\pi}{8}} \\ &= M_c e^{\frac{j\pi}{8}},\ M_c \in \mathcal{G}_{w2} \\ &= M_j \in \mathcal{G}_{we2} \end{aligned} \tag{2.25}$$

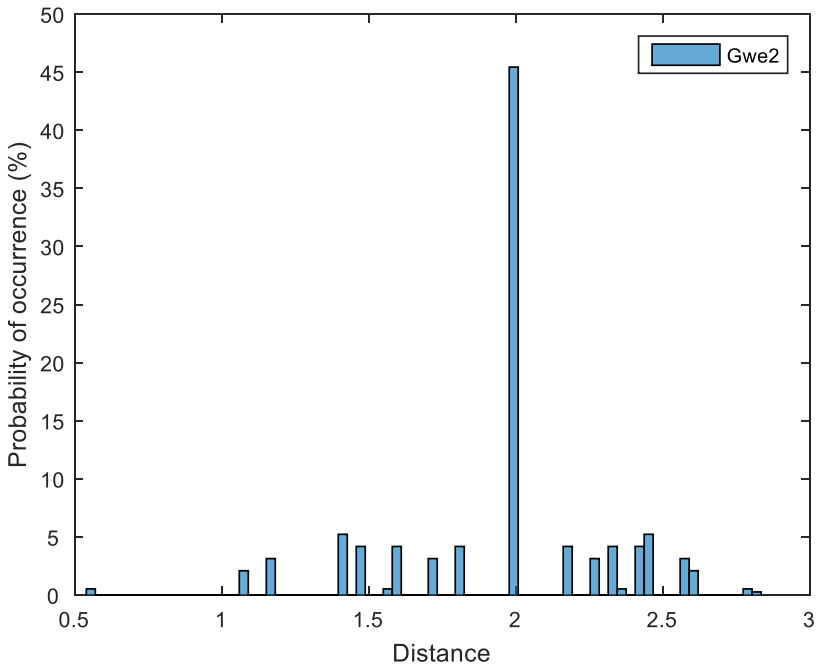

Figure 2.5 – $\mathcal{G}_{we2}$ distance spectrum

— The multiplication of two matrices $M_i M_j \in \mathcal{G}_{w2} e^{\frac{j\pi}{8}}$:

$$\begin{aligned} M_i M_j &= (M_a e^{\frac{j\pi}{8}})(M_b e^{\frac{j\pi}{8}}),\ M_a, M_b \in \mathcal{G}_{w2} \\ &= (M_a M_b)(e^{\frac{j\pi}{8}} e^{\frac{j\pi}{8}}) \\ &= M_c e^{\frac{j\pi}{4}} = M_d \in \mathcal{G}_{w2} \end{aligned} \tag{2.26}$$

3. The inverse of any matrix $M_i \in \mathcal{G}_{w2} e^{\frac{j\pi}{8}}$ is M_j:

$$\begin{aligned} {M_i}^{-1} &= \{M_a e^{\frac{j\pi}{8}}\}^{-1},\ M_a \in \mathcal{G}_{w2} \\ &= {M_a}^{-1} e^{\frac{-j\pi}{8}} \\ &= M_b e^{\frac{15j\pi}{8}} \\ &= M_j \in \mathcal{G}_{we2} \end{aligned} \tag{2.27}$$

4. Associative property is a general property of the product of square matrices thus applies here.

2.3.2 Double extension

Following the same method and in order to further increase the maximum achievable spectral efficiency, we propose a double extension of the Weyl group by multiplying $\mathcal{G}_{we2}$ with $e^{\frac{j\pi}{16}}$ which corresponds to 32-PSK constellation.

$$\mathcal{G}_{wee2} = \mathcal{G}_{we2} \cup \mathcal{G}_{we2} e^{\frac{j\pi}{16}} \tag{2.28}$$

Thus, the amount of matrices is increased in $\mathcal{G}_{wee2}$ to 768 and set the maximum spectral efficiency to 4.5 bps/Hz for a MIMO system with 2 transmit antennas.

This new extension, which we denote by $\mathcal{G}_{wee2}$, corresponds to an optimal rotation of the matrices in $\mathcal{G}_{we2}$. Indeed, the elements of the new extension $\mathcal{G}_{we2} e^{\frac{j\pi}{16}}$ are inserted within an equal footing of the already existing matrices elements of $\mathcal{G}_{we2}$, as in section 2.3.1.1:

The relation (2.28) can be rewritten in the form of:

$$\begin{aligned}
\mathcal{G}_{wee2} &= \mathcal{G}_{we2} \cup \mathcal{G}_{we2} e^{\frac{j\pi}{16}} \\
&= \bigcup_{k=0}^{31} e^{\frac{jk\pi}{16}} Q \\
&= \left\{ \bigcup_{k=0}^{15} e^{\frac{jk\pi}{8}} Q \right\} \cup \left\{ \bigcup_{l} e^{\frac{jl\pi}{16}} Q,\ l = 1, 3, 5, 7, 9, \ldots, 31 \right\} \\
&= \mathcal{G}_{we2} \cup \left\{ \bigcup_{l} e^{\frac{jl\pi}{16}} Q,\ l = 1, 3, 5, 7, 9, \ldots, 31 \right\}
\end{aligned} \tag{2.29}$$

An illustration of the newly added elements are shown in Fig. 2.6. In addition, $\mathcal{G}_{wee2}$ is a group under the multiplication operation following the same reasoning in section 2.3.1.2.

The distance spectrum of $\mathcal{G}_{wee2}$ is presented in Fig. 2.7. The double extension provides larger scope of search for matrices along with higher distances amongst them, as is explained in the next section. In fact, $D(M_a, M_b) = D(M_b, M_a)$ as in the $\mathcal{G}_{w2}$ and $\mathcal{G}_{we2}$ case, which means that there are $767 \times \frac{768}{2} = 294528$ values $D(M_a, M_b)$ with $0 \leq a < b \leq 767$. In addition, following the same reasoning of section 2.3.1.2, $\mathcal{G}_{wee2}$ is indeed a group under the multiplication operation.

Some of the achievable spectral efficiencies for the DSTM system for 2 transmit antennas using the Weyl group and its extensions are summarized in Table 2.2.

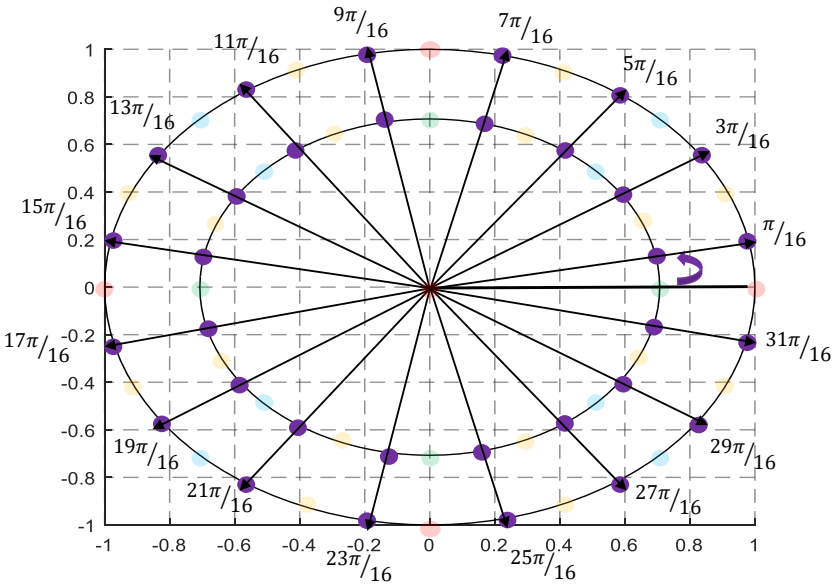

Figure 2.6 – $\mathcal{G}_{wee2}$ matrices, showing new matrices inserted with equal distance from already existing matrices of $\mathcal{G}_{we2}$

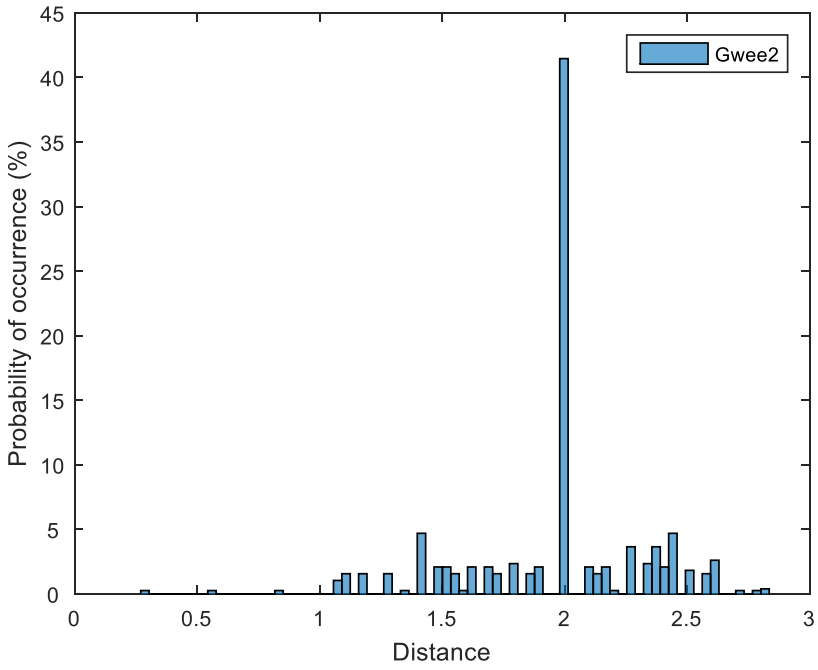

Figure 2.7 – $\mathcal{G}_{wee2}$ distance spectrum

Theoretically, we can keep generating new groups through optimal rotations, but since the resulting matrices grow closer with every extension, further extensions would affect the error performance of the system.

Table 2.2 – Parameters of $\mathcal{G}_{w2}$, $\mathcal{G}_{we2}$ and $\mathcal{G}_{wee2}$

$\mathcal{G}_{w2}$		$\mathcal{G}_{we2}$		$\mathcal{G}_{wee2}$	
192 distinct matrices		384 distinct matrices		768 distinct matrices	
Spectral efficiency (bps/Hz)	Number of selected matrices	Spectral efficiency (bps/Hz)	Number of selected matrices	Spectral efficiency (bps/Hz)	Number of selected matrices
2	16	2	16	2	16
2.5	32	2.5	32	2.5	32
3	64	3	64	3	64
3.5	128	3.5	128	3.5	128
-	-	4	256	4	256
-	-	-	-	4.5	512

2.4 Enhancing Error Performance

2.4.1 Near Optimal Matrix Selection

The information matrices are not randomly chosen, rather they follow a design criterion of the DSTM system studied here, which is maximizing the distances among the chosen matrices. The matrices of the Weyl group can be seen as points distributed on the surface of a high dimension sphere, where the largest distance between two matrices represents the diameter of this sphere. Accordingly, when expanding $\mathcal{G}_{w2}$, the matrices newly generated would be inserted on the same sphere, thus offering for a given spectral efficiency a largest scope of search.

Since the metric used for error performance is the distance between the information matrices selected, this implies that the selection process must use this metric with the aim of enhancing error performance. In this work, a matrix selection algorithm is proposed, maximizing the distances between the matrices selected in order to obtain the best subset $\mathcal{S}$ to be used for a given spectral efficiency where we need to use $K = 2^n$ matrices selected from the group P (n being the length of the binary information vector). A summary of the possible values of K and n for given spectral

Table 2.3 – Summary of the possible values of K and n for given spectral efficiencies from $\mathcal{G}_{w2}$, $\mathcal{G}_{we2}$ and $\mathcal{G}_{wee2}$

R (bps/Hz)	K (Matrices)	n (bits)
1	4	2
2	16	4
3	64	6
3.5	128	7
4	256	8
4.5	512	9

efficiencies are presented in Table 2.3. The matrix selection algorithm is as follows:

1. The first matrix M_1 of the group $\mathcal{P}$, which is in fact the identity matrix I_M (here $M = 2$), is inserted into the set $\mathcal{S}$ as a reference ($S_1 = M_1$) where $S_1 \in \mathcal{S}$. $\mathcal{S}$ is of size K which is determined by the desired spectral efficiency.
2. The distance $D(M_1, M_i)$ is computed for all matrices $M_i \in \mathcal{P} \backslash \mathcal{S}$, then $D_{max} = maxD(M_1, M_i)$. S_2 is inserted in $\mathcal{S}$ as the matrix with $D(M_1, M_i) = D_{max}$. If multiple matrices M_i have the same maximum distance D_{max} with M_1, then we choose one randomly to be inserted in $\mathcal{S}$ as S_2.
3. For each non selected matrix $M_i \in \mathcal{P}$ the vector $D_{M_i} = [D(M_i, S_1) \dots D(M_i, S_k)]$ is calculated, where k is the number of already selected matrices for the set $\mathcal{S}$.
4. The values of vector D_{M_i} are sorted in ascending order.
5. We retain the vectors D_{M_i} which have the maximum minimum value. If only one vector D_{M_i} is retained, then M_i is added to $\mathcal{S}$. If several vectors D_{M_i} are retained, then the second values of the retained vectors are compared and those having the largest second value are retained. If only one vector D_{M_i} is retained, then M_i is added to $\mathcal{S}$. If several vectors D_{M_i} are retained, then the third values of the retained vectors are compared. This can continue to the last values of the vectors D_{M_i}. If in the end all the values of the vectors D_{M_i}

are identical, we choose a random one. Finally, a new vector M_i is added to $\mathcal{S}$.

6. Steps 3-5 are iterated to obtain the set $\mathcal{S}$ having K matrices selected from the group $\mathcal{P}$.

The goals of the proposed extensions are listed as follows:

— Increasing the maximum spectral efficiency achievable through the expansion of the candidate group.

— Enlarging the search scope for the optimal matrices selected for a given spectral efficiency.

This information matrices selection algorithm's performance is analyzed for $\mathcal{G}_{w2}$, $\mathcal{G}_{we2}$, and $\mathcal{G}_{wee2}$ for different spectral efficiencies. The sets selected for different cases are summarized in table 2.4.

Table 2.4 – Sets produced by the selection algorithm

Spectral efficiency (bps/Hz) Group	1	2	3	3.5	4	4.5
$\mathcal{G}_{w2}$	$\mathcal{S}1_A$	$\mathcal{S}2_A$	$\mathcal{S}3_A$	$\mathcal{S}3.5_A$	-	-
$\mathcal{G}_{we2}$	$\mathcal{S}1_A$	$\mathcal{S}2_A$	$\mathcal{S}3_B$	$\mathcal{S}3.5_B$	$\mathcal{S}4_A$	-
$\mathcal{G}_{wee2}$	$\mathcal{S}1_A$	$\mathcal{S}2_A$	$\mathcal{S}3_B$	$\mathcal{S}3.5_B$	$\mathcal{S}4_A$	$\mathcal{S}4.5_A$

For the spectral efficiencies 3 bps/Hz and 3.5 bps/Hz, the selection algorithm produces different sets, $\mathcal{S}3_A$ and $\mathcal{S}3.5_A$ for $\mathcal{G}_{w2}$, then $\mathcal{S}3_B$ and $\mathcal{S}3.5_B$ for $\mathcal{G}_{we2}$ and $\mathcal{G}_{wee2}$. This result leads to the assumption that the newly generated groups $\mathcal{G}_{we2}$ and $\mathcal{G}_{wee2}$ offer better spaced matrices than the ones in $\mathcal{G}_{w2}$ for the mentioned spectral efficiencies. In order to verify this, we study the distance spectrum and error performance of the mentioned sets.

2.4.1.1 3 bps/Hz case

When comparing the distance values between the selected matrices between $\mathcal{G}_{w2}$ and $\mathcal{G}_{we2}$ (or $\mathcal{G}_{wee2}$ since the selected matrices are the same) in table 2.4.1.1 and the histograms in 2.8, it is found that the $\mathcal{G}_{w2}$ set presents the smallest distance of

1.0824 which has an occurrence percentage of 1.58%. On the other hand, the set for $\mathcal{G}_{we2}$ does not present the value 1.0824 and has the lowest distance of 1.1777 with an occurrence rate of 3.17%. Since the smallest distances between the matrices play the largest role in the error performance of the system, this leads to the conclusion that for the same spectral efficiency of 3.5 bps/Hz, the set of selected matrices for $\mathcal{G}_{we2}$ should perform better than the set of $\mathcal{G}_{w2}$. This is verified when reviewing the BER performance of these two cases in Fig. 2.9 (simulation environment is described in section 2.5). Indeed, in the high SNR region, the smallest distance affects the error performance the most, where the set of $\mathcal{G}_{we2}$ outperforms that of $\mathcal{G}_{w2}$ starting 15 dB, to reach a difference of 2×10^{-5} for 26 dB. The difference in performance is explained by the fact that we search for 64 matrices (required to achieve 3 bps/Hz spectral efficiency) among 192 in $\mathcal{G}_{w2}$, whereas for $\mathcal{G}_{wee2}$ we enlarge the search scope to 768 matrices, which allows the search algorithm to select better spaced matrices.

2.4.1.2 3.5 bps/Hz case

The same analysis as in section 2.4.1.1 is conducted for the sets of $\mathcal{G}_{w2}$ and $\mathcal{G}_{we2}$ for the 3.5 bps/Hz case. The histograms in Fig. 2.10 and table 2.4.1.2 show that the smallest distance in the $\mathcal{G}_{w2}$ set is equal to 1.0824 and constitutes 3.54% of the distance values, in contrast to only 0.78% of the distances of $\mathcal{G}_{we2}$. When comparing

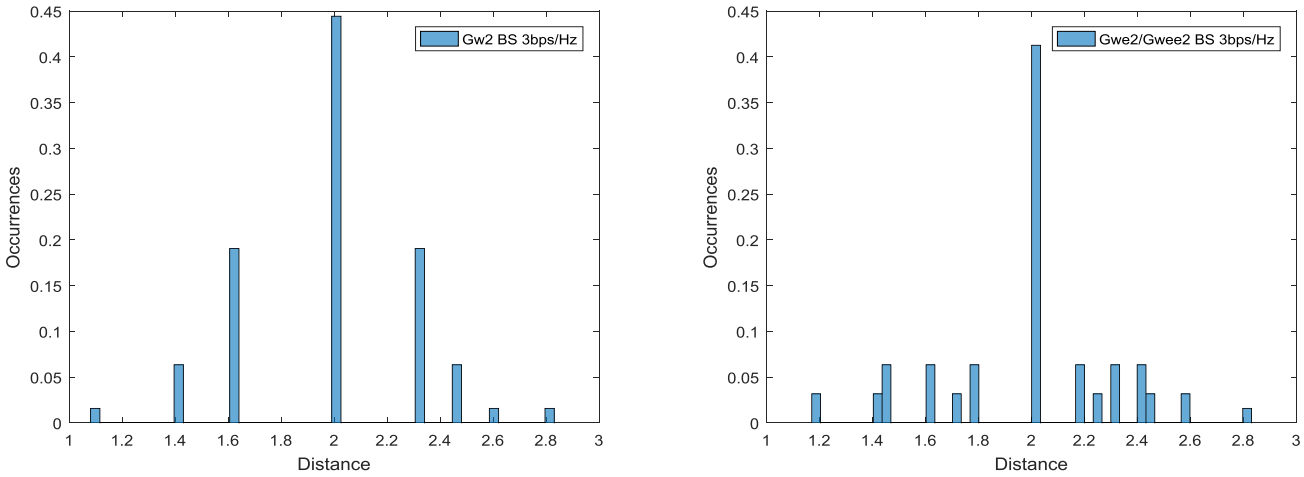

Figure 2.8 – Distance spectra of the sets selected for 3 bps/Hz in the case of $\mathcal{G}_{w2}$ and $\mathcal{G}_{we2}$ or $\mathcal{G}_{wee2}$

Table 2.5 – Distance analysis of selected sets for 3 bps/Hz in $\mathcal{G}_{w2}$,$\mathcal{G}_{we2}$ and $\mathcal{G}_{wee2}$

R=3 bps/Hz	$\mathcal{G}_{w2}$		$\mathcal{G}_{we2}$ or $\mathcal{G}_{wee2}$	
Distance Value	Occurrences amount	Occurrence percentage (%)	Occurrences amount	Occurrence percentage (%)
1.0824	64	1.58	-	-
1.1777	-	-	128	3.17
1.4142	256	6.34	128	3.17
1.4671	-	-	256	6.34
1.608	768	19.04	256	6.34
1.7081	-	-	128	3.17
1.7985	-	-	256	6.34
2	1792	44.44	1664	41.26
2.183	-	-	256	6.34
2.2544	-	-	128	3.17
2.3268	768	19.04	256	6.34
2.4182	-	-	256	6.34
2.4495	256	6.349	128	3.17
2.5716	-	-	128	3.17
2.6131	64	1.58	-	-
2.8284	64	1.58	64	1.58

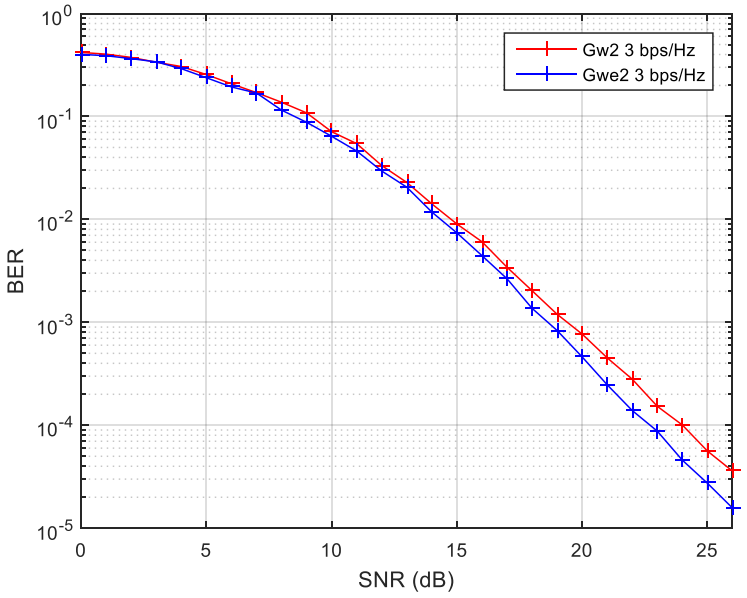

Figure 2.9 – Performance of the selected sets of matrices for $\mathcal{G}_{w2}$ and $\mathcal{G}_{we2}$ (or $\mathcal{G}_{wee2}$) for 3 bps/Hz

the performance of the selected matrices from $\mathcal{G}_{w2}$ versus the ones selected from $\mathcal{G}_{we2}$ for a DSTM MIMO system employing 2 transmit antennas and the same spectral efficiency of 3.5 bps/Hz, it is evident from Fig. 2.11 that the matrices selected from the extended group perform better for high SNR values (above 15 dB). This performance analysis proves the importance of the selection algorithm employed in the selection of the best information matrices to use.

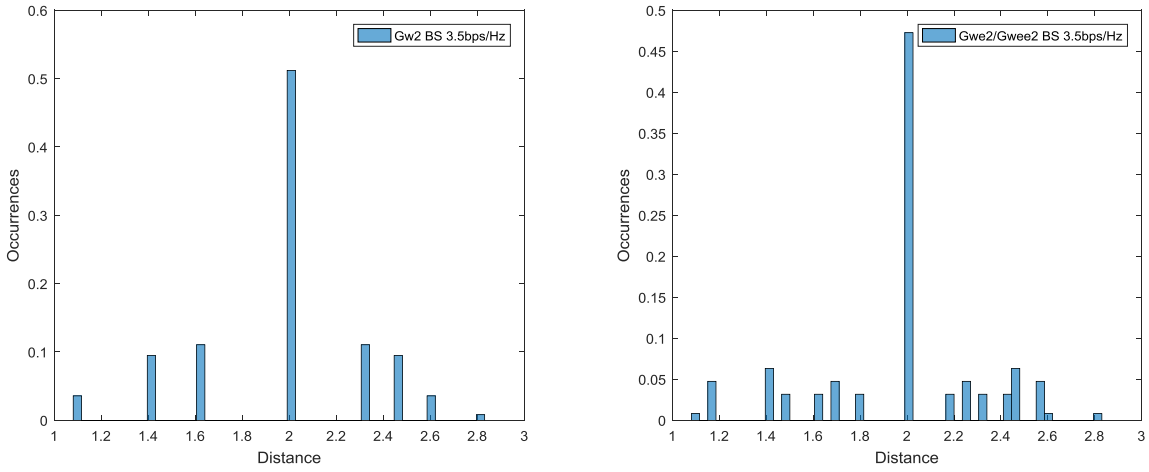

Figure 2.10 – Distance spectra of the sets selected for 3.5 bps/Hz in the case of $\mathcal{G}_{w2}$ and $\mathcal{G}_{we2}$ or $\mathcal{G}_{wee2}$

2.4.2 Optimal mapping rule

With the aim of further enhancing the error performance, it is crucial to adopt a mapping strategy between the information matrices $V_{i_\tau} \in \mathcal{S}$ and the binary vectors. For a given spectral efficiency, the matrices in the set $\mathcal{S}$ that are the farthest from each other in distance, are again sorted so that they are closest in distance. Thereafter, the strategy adopted is based on mapping these matrices which are the closest in distance to the binary vectors having the smallest Hamming distance. Because the closest matrices are the most prone to error, the error occurring would not be as critical. If multiple binary vectors have the same Hamming distance, one is assigned randomly to the corresponding matrix.

Table 2.6 – Distance analysis of selected sets for 3.5 bps/Hz in $\mathcal{G}_{w2}$,$\mathcal{G}_{we2}$ and $\mathcal{G}_{wee2}$

R=3.5 bps/Hz	$\mathcal{G}_{w2}$		$\mathcal{G}_{we2}$ or $\mathcal{G}_{wee2}$	
Distance Value	Occurrences amount	Occurrence percentage (%)	Occurrences amount	Occurrence percentage (%)
1.0824	576	3.54	128	0.78
1.1777	-	-	768	4.72
1.4142	1536	9.44	1024	6.29
1.4671	-	-	512	3.14
1.608	1792	11.02	512	3.14
1.7081	-	-	768	4.72
1.7985	-	-	512	3.14
2	8320	51.18	7680	47.24
2.183	-	-	512	3.14
2.2544	-	-	768	4.72
2.3268	1792	11.02	512	3.14
2.4182	-	-	512	3.14
2.4495	1536	9.44	1024	6.29
2.5716	-	-	768	4.72
2.6131	576	3.54	128	0.78
2.8284	128	0.78	128	0.78

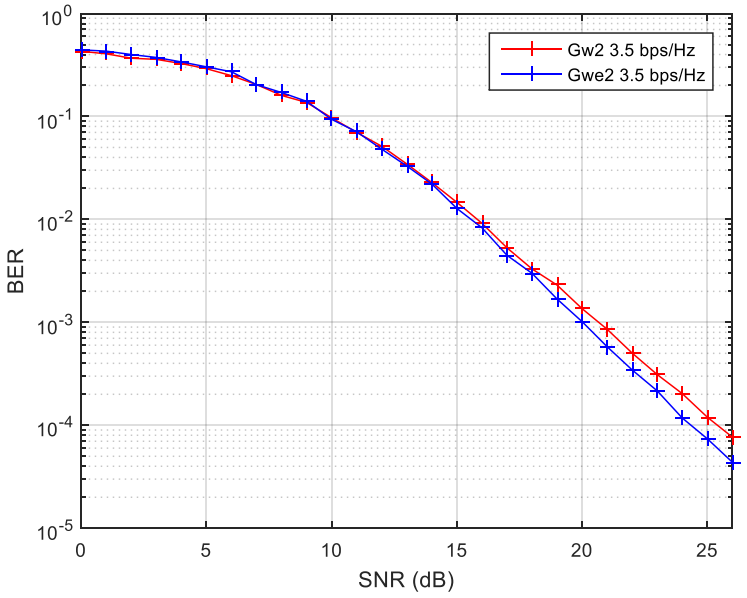

Figure 2.11 – Performance of the selected sets of matrices for $\mathcal{G}_{w2}$ and $\mathcal{G}_{we2}$ (or $\mathcal{G}_{wee2}$) for 3.5 bps/Hz

2.5 Performance of DSTM MIMO system using 2 transmit antennas

In this section we present the performance results of the DSTM MIMO systems for 2 transmit antennas employing the double extension of the Weyl group ($\mathcal{G}_{wee2}$) since according to table 2.4, $\mathcal{G}_{wee2}$ selected matrices are similar to those of $\mathcal{G}_{we2}$ for all spectral efficiencies, and different than that of $\mathcal{G}_{w2}$ for 3 and 3.5 bps/Hz.

2.5.1 Simulation environment

The information matrices are transmitted through a Rayleigh channel characterized by the H channel matrix of dimension 2×2. The elements of the channel matrix are independent complex random variables whose real and imaginary parts are Gaussian random variables of mean zero and variance $\sigma^2 = \frac{1}{2}$. The variance of the noise is inversely proportional to the SNR value by (1.13).
Each received matrix is disturbed by a noise matrix whose elements are also complex. Their real and imaginary parts are also Gaussian random variables, with zero mean and standard deviation which is determined according to the SNR. In addition, constraints are put on the number of errors encountered (1000 error bits) for simulation for a given SNR value that will impose a quality of the results of BER.

We consider that the channel matrix remains constant during the transmission of $L = \frac{T_c}{T_s} = 100$ symbols, thus 50 matrices. Then another random draw is performed to have another channel matrix.

2.5.2 Simulation results

The BER versus SNR of the DSTM MIMO system employing $M = 2$ transmit antennas and $N = 2$ receive antennas for the spectral efficiencies 1, 2, 3, 4, 4.5 bps/Hz and using $\mathcal{G}_{wee2}$ is presented in Fig. 2.12 where for a fixed value of SNR, the stop condition is encountering 10000 errors before continuing to the next SNR value. As expected, when the spectral efficiency increases, more matrices are employed that are closer in distance, thus increasing the error rate of the DSTM system. For

instance, the 1 bps/Hz systems attains BER=10^{-5} at 25 dB, whereas the 4.5 bps/Hz systems attains it for SNR higher than 30 dB.

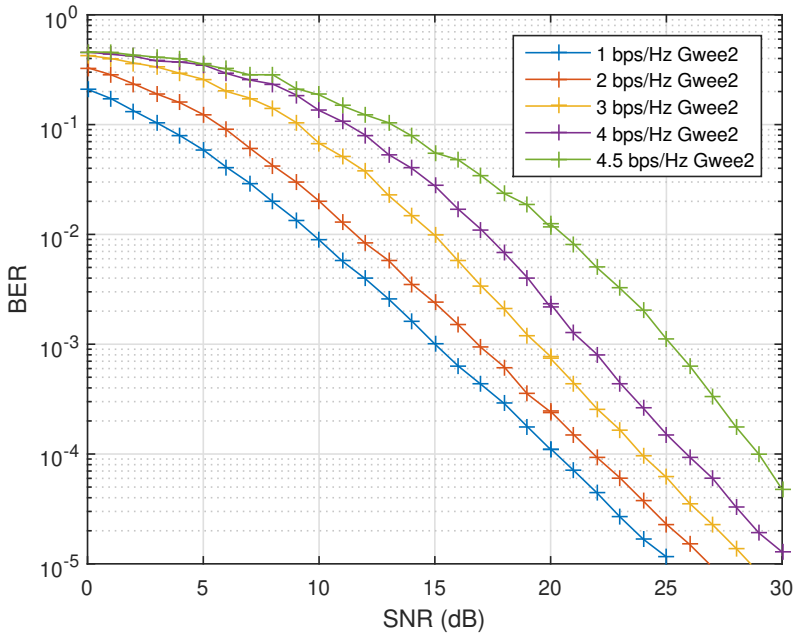

Figure 2.12 – BER performance of DSTM MIMO 2×2 system for different spectral efficiencies

2.6 Conclusion

In this chapter, we propose DSTM MIMO schemes for 2 transmit antennas based on the extensions of the multiplicative Weyl group of unitary matrices with the aim of increasing the maximum spectral efficiency. In addition, we thoroughly study the distance spectrum of the proposed groups and introduce a new matrix selection algorithm and adopt an optimal mapping strategy between binary information vectors and selected matrices to improve the error performance of the overall system. Simulation results illustrate the two main advantages of the use of this new double extension of the Weyl group for DSTM schemes. First, it enlarges the search scope of the matrices, allowing better results for a given spectral efficiency. Secondly, the extensions performed increase the maximum achievable spectral efficiency by the Weyl group.

Chapter 3

DSTM Scheme Employing 4 and 8 Transmit Antennas

In this chapter, we expand the DSTM MIMO system from 2 transmit antennas to 4 and 8 transmit antennas through the use of the Kronecker product on the Weyl group. Furthermore, we apply extensions to the newly generated 4×4 and 8×8 multiplicative groups of unitary matrices with the aim of increasing their maximum achievable spectral efficiencies. The distance spectrum of the generated groups is studied and the information matrices are selected through the selection algorithm conceived in the previous chapter. BER performance results are presented and analyzed.

3.1 DSTM System using 4 Transmit Antennas

In order to expand our DSTM MIMO system to 4 transmit antennas, the Kronecker product operation is applied on $\mathcal{G}_{w2}$.

The Kronecker product is an operation on two matrices of arbitrary size resulting in a matrix of expanded size. More explicitly, if A is an $m \times n$ matrix and B is a $p \times q$ matrix, then the Kronecker product $A \otimes B$ is the $pm \times qn$ block matrix:

$$A \otimes B = \begin{pmatrix} a_{1,1}B & \cdots & a_{1,n}B \\ \vdots & \ddots & \vdots \\ a_{m,1}B & \cdots & a_{m,n}B \end{pmatrix} \tag{3.1}$$

The Kronecker product has the following properties:

1. $A \otimes B$ is invertible if and only if A and B are invertible:

$$(A \otimes B)^{-1} = A^{-1} \otimes B^{-1} \tag{3.2}$$

2. The operation of transposition is distributive over the Kronecker product:

$$(A \otimes B)^T = A^T \otimes B^T \tag{3.3}$$

3. The Kronecker product is linear:

$$A \otimes (\alpha B + \beta C) = \alpha A \otimes B + \beta A \otimes C \tag{3.4}$$

4. The Kronecker product is associative:

$$(A \otimes B) \otimes C = A \otimes (B \otimes C) \tag{3.5}$$

5. The Kronecker product is not commutative:

$$A \otimes B \neq B \otimes A \tag{3.6}$$

In [101], the author attempts to link the distance between two matrices with the Kronecker product and presents the following theorems:

Theorem 3.1. *Consider the complex matrices A, B of size $p \times q$ and M a complex matrix of size $m \times n$. If $\|M\|$ is the Frobenius norm of the matrix M, i.e.,*

$$\|M\| = \sqrt{\sum_{i=1}^{m}\sum_{j=1}^{n} m_{ij}m_{ij}^*}$$

and $D(A, B) = \|A - B\|$, then:

$$D(M \otimes A, M \otimes B) = \|M\|.D(A, B). \tag{3.7}$$

Proof:

$$\begin{aligned} D(M \otimes A, M \otimes B) &= \|M \otimes A - M \otimes B\| = \|M \otimes (A - B)\| \\ &= \sqrt{\sum_{ij}\sum_{kl}[m_{ij}(a_{kl} - b_{kl})][m_{ij}(a_{kl} - b_{kl})]^*} \\ &= \sqrt{\sum_{ij} m_{ij}m_{ij}^* \sum_{kl}[(a_{kl} - b_{kl})][(a_{kl} - b_{kl})]^*} \\ &= \|M\|.\|A - B\| = \|M\|.D(A, B) \end{aligned}$$

Theorem 3.2. *If M is a non-null complex matrix of size $m \times n$ and A, B, C, D are complex matrices of size $p \times q$, then*

$$D(A,B) < D(C,D) \Rightarrow D(M \otimes A, M \otimes B) < D(M \otimes C, M \otimes D) \tag{3.8}$$

Proof:

If $D(A,B) < D(C,D)$ and $\|M\| > 0$, using theorem 3.1, we have:

$$\begin{aligned} D(M \otimes C, M \otimes D) - D(M \otimes A, M \otimes B) &= \|M\|.D(C,D) - \|M\|.D(A,B) \\ &= \|M\|(D(C,D) - D(A,B)) > 0 \end{aligned}$$

3.1.1 Expansion of $\mathcal{G}_{w2}$ to $\mathcal{G}_{w4}$

For a MIMO system using 4 transmit antennas and with the assumption $M = T$ in place, we need to use 4×4 transmission matrices. When the Kronecker product is applied to $\mathcal{G}_{w2}$, a 4×4 group of unitary matrices $\mathcal{G}_{w4} = \mathcal{G}_{w2} \otimes \mathcal{G}_{w2}$ is obtained. The Kronecker product gives $192 \times 192 = 36864$ matrices, among these only 4608 are distinct. Thus, for a MIMO system of 4 transmit antennas, the maximum spectral efficiency is reduced to $R_{max} = \frac{1}{4}\lfloor log_2 4608 \rfloor = 3\, bps/Hz$ using relation (2.7) from chapter 2.

3.1.1.1 Group properties

Similarly to the extension of $\mathcal{G}_{we2}$, it is important that the newly generated set $\mathcal{G}_{w4}$ is a group under the multiplication operation.

Indeed, $\mathcal{G}_{w4}$ also satisfies the group conditions mentioned in section 1.4.2.2:

1. The identity element is indeed in $\mathcal{G}_{w4}$ since:

$$\begin{gathered} I \in \mathcal{G}_{w2},\ \mathcal{G}_{w4} = \mathcal{G}_{w2} \otimes \mathcal{G}_{w2} \\ I_2 \otimes I_2 = \begin{bmatrix} 1 & 0 & 0 & 0 \\ 0 & 1 & 0 & 0 \\ 0 & 0 & 1 & 0 \\ 0 & 0 & 0 & 1 \end{bmatrix} = I_4 \in \mathcal{G}_{w4} \end{gathered} \tag{3.9}$$

2. $\mathcal{G}_{w4}$ is indeed a closed group under multiplication, because if we suppose $M_i, M_j \in \mathcal{G}_{w4}$, then:

$$\begin{aligned} M_i M_j &= (M_a \otimes M_b)(M_c \otimes M_d) \\ &= (M_a M_c) \otimes (M_b M_d) \\ &= M_e \otimes M_f = M_k \in \mathcal{G}_{w4} \end{aligned} \tag{3.10}$$

3. The inverse of any matrix M_i in $\mathcal{G}_{w4}$ is indeed in $\mathcal{G}_{w4}$, since:

$$\begin{aligned} (M_i)^{-1} &= (M_a \otimes M_b)^{-1}, (M_a, M_b) \in \mathcal{G}_{w2} \\ &= M_a^{-1} \otimes M_b^{-1} \\ &= M_c \otimes M_d \\ &= M_j \in \mathcal{G}_{w4} \end{aligned} \tag{3.11}$$

In addition, the matrices in $\mathcal{G}_{w4}$ are unitary. Indeed, since the operation of transposition is distributive over the Kronecker product:

$$(M_a \otimes M_b)^T = M_a^T \otimes M_b^T \tag{3.12}$$

then the matrices in $\mathcal{G}_{w4}$ are unitary, because if we suppose that $M_a, M_b \in \mathcal{G}_{w2}$ and $M_i \in \mathcal{G}_{w4}$, then:

$$\begin{aligned} M_i M_i^T &= (M_a \otimes M_b)(M_a \otimes M_b)^T \\ &= (M_a \otimes M_b)(M_a^T \otimes M_b^T) \\ &= (M_a M_a^T) \otimes (M_b M_b^T) \\ &= I_2 \otimes I_2 = I_4 \end{aligned} \tag{3.13}$$

3.1.1.2 Distance analysis of $\mathcal{G}_{w4}$

The distances occurrences between the matrices of the generated group $\mathcal{G}_{w4}$ are presented in table 3.1 and Fig. 3.1. Indeed, a multiplication of the distances values of the matrices in $\mathcal{G}_{w2}$ is $\sqrt{2}$. The 8 values in table 2.1 multiplied by $\sqrt{2}$ are in table 3.1 amongst other values.

Table 3.1 – Table of distance occurrences between matrices of $\mathcal{G}_{w4}$

Distance	1.5307	2	2.2741	2.4495	2.5663	2.8284	3.0683	3.1623	3.2907	3.4641	3.6955	4
Occurrence percentage (%)	0.30	1.64	4.34	5.55	2.77	70.71	2.77	5.55	4.34	1.64	0.30	0.02

3.2 Simple Extension of $\mathcal{G}_{w4}$

Indeed, this decrease in spectral efficiency becomes more severe with an additional increase of the number of transmission antennas, according to relation (2.7). This is why it becomes important to extend the $\mathcal{G}_{w4}$ group with the aim of increasing the maximum achievable spectral efficiency. We propose to use an extension of $\mathcal{G}_{w4}$ using:

$$\mathcal{G}_{we4} = \mathcal{G}_{w4} \cup \mathcal{G}_{w4} e^{\frac{j\pi}{8}} \tag{3.14}$$

which produces $4608 \times 2 = 9216$ distinct matrices. $\mathcal{G}_{we4}$ is able to upgrade the maximum spectral efficiency to 3.25 bps/Hz compared to the maximum spectral efficiency of 3 bps/Hz for $\mathcal{G}_{w4}$.

3.2.1 Group properties and optimal rotation of $\mathcal{G}_{we4}$

Following the same analysis conducted in chapter 2 section 2.3.1.2, we conclude that $\mathcal{G}_{we4}$ satisfies the group conditions:

1. The identity element is indeed in $\mathcal{G}_{we4}$ since:

$$I \in \mathcal{G}_{w4},\ \mathcal{G}_{we4} = \mathcal{G}_{w4} \cup \mathcal{G}_{w4} e^{\frac{j\pi}{8}} \tag{3.15}$$

2. $\mathcal{G}_{we4}$ is indeed a closed group under multiplication:
   — The multiplication of two matrices $M_a, M_b \in \mathcal{G}_{w4}$:

$$M_a M_b \in \mathcal{G}_{w4} \implies M_a M_b \in \mathcal{G}_{we4} \tag{3.16}$$

   — The multiplication of a matrix $M_a \in \mathcal{G}_{w4}$ with a matrix $M_i \in \mathcal{G}_{w4} e^{\frac{j\pi}{8}}$:

$$M_a M_i = M_a (M_b e^{\frac{j\pi}{8}}) = (M_a M_b) e^{\frac{j\pi}{8}} = M_c e^{\frac{j\pi}{8}} = M_j \in \mathcal{G}_{we4} \tag{3.17}$$

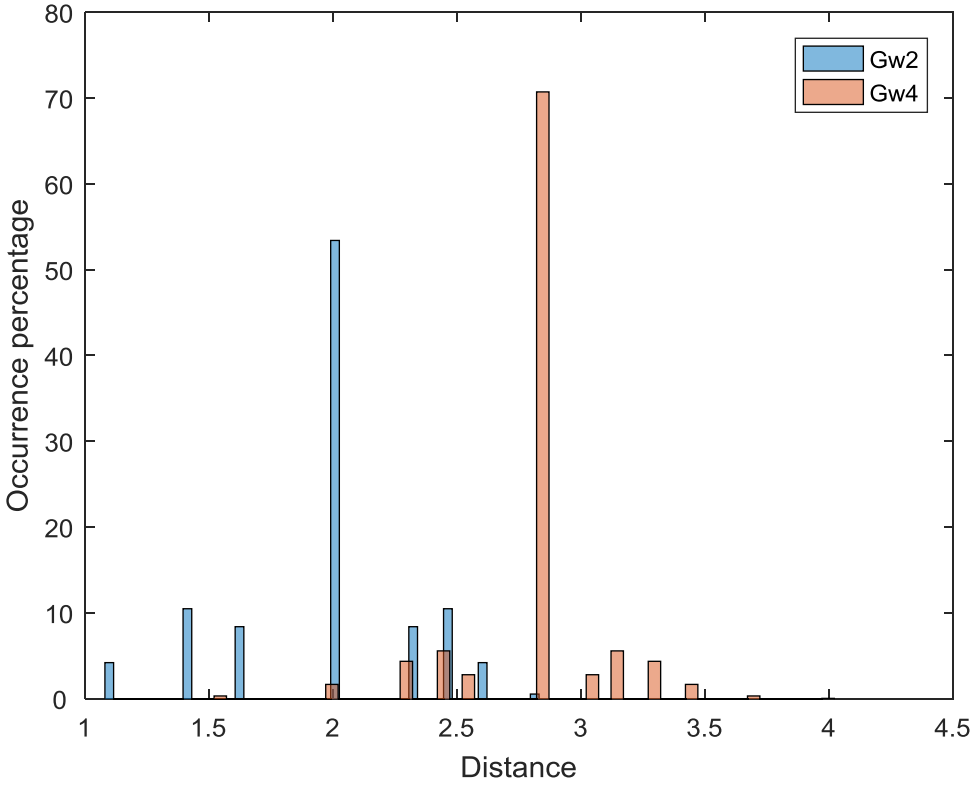

Figure 3.1 – Distance spectra of $\mathcal{G}_{w4}$ and $\mathcal{G}_{w2}$

— The multiplication of two matrices $M_i, M_j \in \mathcal{G}_{w4}e^{\frac{j\pi}{8}}$:

$$\begin{aligned} M_i M_j &= (M_a e^{\frac{j\pi}{8}})(M_b e^{\frac{j\pi}{8}}) \\ &= (M_a M_b)(e^{\frac{j\pi}{8}} e^{\frac{j\pi}{8}}) \\ &= M_c e^{\frac{j\pi}{4}} = M_d \in \mathcal{G}_{w4} \end{aligned} \tag{3.18}$$

3. The inverse of any matrix $M_i \in \mathcal{G}_{w4}e^{\frac{j\pi}{8}}$:

$$\begin{aligned} {M_i}^{-1} &= \{M_a e^{\frac{j\pi}{8}}\}^{-1} \\ &= {M_a}^{-1} e^{\frac{-j\pi}{8}} \\ &= M_b e^{\frac{15j\pi}{8}} \\ &= M_j \in \mathcal{G}_{we4} \end{aligned} \tag{3.19}$$

4. The product of the matrices of $\mathcal{G}_{we4}$ is an associative operation which is a

general property of square matrices.

In addition, the matrices belonging to $\mathcal{G}_{we4}$ are unitary since:

$$\begin{aligned} M_i M_i^H &= (M_a e^{\frac{j\pi}{8}})(M_a e^{\frac{j\pi}{8}})^H \\ &= M_a M_a^H e^{\frac{j\pi}{4}} = I e^{\frac{j\pi}{4}} \end{aligned} \tag{3.20}$$

which is a multiple of the identity matrix. And in the case that M_i is in $\mathcal{G}_{w4}$, since it is a group, then the inverse of M_i exists in $\mathcal{G}_{w4}$ thus in $\mathcal{G}_{we4}$

3.2.2 Optimal rotation

Furthermore, this extension also represents an optimal rotation of $\mathcal{G}_{w4}$, since:

$$\begin{aligned} \mathcal{G}_{w4} &= \mathcal{G}_{w2} \otimes \mathcal{G}_{w2} \\ &= \bigcup_{k=0}^{7} e^{\frac{jk\pi}{4}} (Q \otimes Q) \end{aligned} \tag{3.21}$$

and

$$\begin{aligned} \mathcal{G}_{we4} &= \mathcal{G}_{w4} \cup \mathcal{G}_{w4} e^{\frac{j\pi}{8}} \\ &= \bigcup_{k=0}^{7} e^{\frac{jk\pi}{4}} (Q \otimes Q) \cup \left\{ \bigcup_{k=0}^{7} e^{\frac{jk\pi}{4}} (Q \otimes Q) \right\} e^{\frac{j\pi}{8}} \\ &= \left\{ \bigcup_{k=0}^{7} e^{\frac{jk\pi}{4}} (Q \otimes Q) \right\} \cup \left\{ \bigcup_{l} e^{\frac{jl\pi}{8}} (Q \otimes Q),\ l = 1,3,5,7,9,11,13,15 \right\} \\ &= \mathcal{G}_{w4} \cup \left\{ \bigcup_{l} e^{\frac{jl\pi}{8}} (Q \otimes Q),\ l = 1,3,5,7,9,11,13,15 \right\} \end{aligned} \tag{3.22}$$

which means that the newly generated matrices have elements that are inserted within an equal footing of the already existing matrices elements. This is evidently performed in the generation of $\mathcal{G}_{we4}$, where the elements of the matrices newly added belong to a $16PSK$ constellation thus of equal footing to the already existing elements belonging to $8PSK$.

The distance occurrences in $\mathcal{G}_{we4}$ are presented in Table 3.2, and show compared to the distances between the matrices of $\mathcal{G}_{w4}$, we have more distances, because we add the distances between a matrix of $\mathcal{G}_{w4}$ and a matrix of $\mathcal{G}_{w4} e^{(i\pi/8)}$.

Table 3.2 – Table of distance occurrences between matrices of $\mathcal{G}_{we4}$

Distance	Occurrence (%)
0.7804	0.02
1.5307	0.15
1.6655	0.26
2	0.82
2.0747	1.12
2.2223	0.02
2.2741	2.17
2.321	2.08
2.4156	0.26
2.4495	2.77
2.4804	1.38
2.5435	1.12
2.5663	1.38
2.6301	2.08
2.6897	1.38
2.8284	65.82
2.9606	1.38
3.0137	2.08
3.0683	1.38
3.0872	1.12
3.1381	1.38
3.1623	2.77
3.1882	0.26
3.2578	2.08
3.2907	2.17
3.3259	0.02
3.4199	1.12
3.4641	0.82
3.6368	0.26
3.6955	0.15
3.9231	0.02
4	0.01

3.3 Double Extension of $\mathcal{G}_{w4}$

Attempting to further increase the achievable spectral efficiency, we apply the double extension through:

$$\mathcal{G}_{wee4} = \mathcal{G}_{we4} \cup \mathcal{G}_{we4} e^{\frac{j\pi}{16}} \tag{3.23}$$

generating $9216 \times 2 = 18438$ distinct matrices which upgrades the achievable maximum spectral efficiency to 3.5 bps/Hz. Indeed, following previous analysis from 3.2.1 and 3.2.2, $\mathcal{G}_{wee4}$ forms a group of unitary matrices under the multiplication operation, and is obtained by an optimal rotation of $\mathcal{G}_{we4}$.

The distance spectrum of the newly generated matrices of $\mathcal{G}_{wee4}$ is presented in Table 3.3. And the proposed groups and their achievable spectral efficiencies for the DSTM system employing 4 transmit antennas are summarized in Table 3.4.

3.4 Error Performance of 4 Transmit Antennas DSTM System

3.4.1 Near-Optimal Matrix Selection Algorithm and Optimal Mapping

As in the case of the 2 transmit antennas system, the matrices from the generated groups are selected following a design criterion of maximizing the distances amongst the selected matrices along with an optimal mapping strategy between binary vectors and information matrices as in section 2.4.

When the information matrices selection algorithm is applied on $\mathcal{G}_{w4}$, $\mathcal{G}_{we4}$ and $\mathcal{G}_{wee4}$, the sets produced are summarized in table 3.5.

For the spectral efficiency 3 bps/Hz, the selection algorithm produces different sets, $\mathcal{S}3_A$ for $\mathcal{G}_{w4}$, then $\mathcal{S}3_B$ for $\mathcal{G}_{we4}$ and $\mathcal{G}_{wee4}$. The distance spectrum and error performance of the mentioned sets are studied.

Table 3.3 – Table of distance occurrences between matrices of $\mathcal{G}_{wee4}$

Distance	Occurrence (%)	Distance	Occurrence (%)
0.3921	0.01	2.9606	0.69
0.7804	0.01	2.9632	0.56
1.1611	0.01	3.0137	1.04
1.5307	0.07	3.0172	0.13
1.5658	0.13	3.0185	0.69
1.6655	0.13	3.0683	0.69
1.8156	0.13	3.0872	0.56
1.8856	0.01	3.092	0.01
2	0.41	3.0938	1.04
2.0191	0.56	3.1085	0.69
2.0747	0.56	3.1381	0.69
2.162	0.56	3.1562	0.69
2.2039	0.13	3.1623	1.38
2.2223	0.01	3.1882	0.13
2.2741	1.08	3.1972	0.56
2.286	1.04	3.2174	1.04
2.321	1.04	3.2578	1.04
2.3766	1.04	3.2824	1.04
2.4037	0.56	3.2907	1.08
2.4156	0.13	3.3259	0.01
2.4495	1.38	3.3381	0.13
2.4573	0.69	3.3654	0.56
2.4804	0.69	3.4199	0.56
2.5174	0.69	3.453	0.56
2.5355	1.04	3.4641	0.41
2.5376	0.01	3.5277	0.01
2.5435	0.56	3.5642	0.13
2.5663	0.69	3.6368	0.13
2.6247	0.69	3.6808	0.13
2.6261	0.13	3.6955	0.07
2.6301	1.04	3.8278	0.01
2.6869	0.56	3.9231	0.01
2.6897	0.69	3.9807	0.01
2.7291	1.04	4	0.005
2.7586	0.69	-	-
2.8284	63.38	-	-
2.8966	0.69	-	-
2.9243	1.04	-	-

Table 3.4 – Parameters of $\mathcal{G}_{w4}$, $\mathcal{G}_{we4}$ and $\mathcal{G}_{wee4}$

$\mathcal{G}_{w4}$		$\mathcal{G}_{we4}$		$\mathcal{G}_{wee4}$	
4608 distinct matrices		9216 distinct matrices		18432 distinct matrices	
Spectral efficiency (bps/Hz)	Number of selected matrices	Spectral efficiency (bps/Hz)	Number of selected matrices	Spectral efficiency (bps/Hz)	Number of selected matrices
2	256	2	256	2	256
2.5	1024	2.5	1024	2.5	1024
3	4096	3	4096	3	4096
-	-	3.25	8192	3.25	8192
-	-	-	-	3.5	16384

Table 3.5 – Sets produced by the selection algorithm

Spectral efficiency (bps/Hz) Group	2	3	3.25	3.5
$\mathcal{G}_{w4}$	$\mathcal{S}2_A$	$\mathcal{S}3_A$	-	-
$\mathcal{G}_{we4}$	$\mathcal{S}2_A$	$\mathcal{S}3_B$	$\mathcal{S}3.25_A$	-
$\mathcal{G}_{wee4}$	$\mathcal{S}2_A$	$\mathcal{S}3_B$	$\mathcal{S}3.25_A$	$\mathcal{S}3.5_A$

3.4.2 3 bps/Hz case

When comparing the distance values between the selected matrices between $\mathcal{G}_{w4}$ and $\mathcal{G}_{we4}$ (or $\mathcal{G}_{wee2}$ since the selected matrices are similar) in table 3.4.2, we find that the distance values are fairly close to each other (shown also in histograms of Fig. 3.2), even for the lowest distance present (1.53 and 1.56). This leads to the conclusion that the performance of these two sets should be similar to an extent. This is verified when comparing the performances of these two sets in Fig. 3.3.

Table 3.6 – Distance values for the selected matrices of $\mathcal{G}_{w4}$ and $\mathcal{G}_{wee4}$ for 3 bps/Hz spectral efficiency

	Occurrence Percentage			Occurrence Percentage	
Distance	$\mathcal{G}_{w4}$	$\mathcal{G}_{wee4}$	Distance	$\mathcal{G}_{w4}$	$\mathcal{G}_{wee4}$
1.5307	0.321	0.072688	2.8966		0.607448
1.5658		0.157204	2.9243		1.137057
1.6655		0.146329	2.9606		0.732601
1.8156		0.156441	2.9632		0.517399
2	1.679	0.369734	3.0137		0.836386
2.0191		0.517399	3.0172		0.157204
2.0747		0.596001	3.0185		0.619658
2.162		0.526557	3.0683	2.735	0.787546
2.2039		0.156441	3.0872		0.596001
2.2741	4.319	1.143162	3.0938		1.134005
2.286		1.137057	3.1085		0.619658
2.321		0.836386	3.1381		0.732601
2.3766		1.134005	3.1562		0.607448
2.4037		0.526557	3.1623	5.470	1.462149
2.4156		0.146329	3.1882		0.146329
2.4495	5.470	1.462149	3.1972		0.526557
2.4573		0.607448	3.2174		1.134005
2.4804		0.732601	3.2578		0.836386
2.5174		0.619658	3.2824		1.137057
2.5355		1.134005	3.2907	4.319	1.143162
2.5435		0.596001	3.3381		0.156441
2.5663	2.735	0.787546	3.3654		0.526557
2.6247		0.619658	3.4199		0.596001
2.6261		0.157204	3.453		0.517399
2.6301		0.836386	3.4641	1.679	0.369734
2.6869		0.517399	3.5642		0.156441
2.6897		0.732601	3.6368		0.146329
2.7291		1.137057	3.6808		0.157204
2.7586		0.607448	3.6955	0.321	0.072688
2.8284	70.93	63.63668	4	0.024	0.02442

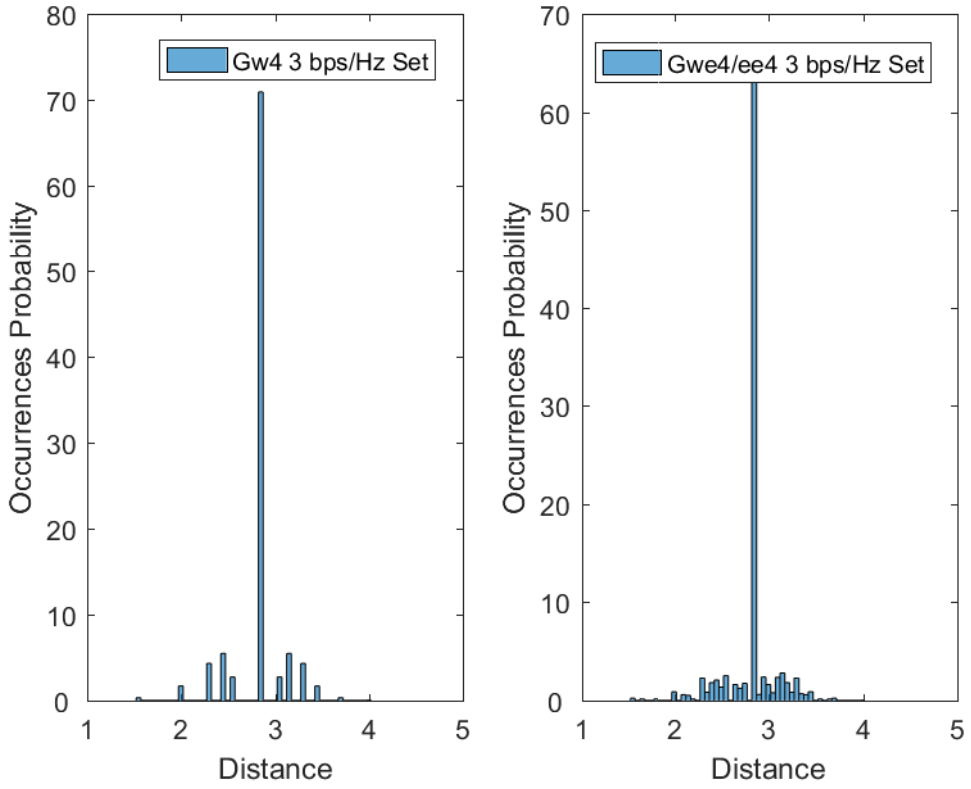

Figure 3.2 – Histograms of the distance values of the selected matrices in $\mathcal{G}_{w4}$ and $\mathcal{G}_{wee4}$

3.4.3 Error Performance

The simulation parameters are similar to the ones used for DSTM schemes with 2 transmit antennas. The information matrices are transmitted through a Rayleigh channel characterized by the H channel matrix of dimension 4×4. The elements of the channel matrix are independent complex random variables whose real and imaginary parts are Gaussian random variables of mean zero and variance $\sigma^2 = \frac{1}{2}$. The transmission of each information matrix is disturbed by the channel matrix and a noise matrix whose elements are also complex. Their real and imaginary parts are also Gaussian random variables, with zero mean and standard deviation which is determined according to the SNR in relation (1.13).

We consider that the channel matrix remains observed during the transmission of $L = \frac{T_c}{T_s} = 100$ symbols, thus 25 matrices. Then another random draw is performed to have another channel matrix. The noise variation is related to the SNR through

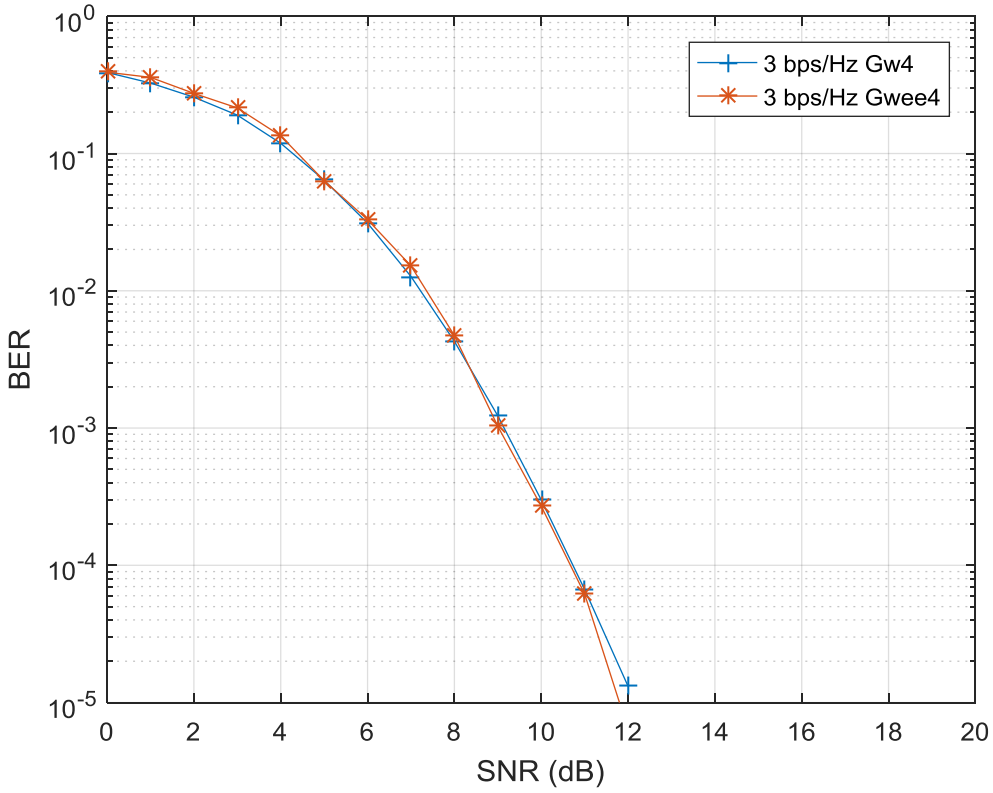

Figure 3.3 – Performance of the two sets of the selected matrices for $\mathcal{G}_{w4}$ and $\mathcal{G}_{we4}$

$\sigma^2 = \frac{1}{SNR}$. The simulation stopping condition is related to reaching 1000 errors before passing to the next SNR.

In Fig. 3.4, the simulation results of the BER for each SNR value are presented for DSTM MIMO systems employing $M = 4$ transmit antennas and $N = 4$ receive antennas using $\mathcal{G}_{wee4}$. To further explain the results in Fig. 3.4, the distance spectra of the lowest distances between the selected matrices for 2, 3, 3.25, 3.5 bps/Hz are presented in Table 3.7. The distance 2.82 appears with an identical frequency of 63% for the 3 systems with spectral efficiencies 3, 3.25 and 3.5 bps/Hz, which explains why these three curves are close for low SNRs ($<$ 8dB). Indeed, in this area, the smallest distances are the most vulnerable to generate error events. The 2.82 distance appears the most for the 2 bps/Hz system but with a lower probability of 43% explaining why its BER curve does not match for low SNR with the systems

with spectral efficiency 3, 3.25 and 3.5 bps/Hz.

In addition, the smallest distances in Table 3.7 explain the error performance of the 3.25 and 3.5 bps/Hz systems for high SNR values. The smallest distance between the matrices selected for 3.5 bps/Hz is 0.3921, which is almost 4 times lower than the smallest distance for the 3 bps/Hz system (1.5307). The same analysis is applied for the 3.25 bps/Hz system where the smallest distance is 0.7804 and 2 times lower than that of the 3 bps/Hz system. As previously mentioned, the smallest distances are the most critical and play the highest role for high SNR values, determining the degradation in the performance of the 3.25 and 3.5 bps/Hz systems.

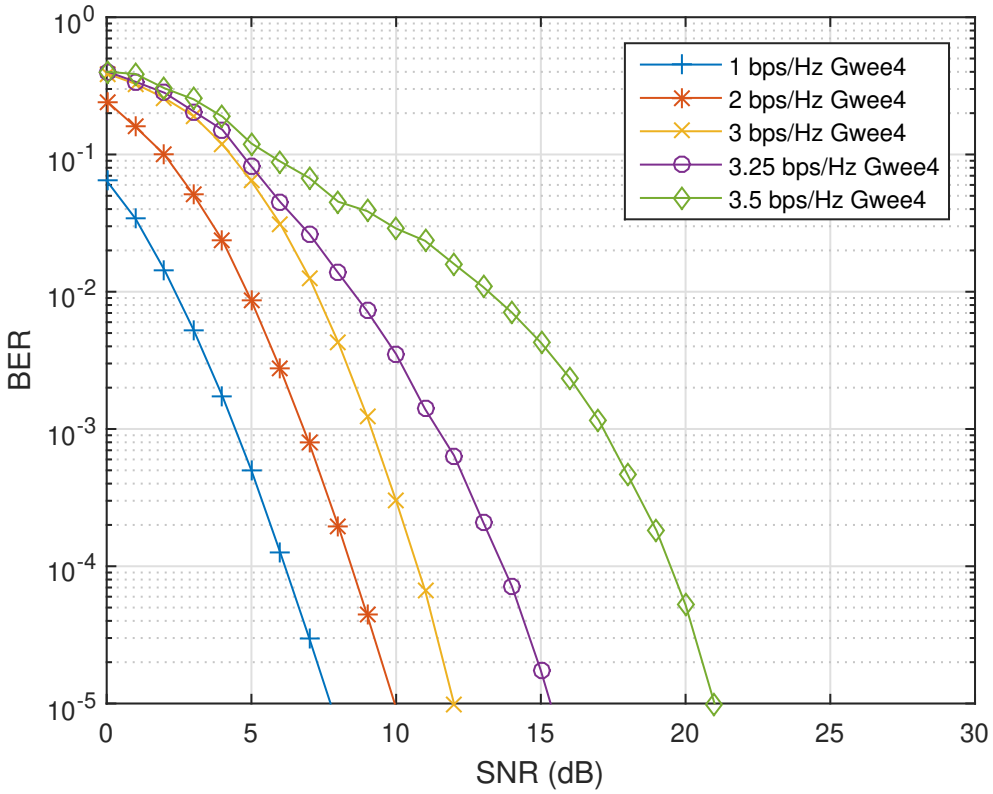

Figure 3.4 – BER performance of DSTM MIMO 4×4 system for different spectral efficiencies

Table 3.7 – Occurrences and distances between selected matrices of $\mathcal{G}_{wee4}$

Spectral efficiency Distance	2(bps/Hz)	3(bps/Hz)	3.25(bps/Hz)	3.5(bps/Hz)
0.3921	-	-	-	0.011%
0.7804	-	-	0.021%	0.011%
1.1611	-	-	0.0%	0.011%
1.5307	-	0.73%	0.080%	0.083%
1.5658	-	0.157%	0.148%	0.128%
1.6655	-	0.146%	0.112%	0.128%
1.8156	-	0.156%	0.148%	0.128%
1.8856	-	-	0.0%	0.011%
2	-	0.370%	0.408%	0.438%
...	...	...	...	...
2.162	1.568%	0.527%	0.539%	0.555%
...	...	...	...	...
2.8284	43.13%	63.63%	63.39%	63.57%

3.4.4 Comparison between the performance of 2 and 4 transmit antenna DSTM systems

When comparing the performances of the 2 transmit antennas system employing $\mathcal{G}_{wee2}$ and the 4 transmit antenna system employing $\mathcal{G}_{wee4}$ in Fig. 3.5, we find a large difference as the 4 transmit antenna system reached BER 10^{-5} for 10 dB whereas the 2 transmit antennas system reaches the same values for 26 dB. This is in fact due to the robustness of the 4 transmit antenna system in the face of channel fading along with the difference in the distances of the matrices employed by both systems as is shown in Fig. 3.6. More explicitly, it is shown that the 4 transmit antenna system has matrices with distances ranging from 2 to 4, whereas the maximum distance between matrices of the 2 transmit antenna system is 2.8.

3.5 DSTM System Using 8 Transmit Antennas

Adopting the same method used to generate the 4×4 unitary matrices, we apply the Kronecker product between the original Weyl group $\mathcal{G}_{w2}$ and $\mathcal{G}_{w4}$ in order to produce 8×8 matrices suitable for MIMO systems employing 8 transmit antennas.

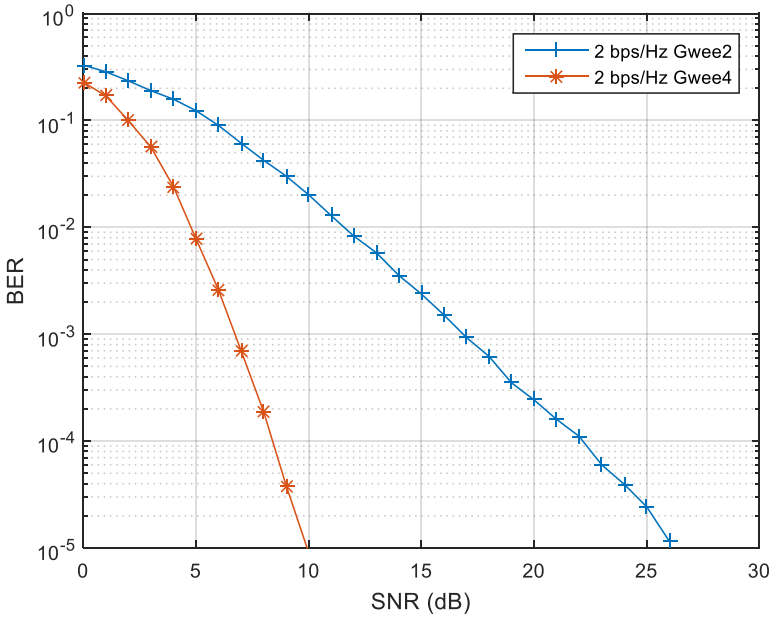

Figure 3.5 – BER performance of DSTM MIMO 2×2 and 4×4 systems for 2 bps/Hz

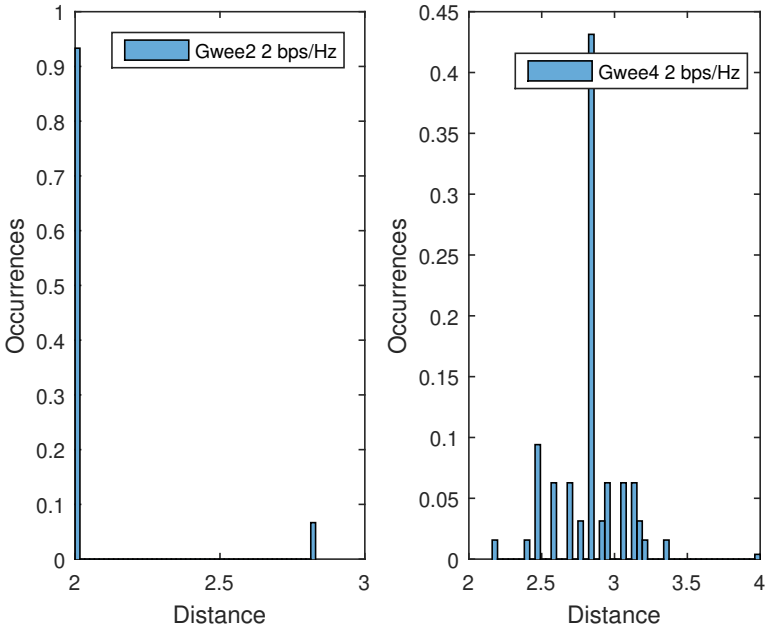

Figure 3.6 – Histogram of distance occurrences for 2 bps/Hz for $\mathcal{G}_{wee2}$ and $\mathcal{G}_{wee4}$

The generated group $\mathcal{G}_{w8} = \mathcal{G}_{w4} \otimes \mathcal{G}_{w2}$ contains 110592 distinct 8×8 matrices having its maximum spectral efficiency further reduced to $R_{max} = \frac{1}{8}\lfloor log_2 110592 \rfloor =$

$2\,bps/Hz$.

3.5.0.1 Group properties

Similarly to the extension of $\mathcal{G}_{w4}$, it is important that the newly generated set $\mathcal{G}_{w8}$ is a group under the multiplication operation.
Indeed, $\mathcal{G}_{w8}$ also satisfies the group conditions mentioned in section 1.4.2.2:

1. The identity element is indeed in $\mathcal{G}_{w8}$ since:

$$\begin{aligned} &I_2 \in \mathcal{G}_{w2},\ I_4 \in \mathcal{G}_{w4},\ \mathcal{G}_{w8} = \mathcal{G}_{w2} \otimes \mathcal{G}_{w4} \\ &I_2 \otimes I_4 = I_8 \in \mathcal{G}_{w8} \end{aligned} \tag{3.24}$$

2. $\mathcal{G}_{w8}$ is indeed a closed group under multiplication, because if we suppose $M_i, M_j \in \mathcal{G}_{w8}$, then:

$$\begin{aligned} M_i M_j &= (M_a \otimes M_b)(M_c \otimes M_d),\ M_a, M_c \in \mathcal{G}_{w2},\ M_b, M_d \in \mathcal{G}_{w4} \\ &= (M_a M_c) \otimes (M_b M_d) \\ &= M_e \otimes M_f = M_k \in \mathcal{G}_{w8} \end{aligned} \tag{3.25}$$

3. The inverse of any matrix $M_i \in \mathcal{G}_{w8}$ is indeed $(M_i)^{-1} = M_j \in \mathcal{G}_{w8}$:

$$\begin{aligned} (M_i)^{-1} &= (M_a \otimes M_b)^{-1} \\ &= M_a^{-1} \otimes M_b^{-1} \\ &= M_c \otimes M_d \\ &= M_j \in \mathcal{G}_{w8} \end{aligned} \tag{3.26}$$

4. The product of the matrices of $\mathcal{G}_{w4}$ is an associative operation which is a general property of square matrices.

In addition, since the operation of transposition is distributive over the Kronecker product:

$$(M_a \otimes M_b)^H = M_a^H \otimes M_b^H \tag{3.27}$$

then the matrices in $\mathcal{G}_{w8}$ are unitary, because if we suppose that $M_a \in \mathcal{G}_{w2}$, $M_b \in \mathcal{G}_{w4}$

and $M_i \in \mathcal{G}_{w8}$, then:

$$\begin{aligned} M_i M_i^T &= (M_a \otimes M_b)(M_a \otimes M_b)^T \\ &= (M_a \otimes M_b)(M_a^T \otimes M_b^T) \\ &= (M_a M_a^T) \otimes (M_b M_b^T) \\ &= I_2 \otimes I_4 = I_8 \end{aligned} \tag{3.28}$$

3.5.1 Simple and Double Extension of $\mathcal{G}_{w8}$

For an 8 transmit antennas system, the maximum spectral efficiency is reduced from 3.5 bps/Hz when employing the group $\mathcal{G}_{w2}$ in 2 transmit antennas systems to 2 bps/Hz. In the aim of resolving the issue of an important decrease in spectral efficiency, and similarly to the extensions performed on the 4 transmit antennas and 2 transmit antennas system, we extend the $\mathcal{G}_{w8}$ through:

$$\mathcal{G}_{we8} = \mathcal{G}_{w8} \cup \mathcal{G}_{w8} e^{\frac{j\pi}{8}} \tag{3.29}$$

then

$$\mathcal{G}_{wee8} = \mathcal{G}_{we8} \cup \mathcal{G}_{we8} e^{\frac{j\pi}{16}} \tag{3.30}$$

allowing an increase to 2.25 bps/Hz for $\mathcal{G}_{wee8}$ using 442368 distinct unitary matrices.

3.5.2 Group properties and optimal rotation of the extensions of $\mathcal{G}_{w8}$

Following the same analysis conducted in chapter 2 section 2.3.1.2, we conclude that $\mathcal{G}_{we8}$ (and consequently $\mathcal{G}_{wee8}$) satisfies the group conditions:

1. The identity element is indeed in $\mathcal{G}_{we8}$ since:

$$I \in \mathcal{G}_{w8},\ \mathcal{G}_{we8} = \mathcal{G}_{w8} \cup \mathcal{G}_{w8} e^{\frac{j\pi}{8}} \tag{3.31}$$

2. $\mathcal{G}_{we8}$ is indeed a closed group under multiplication:
   — The multiplication of two matrices $M_a, M_b \in \mathcal{G}_{w8}$:

$$M_a M_b \in \mathcal{G}_{w8} \implies M_a M_b \in \mathcal{G}_{we8} \tag{3.32}$$

— The multiplication of a matrix $M_a \in \mathcal{G}_{w8}$ with a matrix $M_i \in \mathcal{G}_{w8}e^{\frac{j\pi}{8}}$:

$$M_aM_i = M_a(M_be^{\frac{j\pi}{8}}) = (M_aM_b)e^{\frac{j\pi}{8}} = M_ce^{\frac{j\pi}{8}} = M_j \in \mathcal{G}_{we8} \tag{3.33}$$

— The multiplication of two matrices $M_i, M_j \in \mathcal{G}_{w8}e^{\frac{j\pi}{8}}$:

$$\begin{aligned} M_iM_j &= (M_ae^{\frac{j\pi}{8}})(M_be^{\frac{j\pi}{8}}) \\ &= (M_aM_b)(e^{\frac{j\pi}{8}}e^{\frac{j\pi}{8}}) \\ &= M_ce^{\frac{j\pi}{4}} = M_d \in \mathcal{G}_{w8} \end{aligned} \tag{3.34}$$

3. The inverse of any matrix $M_i \in \mathcal{G}_{w8}e^{\frac{j\pi}{8}}$:

$$\begin{aligned} {M_i}^{-1} &= \{M_ae^{\frac{j\pi}{8}}\}^{-1},\ M_a \in \mathcal{G}_{w8} \\ &= {M_a}^{-1}e^{\frac{-j\pi}{8}} \\ &= M_be^{\frac{15j\pi}{8}} \\ &= M_j \in \mathcal{G}_{we8} \end{aligned} \tag{3.35}$$

4. The product of the matrices of $\mathcal{G}_{we8}$ is an associative operation which is a general property of square matrices.

In addition, the matrices belonging to $\mathcal{G}_{we8}$ are unitary since:

$$\begin{aligned} M_iM_i^H &= (M_ae^{\frac{j\pi}{8}})(M_ae^{\frac{j\pi}{8}})^H \\ &= M_aM_a^He^{\frac{j\pi}{4}} = Ie^{\frac{j\pi}{4}} \end{aligned} \tag{3.36}$$

which is a multiple of the identity matrix.

In a similar way that $\mathcal{G}_{we4}$ is an optimal rotation of $\mathcal{G}_{w4}$, $\mathcal{G}_{we8}$ is also an optimal rotation, which means that the newly generated matrices have elements that are inserted within an equal footing of the already existing matrices elements. The elements of the matrices newly added belong to a $16PSK$ constellation thus of equal footing to the already existing elements belonging to $8PSK$. This analysis is extended to $\mathcal{G}_{wee8}$ in a straightforward manner as in previous sections.

Table 3.8 summarizes the achievable spectral efficiencies of the proposed groups for 8 transmit antennas.

Table 3.8 – Parameters of $\mathcal{G}_{w8}$, $\mathcal{G}_{we8}$ and $\mathcal{G}_{wee8}$

$\mathcal{G}_{w8}$		$\mathcal{G}_{we8}$		$\mathcal{G}_{wee8}$	
110592 distinct matrices		221184 distinct matrices		442368 distinct matrices	
Spectral efficiency (bps/Hz)	Number of selected matrices	Spectral efficiency (bps/Hz)	Number of selected matrices	Spectral efficiency (bps/Hz)	Number of selected matrices
0.5	16	0.5	16	0.5	16
1	256	1	256	1	256
2	65536	2	65536	2	65536
-	-	2.125	131072	2.125	131072
-	-	-	-	2.25	262144

3.5.3 Error Performance of 8 Transmit Antennas DSTM System

For the DSTM MIMO system having $M = 8$ and $N = 8$ and using $\mathcal{G}_{wee8}$ and $L = 120$ transmitted symbols (15 matrices transmitted of size 8×8), and in order to achieve the low spectral efficiencies of 0.5 and 1 bps/Hz, we need 16 and 256 matrices respectively according to Table 3.8. Whereas for higher spectral efficiencies of 2, 2.125 and 2.25 bps/Hz, we need 65536, 131072 and 262144 matrices respectively. Running the search algorithm mentioned in previous sections for this large amount of matrices becomes prohibitive. This is because for the 2.125 bps/Hz case, 131072 8×8 matrices are needed, thus in a simulation, a data table of size 92.2 Gigabytes is required to hold the distance amongst the matrices.

Following this, the BER versus SNR simulation is presented in Fig. 3.7, following the same stopping condition as previous simulations, for the DSTM MIMO systems having $M = 8$ and $N = 8$ and using $\mathcal{G}_{wee8}$ and $L = 120$ transmitted symbols for the spectral efficiencies 0.5, 1, 2 bps/Hz. The systems with spectral efficiencies 0.5 and 1 bps/Hz attain BER=10^{-5} for 1 and 3 dB respectively and no partitioning is needed. Whereas for the 2 bps/Hz spectral efficiency, BER=10^{-5} is attained for 4 dB.

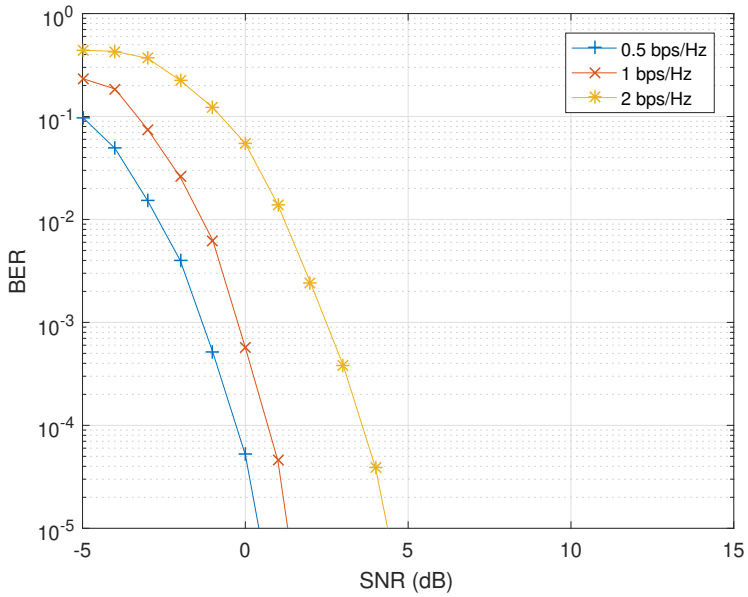

Figure 3.7 – BER performance of DSTM MIMO 8×8 system for different spectral efficiencies

3.6 Conclusion

In this chapter, we expand the Weyl group from matrices of size 2×2, to matrices of size 4×4 and 8×8 in $\mathcal{G}_{w4}$ and $\mathcal{G}_{w8}$ respectively using the Kronecker product. This expansion entails a loss in the maximum achievable spectral efficiencies of the newly generated groups in comparison to the 2 transmit antenna group. This is lead to the extension of the newly generated groups in a similar way to the extension applied to the $\mathcal{G}_{w2}$ group in chapter 2. In addition, an near optimal matrix selection algorithm is employed along with an optimal mapping strategy in order to enhance the error performance of the proposed systems. Simulations of the error performance are presented.

Chapter 4

DSTM Under Time Selective Channel Model

In this chapter, rather than using the conventional step channel model, where the channel remains constant for one coherence time and changes randomly from one coherence time to another, we propose a new time selective channel model for DSTM schemes. The new channel model tries to adopt a real case scenario, where the channel varies slightly with each column of the transmitted matrix. Then we evaluate the performance and robustness of the DSTM schemes with 2, 4 and 8 transmit antennas over this time selective channel model using the Weyl group and its extensions.

4.1 Usual channel model for differential MIMO systems

The conventional channel model used for DSTM schemes is constant during one coherence time and changes randomly for the next one. For instance, with the normalized coherence time $L = 100$, during the transmission of the first frame of 100 symbols, the same channel matrix H_τ is used. The next channel $H_{\tau+1}$ is randomly generated to be used for the next 100 symbols. This is an idealized model since in a real case, the channel undergoes changes constantly. The use of this channel

model also means that at the start of every frame, the differential process must be reinitialized, which is not practical.

In [83, 102], Jakes' model [103] assumes that each of the channel coefficients $h_{nm,t}$ is spatially independent but time correlated with auto-correlation function $J_0(2\pi f_d t)$ where $J_0(.)$ is the zero-order Bessel function of the first kind and f_d is the maximum Doppler frequency. In fact, Jake's simulator is a kind of sum-of-sinusoids based fading channel simulator where the received signal is represented as a superposition of a finite number of waves. It is a simplified model of Clarke's Rayleigh fading model. Clarke's model is given by [104]:

$$h(t) = \sum_{n=1}^{N} \alpha_n exp[j(2\pi f_d t cos\theta_n + \phi_n)] \tag{4.1}$$

where N is the number of propagation paths, $0 < \alpha_n < 1$ is the attenuation of the nth path, f_d is the maximum Doppler frequency and θ_n and ϕ_n are, respectively, the angle of arrival and the random phase of the n^{th} propagation path. Both θ_n and ϕ_n are uniformly distributed over $[-\pi, \pi)$ for all n and they are mutually independent.

Jakes approximates Clarkes's model by setting equal strength multipath components, i.e., $\alpha_n = \frac{1}{\sqrt{N}}$ and choosing the N components to be uniformly distributed in angle i.e.,

$$\theta_n = \frac{2\pi n}{N},\ n = 1, 2, \ldots N. \tag{4.2}$$

The normalized low-pass fading process of this model is given by [103]

$$h(t) = \frac{1}{\sqrt{N}} \Bigg\{ \sqrt{2} \sum_{n=1}^{N_0} [e^{j(2\pi f_d t cos\theta_n + \phi_n)} + e^{-j(2\pi f_d t cos\theta_n + \phi_{-n})}] + e^{j(2\pi f_d t + \phi_N)} + e^{-j(2\pi f_d t + \phi_{-N})} \Bigg\},\ N_0 = \frac{1}{2}\left(\frac{N}{2} - 1\right) \tag{4.3}$$

where ϕ_n is given by

$$\phi_N = \phi_{-N} = 0,\ \phi_n = \frac{n\pi}{N_0 + 1},\ n = 0, 1, \ldots, N_0. \tag{4.4}$$

4.2 Time selective channel model

In [105], instead of assuming that the channel is constant during a fixed long time, the channel changes continuously. The narrow-band impulse response $h(t)$ is

a random process with a Rayleigh distributed envelop, and the flat fading channel is considered. Aiming to obtain intermediate $h(t)$ values between two successive Rayleigh samples, $h(t)$ should be sampled with a certain high frequency. From Nyquist's sampling theorem, it is known that if the channel is sampled with sufficient large frequency, the impulse response of the channel can be reconstructed by the sampled points. This method is used in the conceived channel model.

This channel model is inspired from the Nyquist sampling theorem where a band-limited signal $x(t)$ can be reconstructed from its samples $x(kT_0)$ with the sinc function as long as the sampling frequency $f_0 = \frac{1}{T_0} > 2f_m$, where f_m is the maximum frequency of the signal:

$$\begin{aligned} x(t) &= \sum_{k=-\infty}^{+\infty} x(kT_0) \frac{sin f_0\pi(t - kT_0)}{f_0\pi(t - kT_0)} \\ &= \sum_{k=-\infty}^{+\infty} x(kT_0) \frac{sin\pi(f_0 t - k)}{\pi(f_0 t - k)} \end{aligned} \tag{4.5}$$

With Clarke's model, the channel impulse response $h(t)$ has auto-correlation:

$$R_h(\tau) = 2\sigma^2 J_0(2\pi f_d \tau) \tag{4.6}$$

where $J_0(.)$ is the zero-order Bessel function of the first kind and $\sigma^2 = 0.5 \sum_n E[\alpha_n^2]$. Conventionally, it is assumed that $\sum_n E[\alpha_n^2] = 1$ to ensure that the received signal power equal to the transmitted signal power which results $R_h = J_0(2\pi f_d \tau)$. The function of $h(t)$ has the maximum frequency f_d, meaning that attempting to reconstruct $h(t)$, results that the sampling frequency should be $f_0 > 2f_d$ and the sample period $T_0 < \frac{0.5}{f_d}$. Therefore it is possible to reconstruct the channel response with independently generated Rayleigh distributed random variables.

4.2.1 Model description

The channel model in [105] is applied in our work with improvements to the initialization process. L is considered being the normalized coherence interval meaning that $N_m = \frac{L}{M}$ matrices are transmitted during the coherence interval. $2K$ Rayleigh matrices are generated with $K = 30$, a number large enough to have a good precision. Then $L-1$ channel matrices $H(1), H(2), \ldots, H(L-1)$ are interpolated between

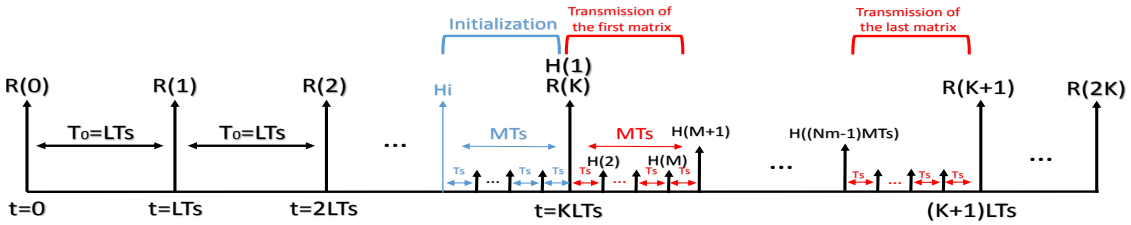

Figure 4.1 – Continuous Rayleigh Channel Model

$R(K)$ and $R(K+1)$. This is done instead of considering one constant matrix $R(K)$. The process is described as follows:

1. A fix number $2K$ of Rayleigh distributed matrices is generated, i.e., $R(1), R(2), \ldots, R(2K)$.
2. Using (4.7), $L-1$ channel matrices are generated.

The Rayleigh random matrices $R(k)$ act as samples of a continuous channel matrix H separated by the coherence interval $T_0 = T_c = L \times T_s$. With the $2K$ randomly generated matrices, $L-1$ interpolated channel matrices are obtained between $R(K)$ and $R(K+1)$:

$$
\begin{aligned}
H(1) &= R(K) \qquad (4.7)\\
H(i+1) &= \sum_{k=1}^{2K} R(k) \frac{sin\pi(f_0 t - k)}{\pi(f_0 t - k)} \\
&= \sum_{k=1}^{2K} R(k) \frac{sin\pi(K + \frac{i}{L} - k)}{\pi(K + \frac{i}{L} - k))}
\end{aligned}
$$

where,

$$
f_0 t(i) = K + \frac{i}{L} \qquad (4.8)
$$

In this model, the matrices $H_i(l)$, where $l = \overline{1, M}$, are used for the transmission of the identity matrix. These H_i matrices are obtained as follows:

$$
H_i(l) = \sum_{k=1}^{2K} R(k) \frac{sin\pi(K - \frac{(M+1)-l}{L} - k)}{\pi(K - \frac{(M+1)-l}{L} - k))}, l = \overline{1, M}
$$

This procedure is illustrated in Fig. 4.1. Here, the module of $R(k)$ is Rayleigh distributed, and as mentioned before, the samples $R(k)\,(k = 1, 2, \ldots, K)$ are separated by $\tau_0 = LT_S$.

4.3 Performance analysis

The performance of the proposed DSTM system using the extension of the Weyl Group for 2, 4 and 8 transmit antennas is presented in this section using the suggested time varying channel. The results are given for two values of the normalized coherence interval of the channel, L=100 and L=20 for 2 and 4 transmit antennas system and L=120 and L=24 for the 8 transmit antennas system. The noise variation is related to the SNR through $\sigma^2 = \frac{1}{SNR}$. The simulation stopping condition is related to reaching 1000 errors before passing to the next SNR. .

4.3.1 2 transmit antennas system performance analysis

We present the performance results of DSTM MIMO system with $M = 2$ and $N = 2$ employing the $\mathcal{G}_{wee2}$ group since it was proved to have the best selected matrices in comparison to $\mathcal{G}_{w2}$. The simulation environment is similar to the ones used in chap 2 and 3, though the channel model used is the continuously fading model described in this chapter.

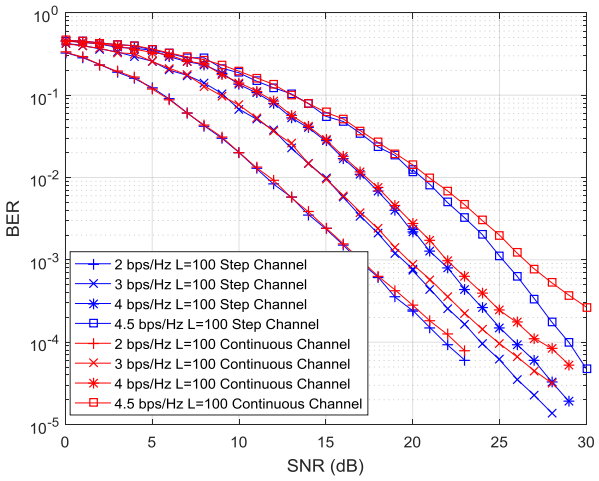

Figure 4.2 – BER performance of DSTM MIMO 2×2 system for different spectral efficiencies employing $\mathcal{G}_{wee2}$ under continuously fading channel and Step Channel for L=100

When comparing the performance of DSTM MIMO scheme under the step chan-

nel model and the continuously fading model for $L = 100$ and different spectral efficiencies in Fig. 4.2, we conclude that the results are similar in the low SNR region, whereas in the high SNR region, the BER in the step channel model continuously decreases though it is limited under the continuously fading channel, due to the continuously varying nature of the channel.

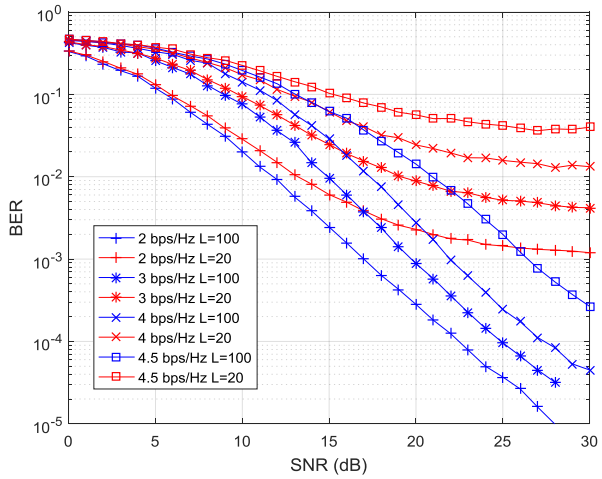

Figure 4.3 – BER performance of DSTM MIMO 2×2 system for different spectral efficiencies employing $\mathcal{G}_{wee2}$ under continuously fading channel for L=100 and L=20

On the other hand, Fig. 4.3 provides the BER simulations versus the Signal-to-Noise-Ratio (SNR) of the DSTM system for 2 bps/Hz up to 4.5 bps/Hz for a coherence interval L=100 and L=20. Predictably, the performance decreases with the spectral efficiency for each set (L=100 and L=20) individually due to the reduction of the distances between the used matrices. For the same simulation environment, employing a normalized coherence interval L=20, a reduction of the system performance is observed in comparison to the results of L=100, due to the fast variation of the propagation channel. Hence it is evident that when adopting the more realistic time varying channel model, the DSTM system's performance degrades for a fast varying channel.

4.3.2 4 transmit antennas system performance analysis

Here, we present the performance results of DSTM MIMO system for $M = 4$ and $N = 4$ employing the $\mathcal{G}_{wee4}$ group since it was proved to have the best selected matrices in comparison to $\mathcal{G}_{w4}$. The simulation environment is similar to the previous section.

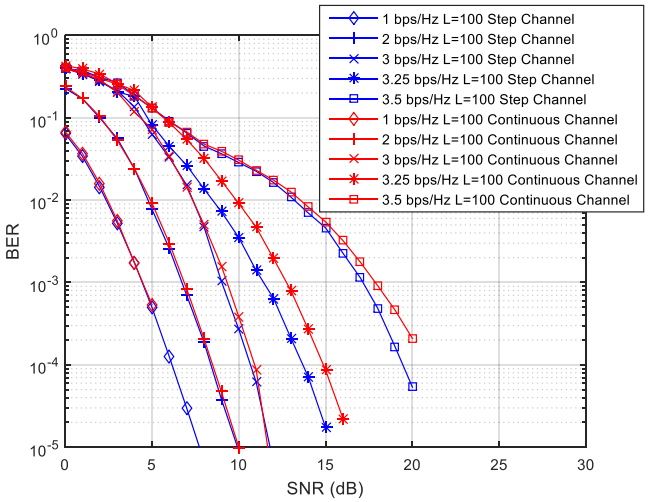

Figure 4.4 – BER performance of DSTM MIMO 4×4 system for different spectral efficiencies employing $\mathcal{G}_{wee4}$ under continuously fading channel and Step Channel for L=100

When comparing the performance of DSTM MIMO scheme under the step channel model and the continuously fading model for $L = 100$ and different spectral efficiencies in Fig. 4.4, we conclude as in the case of the 2 transmit antennas system, that the results are similar in the low SNR region, although the results under the continuous channel begin to degrade as the SNR increases.

In addition, Fig. 4.5 provides the BER simulations versus the Signal-to-Noise-Ratio (SNR) of the DSTM system for 2 bps/Hz up to 3.5 bps/Hz for a coherence interval L=100 and L=20. As in the case of the 2 transmit antenna system a reduction of the system performance is observed in system under L=20 in comparison to the results of L=100, due to the fast variation of the propagation channel.

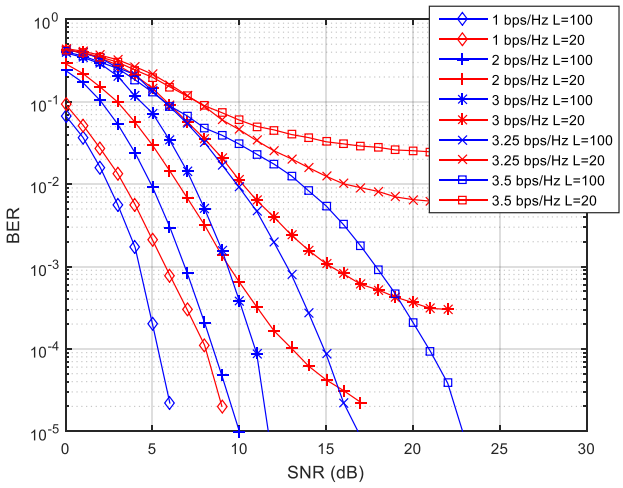

Figure 4.5 – BER performance of DSTM MIMO 4×4 system for different spectral efficiencies employing $\mathcal{G}_{wee4}$ under continuously fading channel for L=100 and L=20

4.3.3 8 transmit antennas system performance analysis

Under the same conditions, the BER performance of the DSTM MIMO system for $M = 8$ and $N = 8$ employing the $\mathcal{G}_{wee8}$ group is presented.

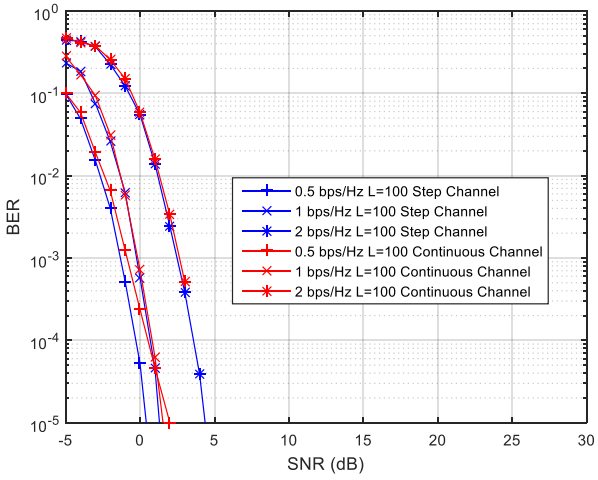

Figure 4.6 – BER performance of DSTM MIMO 8×8 system for different spectral efficiencies employing $\mathcal{G}_{wee4}$ under continuously fading channel and Step Channel for L=100

When comparing the performance of the DSTM scheme under the step chan-

nel model and the continuously fading channel model in Fig. 4.6, we conclude as previously seen, a degradation in the performance under the continuous channel.

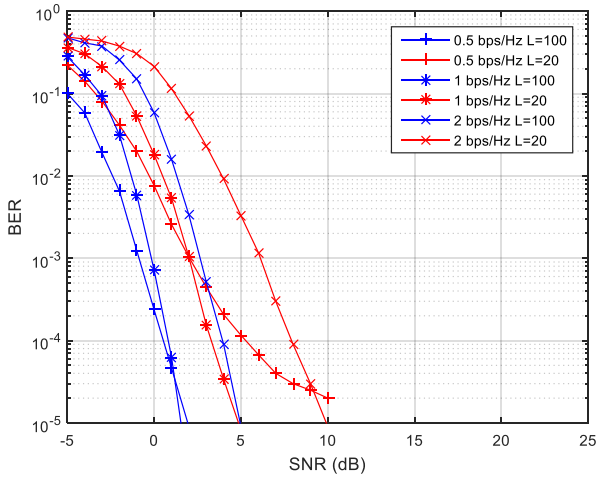

Figure 4.7 – BER performance of DSTM MIMO 8×8 system for different spectral efficiencies employing $\mathcal{G}_{wee4}$ under continuously fading channel for L=100 and L=20

Fig. 4.7 provides the BER simulations versus the Signal-to-Noise-Ratio (SNR) of the DSTM system for 0.5 bps/Hz up to 2.25 bps/Hz for a coherence interval L=100 and L=20. As in the case of the 2 and 4 transmit antenna system a reduction of the system performance is observed in system under L=20 in comparison to the results of L=100.

4.4 Conclusion

In this chapter, the DSTM MIMO scheme is studied under a continuously fading channel model which is inspired from the Nyquist sampling theorem. More explicitly, each column of the transmission matrix is multiplied by an interpolated channel matrix from randomly generated channel matrices. This model has been previously adopted in [105], we add new improvements to it through adding an initialization process. The extensions of the Weyl group have been used for 2, 4 and 8 transmit antennas and the performance results under the new channel model are compared to the results under the step channel model used in previous chapters which show

a degradation of the results under the new model in high SNR region due to the continuous variation of the channel, which depicts a real case scenario. Simulation results also show how the fast variation of the channel degrades the performance of the DSTM schemes.

Chapter 5

DSTM System Analysis Under New Optimization Metric

In this chapter, based on the results produced in [1], an analytical study of the performance of the DSTM system employing the Weyl group is presented, which leads to closed form expressions of the exact and upper bound of the PEP. Theoretical results are then compared to simulation results for validation. Consequently, the exact PEP is used as a new optimization metric in the optimal selection of the transmission matrices,leading to improvements in the error performance of the DSTM system.

5.1 Performance analysis of DSTM

The performance analysis conducted here is inspired from the work achieved in [1], where the author proposes a generalized framework for the study of the performance of DSTM systems. The analysis conducted does not require the information matrices used to belong to a specific space-time modulated constellation, though the only restriction is that the constellation should be unitary. In light of this generalization, the metric employed for the performance analysis is the PEP. The performance of DSTM system has been analyzed in various Rayleigh fading environments, though in our work we are mainly concerned with the slow fading channel case scenario. In this next section, we remind the work achieved in [1] leading to

the closed form expressions of the PEP for the DSTM system.

5.1.1 Preliminaries

5.1.1.1 System model employed

A wireless communication system is considered with M transmit antennas and N receive antennas. At each time t, the encoder produces M outputs $x_t^1\, x_t^2 \ldots x_t^M$, where $x_t^m \in \mathbb{C}$. These outputs are then simultaneously transmitted by M antennas. At the receiver, the signal received by the antenna n at a time t is given by

$$r_t^n = \sum_{m=1}^{M} \sqrt{E_s} h^{m,n} x_t^m + v_t^n \tag{5.1}$$

where E_s is the average transmitted signal energy per symbol period, and v_t^n are independent samples of a zero-mean complex Gaussian random variable with variance $\frac{\sigma_v^2}{2}$ per complex dimension. The coefficient $h^{m,n}$ is the fading gain for the path from transmitter antenna m to receive antenna n. It is assumed to be flat Rayleigh fading and remain constant within T symbol periods. By collecting the transmitted symbols over T time intervals into a code matrix $\mathbf{X} \in \mathbb{C}^{T \times M}$, the received signals at antenna n during T symbol periods can be written in a vector form as

$$\mathbf{r}^n = \sqrt{E_s}\mathbf{X}\mathbf{h}^n + \mathbf{v}^n \tag{5.2}$$

where $\mathbf{h}^n = [h^{1,n}\, h^{2,n} \ldots h^{M,n}]^T$ and $\mathbf{v}^n = [v_1^n\, v_2^n \ldots v_T^n]^T$. In this notation, the mth column of the matrix $\mathbf{X}$ represents the signals sent by the transmitter antenna m as a function of time. The code matrix $\mathbf{X}$ is normalized so that it satisfies the total transmitted power constraint

$$tr(\mathbf{X}\mathbf{X}^H) = T \tag{5.3}$$

By stacking the signals from N receiver antennas into a vector, we obtain

$$\mathbf{r} = \sqrt{E_s}\mathcal{X}\mathbf{h} + \mathbf{v} \tag{5.4}$$

where $\mathbf{r} = vec([\mathbf{r}^1\, \mathbf{r}^2 \ldots \mathbf{r}^N])$, $\mathbf{h} = vec([\mathbf{h}^1\, \mathbf{h}^2 \ldots \mathbf{h}^N])$, $\mathbf{v} = vec([\mathbf{v}^1\, \mathbf{v}^2 \ldots \mathbf{v}^N])$, and $\mathcal{X} = \mathbf{I}_N \otimes \mathbf{X}$. The additive noise is assumed to be white in space and time (i.e., $E[\mathbf{v}\mathbf{v}^H] = \sigma_v^2 \mathbf{I}_{TN}$).

5.1.1.2 Differential space-time encoding

The differential encoding process in [1], is similar to the one described in previous chapters. Since signals are transmitted matrix by matrix, it is convenient to use $k = 1, 2, \ldots$ to denote the matrix index. Likewise, it is assumed that $T = M$ and we denote the $M \times M$ code matrix transmitted over M antennas during the kth matrix as $\mathbf{X}_k$. At the start of the transmission, the transmitter sends the code matrix $\mathbf{X}_0 = \mathbf{I}_M$. Thereafter, data are differentially encoded according to

$$\mathbf{X}_k = \mathbf{S}_{l(k)}\mathbf{X}_{k-1} \tag{5.5}$$

where $\mathbf{S}_{l(k)}$, with $l(k) \in \{0,\ 1, \ldots,\ S-1\}$, is the $M \times M$ information matrix having index k which is selected from a unitary space-time modulated constellation $\mathcal{V}$ of size S. Fitting this description is the space-time code constellation from the Weyl group employed from previous chapters.

5.1.1.3 Channel model

Considering a sequence of K transmitted matrices $\mathbf{X}_1, \mathbf{X}_2, \ldots, \mathbf{X}_K$, the received signal for the kth block over N antennas is given by

$$\mathbf{r}_k = \sqrt{E_s}\mathcal{X}_k + \mathbf{v}_k \tag{5.6}$$

where $\mathcal{X}_k = \mathbf{I}_N \otimes \mathbf{X}_k$.

It has been shown in [106] that the time-varying Rayleigh fading channels can be well described by a hidden Markov model. As has been done in [107] and [108] for channel equalization problems, the time varying fading channels can be modeled by a multi-channel auto-regressive (AR) process of order P

$$\mathbf{h}_k = \sum_{p=1}^{P} \mathbf{A}_p \mathbf{h}_{k-p} + \mathbf{G}\mathbf{n}_k \tag{5.7}$$

where $\mathbf{A}_p$ and $\mathbf{G}$ are the time-invariant matrices which can be determined from the second-order statistics of the fading channels and $\mathbf{n}_k$ is a zero mean complex white Gaussian noise process with covariance $\mathbf{I}_{MN}$. By postmultiplying (5.7) with $\mathbf{h}_{k-\tau}^H$ and taking the expectation on both sides, we arrive at

$$\mathbf{R}_{-\tau} = \sum_{p=1}^{P} \mathbf{A}_p \mathbf{R}_{p-\tau} + \mathbf{G}\mathbf{G}^H \delta(\tau),\ \tau = 0, \ldots, P \tag{5.8}$$

where $\mathbf{R}_\tau \triangleq E[\mathbf{h}_k \mathbf{h}_{k+\tau}^H]$ is the cross correlation matrix of the channels. The matrices $\mathbf{A}_p$ and $\mathbf{G}$ can be obtained by solving the aforementioned equations. In [1] the author considers the time varying channels that can be well approximated by the first order AR process (i.e., $P = 1$)

$$\mathbf{h}_k = \mathbf{A}\mathbf{h}_{k-1} + \mathbf{G}\mathbf{n}_k \tag{5.9}$$

By solving (5.8) for $\tau = 0, 1$, the matrices $\mathbf{A}$ and $\mathbf{G}$ are given by

$$\mathbf{A} = \mathbf{R}_{-1}\mathbf{R}_0^{-1}$$

$$\mathbf{G}\mathbf{G}^H = \mathbf{R}_0 - \mathbf{A}\mathbf{R}_1$$

This channel model is quite general and permits both temporal and spatial correlations in the fading gains. Several channel models widely adopted in literature for the space-time coded systems can be considered as special cases of this model. In our work, we are mainly concerned with the slow fading spatially independent channel model used in [24, 78, 84, 102], the channel cross-correlation matrix $\mathbf{R}_\tau = \mathbf{I}_{MN} \forall \tau$ with $I_{MN} is of size MN \times MN$. Consequently, it can be represented by this general model with $\mathbf{A} = \mathbf{I}_{MN}$ and $\mathbf{G} = 0_{MN}$.

5.1.1.4 Differential detection

At the receiver , the transmitted signal can be non-coherently demodulated by using two consecutive observations, $\mathbf{r}_{k-1}$ and $\mathbf{r}_k$. By substituting (5.9) into (5.6), we have

$$\mathbf{r}_k = \sqrt{E_s}\mathcal{S}_{l(k)}\mathcal{X}_{k-1}\mathbf{A}\mathbf{h}_{k-1} + \sqrt{E_s}\mathcal{X}_k\mathbf{G}\mathbf{n}_k + \mathbf{v}_k$$

where $\mathcal{S}_{l(k)} = \mathbf{I}_N \otimes \mathbf{S}_{l(k)}$. Since $\mathcal{X}_{k-1}$ is unitary, the received signal during the kth block can be rewritten in terms of the received signal of the previous block as

$$\begin{aligned} \mathbf{r}_k &= \sqrt{E_s}\mathcal{S}_{l(k)}\mathcal{X}_{k-1}\mathbf{A}\mathcal{X}_{k-1}^H\mathcal{X}_{k-1}\mathbf{h}_{k-1} \\ &\quad + \sqrt{E_s}\mathcal{X}_k\mathbf{G}\mathbf{n}_k + \mathbf{v}_k \\ &= \mathcal{S}_{l(k)}\mathcal{Z}_{k-1}\mathbf{r}_{k-1} + \mathbf{z}_k \end{aligned} \tag{5.10}$$

where we define $\mathcal{Z}_{k-1} \triangleq \mathcal{X}_{k-1}\mathbf{A}\mathcal{X}_{k-1}^H$ and $z_k \triangleq \sqrt{E_s}\mathcal{X}_k\mathbf{G}\mathbf{n}_k + \mathbf{v}_k - \mathcal{S}_{l(k)}\mathcal{Z}_{k-1}\mathbf{v}_{k-1}$. From (5.10), the transmitted data matrix can be detected according to

$$\hat{\mathbf{S}}_{l(k)} = argmin_{S \in \mathcal{V}} ||\mathbf{r}_k - (\mathbf{I}_N \otimes \mathbf{S})\mathcal{Z}_{k-1}\mathbf{r}_{k-1}||^2 \tag{5.11}$$

When the fading channel is spatially independent, this minimum Euclidean distance detector is optimal and is equivalent to the maximum likelihood detector.

5.1.2 PEP analysis

In this section, the PEP of the DSTM system is analyzed. The PEP , denoted by $P(\mathbf{S}_i \rightarrow \mathbf{S}_j)$, is the probability that the receiver erroneously selects $\mathbf{S}_j$ when $\mathbf{S}_i$ is transmitted. By using the Moment Generating Function (MGF) approach, closed form expressions for the PEP in various fading environments are derived.

With the minimum Euclidean distance detection rule, the receiver will decide in favor of $\mathbf{S}_j$ is

$$||\mathbf{r}_k - \mathcal{S}_i \mathcal{Z}_{k-1} \mathbf{r}_{k-1}||^2 > ||\mathbf{r}_k - \mathcal{S}_j \mathcal{Z}_{k-1} \mathbf{r}_{k-1}||^2$$

Through simple manipulation, it can be shown that this condition is equivalent to

$$f^2(\mathbf{S}_i, \mathbf{S}_j) < -2Re\{\mathbf{r}_{k-1}^H \mathcal{Z}_{k-1}^H \varepsilon_{i,j}^H \mathbf{z}_k\} \tag{5.12}$$

where $f^2(\mathbf{S}_i, \mathbf{S}_j) \triangleq \mathbf{r}_{k-1}^H \mathcal{Z}_{k-1}^H \varepsilon_{i,j}^H \varepsilon_{i,j} \mathcal{Z}_{k-1} \mathbf{r}_{k-1}$ and $\varepsilon_{i,j} = \mathbf{I}_N \otimes \mathbf{E}_{i,j}$ with $\mathbf{E}_{i,j} \triangleq \mathbf{S}_i - \mathbf{S}_j$. The term $y \triangleq -2Re\{\mathbf{r}_{k-1}^H \mathcal{Z}_{k-1}^H \varepsilon_{i,j}^H \mathbf{z}_k\}$ is a Gaussian random variable. Given that $\mathbf{S}_i$ was sent during the kth block, the mean and variance of y conditioned on $\mathbf{r}_{k-1}$ is given by

$$\bar{m}_{y|\mathbf{r}_{k-1}} = 2Re\{\mathbf{r}_{k-1}^H \mathcal{Z}_{k-1}^H \varepsilon_{i,j}^H \mathcal{S}_i \mathcal{Z}_{k-1} \bar{\mathbf{m}}_{\mathbf{v}_{k-1}|\mathbf{r}_{k-1}}\} \tag{5.13}$$

$$\begin{aligned} \sigma^2_{y|\mathbf{r}_{k-1}} &= 2E_s \mathbf{r}_{k-1}^H \mathcal{Z}_{k-1}^H \varepsilon_{i,j}^H \mathcal{X}_k \mathbf{G}\mathbf{G}^H \mathcal{X}_k^H \varepsilon_{i,j} \mathcal{Z}_{k-1} \mathbf{r}_{k-1} \\ &\quad + 2\mathbf{r}_{k-1}^H \mathcal{Z}_{k-1}^H \varepsilon_{i,j}^H \mathcal{S}_i \mathcal{Z}_k - 1 \Sigma_{\mathbf{v}_{k-1}|\mathbf{r}_{k-1}} \mathcal{Z}_{k-1}^H \mathcal{S}_i^H \varepsilon_{i,j} \mathcal{Z}_{k-1} \mathbf{r}_{k-1} \\ &\quad + 2\sigma_v^2 \mathbf{r}_{k-1}^H \mathcal{Z}_k^H - 1 \varepsilon_{i,j}^H \varepsilon_{i,j} \mathcal{Z}_{k-1} \mathbf{r}_{k-1} \end{aligned} \tag{5.14}$$

where $\bar{\mathbf{m}}_{\mathbf{v}_{k-1}|\mathbf{r}_{k-1}}$ and $\Sigma_{\mathbf{v}_{k-1}|\mathbf{r}_{k-1}}$ are the mean and covariance of $\mathbf{v}_{k-1}$ conditioned on $\mathbf{r}_{k-1}$

$$\bar{\mathbf{m}}_{\mathbf{v}_{k-1}|\mathbf{r}_{k-1}} = \left(\frac{E_s}{\sigma_v^2} \mathcal{X}_{k-1}^H + \mathbf{I}_{MN}\right)^{-1} \mathbf{r}_{k-1} \tag{5.15}$$

$$\Sigma_{\mathbf{v}_{k-1}|\mathbf{r}_{k-1}} = \sigma_v^2 \mathbf{I}_{MN} - \sigma_v^2 \left(\frac{E_s}{\sigma_v^2} \mathcal{X}_{k-1}^H + \mathbf{I}_{MN}\right)^{-1} \tag{5.16}$$

We recall that $\mathbf{R}_0 = E[\mathbf{h}_k \mathbf{h}_k^H]$ is the correlation matrix of the channels. From 5.12, the probability that the receiver erroneously selects $\mathbf{S}_j$ when $\mathbf{S}_i$ was sent will depend on the variance of y conditioned on $\mathbf{r}_{k-1}$. As from 5.14, this conditional variance $\sigma^2_{y|\mathbf{r}_{k-1}}$ is made up of three parts. The first part depends on the fading channel and is independent of the noise variance σ_v^2 while the second and third parts depend on the noise variance σ_v^2. In the case of slow fading, we have $\mathbf{G} = 0$. Thus, the conditional variance $\sigma^2_{y|\mathbf{r}_{k-1}}$ reduces to the second and third parts. Both of these parts approach zero as the SNR goes to infinity (i.e., $\frac{E_s}{\sigma_v^2} \to \infty$).

Based on (5.12) the conditional PEP is, therefor, given by

$$P(\mathbf{S}_i \to \mathbf{S}_j | \mathbf{r}_{k-1}) = \mathcal{Q}\left(\sqrt{\frac{(f^2(\mathbf{S}_i, \mathbf{S}_j) - \bar{m}_{y|\mathbf{r}_{k-1}})^2}{\sigma^2_{y|\mathbf{r}_{k-1}}}}\right) \tag{5.17}$$

where $Q(x)$ is the Gaussian Q-function. To compute the unconditional PEP, we need to average (5.17) over the probability distribution of $\mathbf{r}_{k-1}$. By making use of Craig's formula [109] for the Gaussian Q-function and the MGF-based techniques in [110], the unconditional PEP can, then, be computed as

$$P(\mathbf{S}_i \to \mathbf{S}_j) = \frac{1}{\pi} \int_0^{\frac{\pi}{2}} M_\Gamma\left(-\frac{1}{2sin^2\theta}\right) d\theta \tag{5.18}$$

where $M_\Gamma(s) \triangleq \int_0^\infty e^{s\Gamma} p_\Gamma(\Gamma) d\Gamma$ is the MGF of

$$\Gamma = \frac{(f^2(\mathbf{S}_i, \mathbf{S}_j) - \bar{m}_{y|\mathbf{r}_{k-1}})^2}{\sigma^2_{y|\mathbf{r}_{k-1}}} \tag{5.19}$$

Evaluating the PEP in (5.18) is difficult for the general case since the MGF of Γ cannot be readily calculated. In the following section the closed-form expression of the PEP for the fast fading spatially independent case is presented in order to then produce the special case of slow-fading scenario.

5.1.2.1 Spatially independent fast-fading channels

When the channels undergo spatially independent fast fading, we have $\mathbf{R}_0 = \mathbf{I}$, $\mathbf{A} = \alpha \mathbf{I}_{MN}$, $\mathbf{G} = \sqrt{1-\alpha^2}\mathbf{I}_{MN}$, and $\mathcal{Z}_{k-1} = \alpha \mathbf{I}_{MN}$ where α is given by the Jakes's model with $\alpha = J_0(2\pi f_D T_B)$. Hence, the first order AR model in (5.9) reduces to

$$\mathbf{h}_k = \alpha \mathbf{h}_{k-1} + \sqrt{1-\alpha^2}\mathbf{n}_k \tag{5.20}$$

With $\mathbf{R}_0 = \mathbf{I}$, the mean and covariance of $\mathbf{v}_{k-1}$ conditioned on $\mathbf{r}_{k-1}$simplify to

$$\bar{\mathbf{m}}_{\mathbf{v}_{k-1}|\mathbf{r}_{k-1}} = \frac{\sigma_v^2}{E_s + \sigma_v^2}\mathbf{r}_{k-1} \tag{5.21}$$

$$\Sigma_{\mathbf{v}_{k-1}|\mathbf{r}_{k-1}} = \frac{E_s\sigma_v^2}{E_s + \sigma_v^2}\mathbf{I}_{MN} \tag{5.22}$$

Thus the expression for $f^2(\mathbf{S}_i, \mathbf{S}_i)$, $\bar{m}_{y|\mathbf{r}_{k-1}}$ and $\sigma^2_{y|\mathbf{r}_{k-1}}$ can be rewritten as

$$\begin{aligned}
f^2(\mathbf{S}_i, \mathbf{S}_i) &= \alpha^2 d^2(\mathbf{S}_i, \mathbf{S}_i) \\
\bar{m}_{y|\mathbf{r}_{k-1}} &= \frac{2\alpha^2\sigma_v^2}{E_s + \sigma_v^2} Re\{\mathbf{r}_{k-1}^H(\mathbf{I}_{MN} - \mathcal{S}_j^H\mathcal{S}_i)\mathbf{r}_{k-1}\} \\
&= \frac{\alpha^2\sigma_v^2}{E_s + \sigma_v^2}\mathbf{r}_{k-1}^H(2\mathbf{I}_{MN} - \mathcal{S}_j^H\mathcal{S}_i - \mathcal{S}_i^H\mathcal{S}_j)\mathbf{r}_{k-1} \\
&= \frac{\alpha^2\sigma_v^2}{E_s + \sigma_v^2} d_{i,j}^2(\mathbf{S}_i, \mathbf{S}_j) \\
\sigma^2_{y|\mathbf{r}_{k-1}} &= 2\alpha^2\left(E_s(1-\alpha^2) + \sigma_v^2 + \frac{\alpha^2 E_s\sigma_v^2}{E_s + \sigma_v^2}\right) d_{i,j}^2(\mathbf{S}_i, \mathbf{S}_j)
\end{aligned}$$

with $d^2(\mathbf{S}_i, \mathbf{S}_j) \triangleq \mathbf{r}_{k-1}^H \varepsilon_{i,j}^H \varepsilon_{i,j}\mathbf{r}_{k-1}$. By substituting $\bar{m}_{y|\mathbf{r}_{k-1}}$ and $\sigma^2_{y|\mathbf{r}_{k-1}}$ into (5.19), we have

$$\Gamma = \frac{\gamma}{E_s + \sigma_v^2} d_{i,j}^2(\mathbf{S}_i, \mathbf{S}_j)$$

where

$$\gamma = \frac{\alpha^2 E_s^2}{2(E_s + \sigma_v^2)[E_s(1-\alpha^2) + \sigma_v^2] + 2\alpha^2 E_s\sigma_v^2} \tag{5.23}$$

Since $d^2(\mathbf{S}_i, \mathbf{S}_j)$ is in the quadratic form, the MGF of Γ can be readily found. By using the result from [111], the MGF of Γ is, therefor, given by

$$M_\Gamma(s) = \left|\mathbf{I}_{MN} - \frac{s\gamma}{E_s + \sigma_v^2}\Omega\varepsilon_{i,j}^H\varepsilon_{i,j}\right|^{-1} \tag{5.24}$$

where $|.|$ is the determinant of a matrix and $\Omega \triangleq E[\mathbf{r}_{k-1}\mathbf{r}_{k-1}^H]$ is the covariance matrix of the received signal. For this case of spatially independent fading, the covariance matrix $\Omega = (E_s + \sigma_v^2)\mathbf{I}_{MN}$ thus the MGF of Γ becomes

$$M_\Gamma(s) = \prod_{l=1}^{L}(1 - s\gamma\lambda_l)^{-\mu_l} \tag{5.25}$$

where L is the number of distinct non-zero eigenvalues λ_l of the distance matrix $\varepsilon_{i,j}^H\varepsilon_{i,j}$ with multiplicity μ_l.

By using (5.18), the exact PEP of the DSTM in spatially independent fast-fading channels is

$$P(\mathbf{S}_i \to \mathbf{S}_j) = \frac{1}{\pi}\int_0^{\frac{\pi}{2}} \prod_{l=1}^{L}\left(\frac{1}{1+\frac{1}{2sin^2\theta}\gamma\lambda_l}\right)^{\mu_l} d\theta \tag{5.26}$$

By applying the partial-fraction expansion as in [112], the integrand in the aforementioned equation can be rewritten as

$$\prod_{l=1}^{L}\left(\frac{1}{1+\frac{1}{2sin^2\theta}\gamma\lambda_l}\right)^{\mu^l} = \sum_{l=1}^{L}\sum_{p=1}^{\mu_l} c_{p,l}\left(\frac{1}{1+\frac{1}{2sin^2\theta}\gamma\lambda_l}\right)^{p} \tag{5.27}$$

where

$$c_{p,l} = \frac{\left\{\frac{d^{\mu_l-p}}{dx^{\mu_l-p}}\prod_{n=1,n\neq l}^{L}\left(\frac{1}{1+\lambda_n x}\right)^{\mu}_{n}\right\}\Big|_{x=-\lambda_l^{-1}}}{(\mu_l-p)!\lambda_l^{\mu_l-p}} \tag{5.28}$$

If we set $\gamma = 0$, it can be observed from (5.27) that $\sum_{l=1}^{L}\sum_{p=1}^{\mu_l} c_{p,l} = 1$. Using (5.26), (5.27), and the following result from [110]

$$\frac{1}{\pi}\int_0^{\frac{\pi}{2}}\left(\frac{sin^2\theta}{sin^2\theta+\zeta}\right)^{Q} = \frac{1}{2}\left\{1-\sqrt{\frac{\zeta}{1+\zeta}}\sum_{q=0}^{Q-1}\binom{2q}{q}\left(\frac{1}{4(1+\zeta)}\right)^{q}\right\}$$

we can obtain the following closed form expression for the exact PEP of the DSTM in spatially independent fast-fading channels

$$\begin{aligned} P(\mathbf{S}_i \to \mathbf{S}_j) &= \frac{1}{\pi}\int_0^{\frac{\pi}{2}}\sum_{l=1}^{L}\sum_{p=1}^{\mu_l} c_{p,l}\left(\frac{sin^2\theta}{sin^2\theta+\frac{1}{2}\gamma\lambda_l}\right)^{p} d\theta \\ &= \frac{1}{2}\Big\{\sum_{l=1}^{L}\sum_{p=1}^{\mu_l} c_{p,l} \\ &- \sum_{l=1}^{L}\sum_{p=1}^{\mu_l} c_{p,l}\sqrt{\frac{\gamma\lambda_l}{2+\gamma\lambda_l}}\sum_{q=0}^{p-1}\binom{2q}{q}\left(\frac{1}{4+2\gamma\lambda_l}\right)^{q}\Big\} \\ &= \frac{1}{2} - \frac{1}{2}\sum_{l=1}^{L}\sqrt{\frac{\gamma\lambda_l}{2+\gamma\lambda_l}}\sum_{p=1}^{\mu_l} c_{p,l}\sum_{q=0}^{p-1}\binom{2q}{q}\left(\frac{1}{4+2\gamma\lambda_l}\right)^{q} \end{aligned} \tag{5.29}$$

5.1.2.2 Spatially independent slow-fading channels

The spatially independent slow-fading channels can be viewed as a special case of the spatially independent fast-fading channels where the fading rate $f_D T_B = 0$ (i.e.,$\alpha = 1$). In this slow fading case, $\mathbf{A} = \mathbf{I}_{MN}$, $\mathbf{G} = 0_{MN}$, and $\mathcal{Z}_{k-1} = \mathbf{I}_{MN}$ which

is the step channel model used in the previous chapters. Consequently, the exact PEP is still being given by (5.29) with γ now reduces to

$$\gamma = \frac{E_s^2}{2\sigma_v^2(2E_s + \sigma_v^2)} \tag{5.30}$$

5.1.2.3 Upper-bound of PEP

It is noted that the Chernoff bound derived in [84] can also be derived from this MGF-based approach. By substituting the aforementioned expression of γ into (5.26) and setting $\theta = \frac{\pi}{2}$, it can be observed that the PEP of the DSTM in spatially independent slow-fading channels can be upper bounded by

$$P(\mathbf{S}_i, \mathbf{S}_j) \leq \frac{1}{2} \prod_{l=1}^{L} \Big(\frac{1}{1 + \frac{E_s^2}{4\sigma_v^2(2E_s+\sigma_v^2)}\lambda_l} \Big)^{\mu_l} \tag{5.31}$$

5.2 PEP analysis for the Weyl group and its extensions

In the previous section, expression (5.29) from [1] represents the closed form expression for the exact PEP in a spatially independent slow fading channel scenario. This expression assumes that the distance matrix $\varepsilon_{i,j}^H \varepsilon_{i,j}$ has multiple eigenvalues for each PEP in a space-time coded constellation. In fact, when analyzing the matrices of $\mathcal{G}_{w2}$, $\mathcal{G}_{we2}$ and $\mathcal{G}_{wee2}$, it was found that for multiple distance matrices ($\varepsilon_{i,j}^H \varepsilon_{i,j}$) there are identical eigenvalues, meaning that L, which is the number of distinct non-zero eigenvalues is equal to 1.

5.2.0.1 Analysis of distinct non-zero eigenvalues of $\mathcal{G}_{w2}$, $\mathcal{G}_{we2}$ and $\mathcal{G}_{wee2}$

For M the number of transmit antennas and N the number of receive antennas, the distance matrix between one couple of matrices is

$$\varepsilon_{i,j} = \mathbf{I}_N \otimes E_{i,j}$$

where $E_{i,j} = S_i - S_j$. L is the number of distinct non-zero eigenvalues λ_l of the distance matrix $\varepsilon_{i,j}^H \varepsilon_{i,j}$. Table 5.1 shows the percentage occurrences of the values of L for the couple of matrices in $\mathcal{G}_{w2}$, $\mathcal{G}_{we2}$ and $\mathcal{G}_{wee2}$.

Table 5.1 – Percentage occurrences of the values of L for the couple of matrices in $\mathcal{G}_{w2}$, $\mathcal{G}_{we2}$ and $\mathcal{G}_{wee2}$

	$\mathcal{G}_{w2}$	$\mathcal{G}_{we2}$	$\mathcal{G}_{wee2}$
$L=1$	42%	19.6%	10%
$L=2$	58%	80.4%	90%

Since $L=1$ for multiple couples of matrices in the mentioned groups, this means that, for these specific cases, the product operator in expression (5.26), which is solved by using the partial fraction expansion (5.27) is no longer needed. This is why for the case of $L=1$ we use the PEP relation derived in the next section.

5.2.0.2 Special case of the Weyl group

In this section, we derive a closed expression for the special case of the couples of matrices of the Weyl group and its extensions having $L=1$. Based on (5.24)

$$M_\zeta(s) = \left|\mathbf{I}_{MN} - \frac{s\gamma}{E_s+\sigma_v^2}\Omega\varepsilon_{i,j}^H\varepsilon_{i,j}\right|^{-1} \tag{5.32}$$

and $\Omega = (E_s+\sigma_v^2)\mathbf{I}_{MN}$. This leads to, based on $det(A) = \prod_{l=1}^{L}\lambda_l$, to

$$M_\zeta(s) = \prod_{l=1}^{L}(1-s\gamma\lambda_l)^{-}\mu_l \tag{5.33}$$

Having $L=1$ leads to

$$M_\zeta(s) = (1-s\gamma\lambda)^{-\mu} \tag{5.34}$$

where λ is the single distinct non-null eigenvalue of $\varepsilon_{i,j}^H\varepsilon_{i,j}$ and μ is the multiplicity of λ. Now by using expression (5.18), the exact PEP of the DSTM in spatially independent slow fading channel for the special case of identical eigenvalues is

$$\begin{aligned} P(\mathbf{S}_i\to\mathbf{S}_j) &= \frac{1}{\pi}\int_0^{\frac{\pi}{2}}\big(1-\big(-\frac{1}{2sin^2\theta}\big)\gamma\lambda\big)^{-\mu}d\theta \\ &= \frac{1}{\pi}\int_0^{\frac{\pi}{2}}\big(\frac{sin^2\theta}{sin^2\theta+\frac{\gamma\lambda}{2}}\big)^{\mu}d\theta \end{aligned} \tag{5.35}$$

The solution to such an integral is mentioned in the PEP analysis previously, and is evaluated without the need for the partial fraction expansion, thus solving the

problem of the product operator issue produced for $L = 1$

$$P(\mathbf{S}_i \to \mathbf{S}_j) = \frac{1}{2}\{1 - \sqrt{\frac{\gamma\lambda}{2+\gamma\lambda}} \sum_{q=0}^{\mu-1} \binom{2q}{q} (\frac{1}{4+2\gamma\lambda})^q\} \tag{5.36}$$

Thus, when deriving the exact PEP of the couple of matrices of the Weyl group and its extensions, we study the condition of the eigenvalues of their distance matrix, and based on it, we either derive the PEP according to the special case in (5.36) or the general case in (5.29).

5.3 Interpretation of theoretical results of PEP

In order to validate the PEP closed form expressions stated in the previous section, we calculate the PEP values for couples of matrices belonging to the Weyl group. Then, we produce simulation results of the exact and upper bound PEP of these matrices couples in the aim of comparing the theoretical and simulations results.

5.3.1 Simulation environment

We consider a MIMO system with 2 transmitting antennas and 2 receiving antennas. On transmission, we consider the equally likely transmission of the information matrices M_1, M_6 and M_7 through a Rayleigh channel characterized by the H channel matrix of dimension 2×2. The elements of the channel matrix are independent complex random variables whose real and imaginary parts are Gaussian random variables of zero mean and variance $\sigma^2 = \frac{1}{2}$. It is considered that the channel matrix remains constant during the transmission of $L = 100$ symbols, therefore 50 matrices. Then, we perform another random draw to have another channel matrix. The transmission of each matrix M_i is disturbed by a noise matrix W_i whose elements are also complex. Their real and imaginary parts are also Gaussian random variables, with zero mean and standard deviation, which is determined as a function of the signal to noise ratio SNR as in relation (1.13).

The matrices M_6 and M_7 have equal distance of value 2 towards M_1, though we find that their PEP values towards M_1 are different. This means that the distance

between two matrices does not uniquely govern the PEP values hence the BER performance obtained with the information matrices chosen.

5.3.1.1 Simulation results

For the matrices $M_1 = \begin{pmatrix} 1 & 0 \\ 0 & 1 \end{pmatrix}$, $M_6 = \begin{pmatrix} 0 & 1 \\ 1 & 0 \end{pmatrix}$ and $M_7 = \begin{pmatrix} 0 & 1 \\ -1 & 0 \end{pmatrix}$, the program which allowed their equally likely generation ($P(M_1) = P(M_6) = P(M_7) = \frac{1}{3}$) and the calculation of probabilities of type $P(M_i \to M_j)$, considered a number of minimum 400 errors for all the pairs of matrices $(M_i \to M_j)$ separated by the minimum distance of 2. Except for SNR of 17 dB and 18 dB, we reduced this number of errors to 300, in order to decrease the calculation time. It was also verified that the PEP values are not affected by the transmission of two matrices ($P(M_1) = P(M_6) = \frac{1}{2}$) or three matrices ($P(M_1) = P(M_6) = P(M_7) = \frac{1}{3}$). For the simulation, we have considered a Rayleigh channel of the step channel type with $L = 100$, therefore the same matrix H of channel for 50 successive matrices emitted. these simulation results are presented in Fig. 5.1.

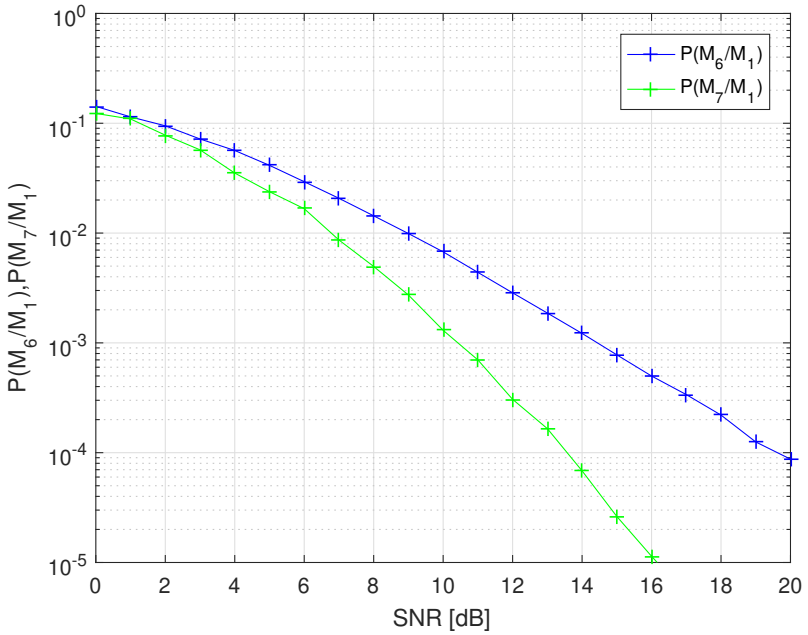

Figure 5.1 – Simulation results of the exact PEP of the couple of matrices (M_6, M_1) and (M_7, M_1)

Even though the couple of matrices used have the same distance values, the corresponding PEP values are quite different, as M_7 performance is considerably better than M_6, specially in the high SNR region. We then validate these results with the theoretical ones under the same conditions.

5.3.1.2 Theoretical results

Using the closed form expressions derived in previous sections, we produce theoretical results for the exact PEP and upper bound PEP for the matrices couples studied, and compare these results to the simulation performance in Fig.5.2.

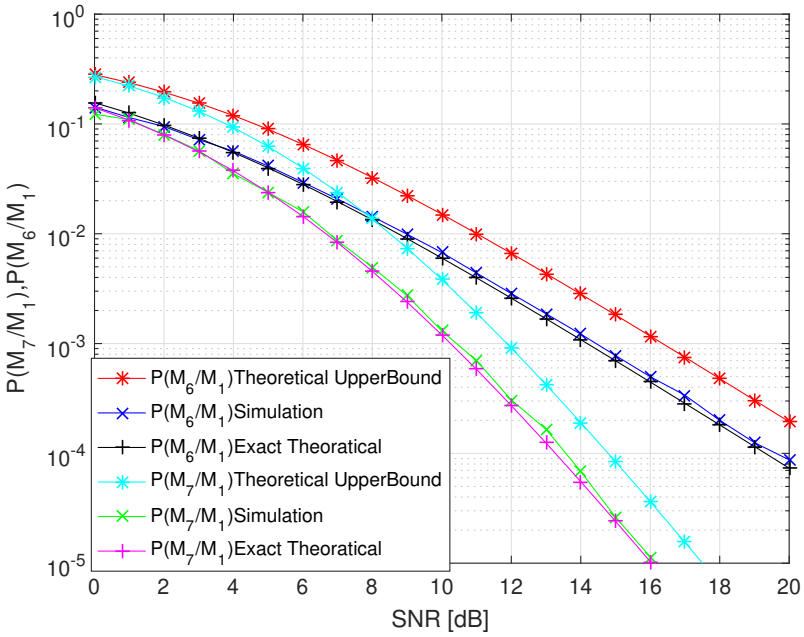

Figure 5.2 – Theoretical versus simulation results of the exact and upper bound on PEP of the couple of matrices (M_6, M_1) and (M_7, M_1)

The theoretical results of the exact PEP value are a perfect match with the simulation results. This validates the simulation results produced and inspire us to adopt a different performance metric than the distance in the selection of the information matrices, which will be explored in the next section.

5.4 New optimal search algorithm based on the exact PEP value

Instead of using the distance between couple of matrices in our search for the optimal information matrices to employ in the DSTM system, we produce all the exact PEP values between all the couple of matrices of a given group according the closed forms expressions indicated previously for a fixed SNR (section 5.6). Then, using the generated PEP values we apply an optimal search algorithm to select the best possible matrices.

5.4.1 First step of optimal search algorithm

Suppose we employ the group $\mathcal{G}_{w2}$, the first step is to generate all possible exact PEP values as is shown in table 5.2.

Table 5.2 – Table of exact PEP values for $\mathcal{G}_{w2}$

Exact PEP	M_1	M_2	...	M_{192}
M_1	x	$P(M_1, M_2)$	...	$P(M_1, M_{192})$
M_2	$P(M_2, M_1)$	x	...	$P(M_2, M_{192})$
$\vdots$	$\vdots$	$\vdots$	$\vdots$	$\vdots$
M_{192}	$P(M_{192}, M_1)$	$P(M_{192}, M_2)$	...	x

5.4.2 Second step of optimal search algorithm

The optimal search algorithm is as follows: Let P be the candidate group of matrices to search, and S the set of optimal matrices to be selected.

1. The first matrix V_1 of P is added to S as a first entry ($S_1 = I$).
2. The second matrix V_{2_i} to be selected ($V_{2_i} \in P \setminus S$) has the smallest exact PEP value towards S_1: $min(PEP(V_{2_i} \to S_1))$. If multiple matrices have the minimum value, the tree search explained later on is used.

3. For the next matrix to be added to the optimal set S, we produce the set $\mathcal{P}$ of PEP values: $\mathcal{P}_{3_i} = [PEP(V_{3_i} \rightarrow S_1), PEP(V_{3_i} \rightarrow S_2)]$, where $V_{3_i} \in P, V_{3_i} \notin S$. Meaning a vector $\mathcal{P}_{3_i}$ is created for each matrix V_{3_i}. $\mathcal{P}_3 = [\mathcal{P}_{3_1}, \mathcal{P}_{3_2}]$.
4. The vectors $\mathcal{P}_{3_i}$ are sorted in descending order, with the aim of selecting the matrix belonging to the vector $\mathcal{P}_{3_i}$ having the lowest maximum PEP values. This is done by comparing the PEP values after sorting the set in descending order and choosing the set with the smallest first value. If the first values are identical, the second PEP values are checked, and so on until the end of the vector.
5. In the case where one set $\mathcal{P}_{3_i}$ remains (having unique set of PEP matching the *"lowest maximum criterion"*), we choose the matrix V_{3_i} associated with it.
6. Otherwise, if multiple $\mathcal{P}_{3_i}$ have the *"lowest maximum criterion"* and are indeed matching, we invoke a tree search
   (a) Suppose the two sets $\mathcal{P}_{3_1}$ and $\mathcal{P}_{3_2}$ match the *"lowest maximum criterion"* and are indeed matching
   (b) We run a tree search through adding the matrices V_{3_1} (associated to $\mathcal{P}_{3_1}$) and V_{3_2} (associated to $\mathcal{P}_{3_2}$) to two temporary optimal sets S_α and S_β respectively.
   (c) We run the search algorithm from step 3 in the two temporary optimal sets, for each matrix added to each set, we compare both S_α and S_β in the same manner as step 4.
   (d) We select the set having the better matrix added (in terms of *"lowest maximum criterion"*), we see to which set $\mathcal{P}_{3_1}$ or $\mathcal{P}_{3_2}$ is related and continue to step 5.
   (e) If for both added matrices, the sets S_α and S_β give identical PEP vectors, we continue by rerunning the search again from step 3, and so on. This is repeated until we reach the required size of the optimal set. In that case, and if the sets S_α and S_β remain matching, we select one randomly and proceed from step 5.

7. The matrix V_{3_i} is then added to the set S, and we repeat the search from step 3 until we reach the required size according to the chosen spectral efficiency.

5.5 Optimal mapping

After selecting the optimal set of matrices to be employed, and to further enhance error performance, an optimal mapping strategy is adopted.
For a given spectral efficiency that requires a specific set of matrices optimally chosen according to the PEP criteria, the closest binary vectors in Hamming distance, are mapped to the matrices that have the biggest PEP amongst them. By doing this, the effect of the matrices that are most prone to error on the binary vectors will not be as critical.

5.6 Choice of SNR value for the generation of the exact PEP

In this section, the performance of the groups $\mathcal{G}_{w2}$, $\mathcal{G}_{we2}$ and $\mathcal{G}_{wee2}$ are studied in light of exact PEP values generated for different SNR values. The aim of this is to select the SNR value for which the exact PEPs give the best performance, which will be referred to with χ.

We generate the exact PEP values for χ = 10, 12, 15 and 30 dB and employ the optimal search algorithm and optimal mapping strategy. This performance is presented for the maximum spectral efficiency 3.5 bps/Hz of $\mathcal{G}_{w2}$. In Fig.5.3 is a comparison between $\mathcal{G}_{w2}$ and $\mathcal{G}_{we2}$ in the previously mentioned scenarios.

It is found that in all of the scenarios in Fig. 5.3, the performance of $\mathcal{G}_{w2}$ and $\mathcal{G}_{we2}$ are similar in the low SNR region up until 10 dB, where $\mathcal{G}_{w2}$ outperforms $\mathcal{G}_{we2}$ slightly from 10 dB to 20 dB. Afterwards, $\mathcal{G}_{we2}$ performs better in the high SNR region. This is explained by the fact that the PEP closed form expression used is intended for the high SNR region, which is evident when reviewing the performances in Fig. 5.3. The question remains on the optimal choice of χ. This is why, the performance for the same group are compared for PEP values generated at χ in Fig 5.4. It is found

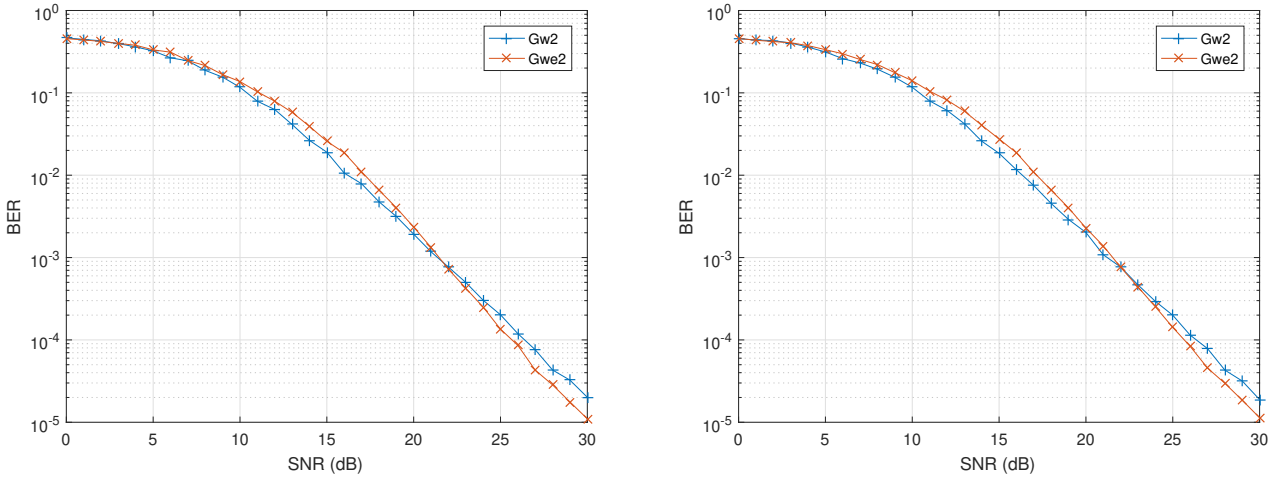

(a) $\chi = 10\,dB$

(b) $\chi = 12\,dB$

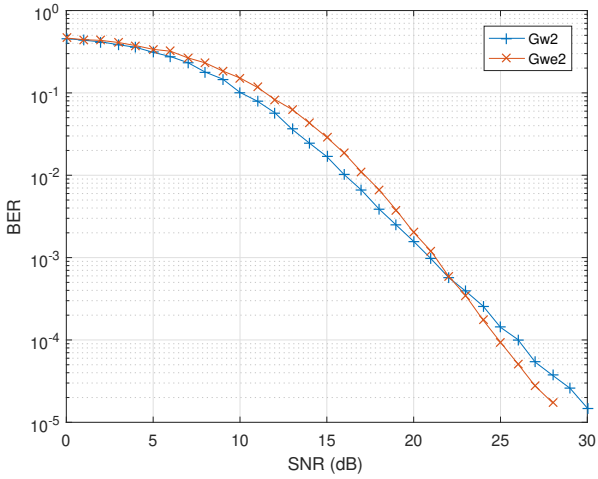

(c) $\chi = 15\,dB$

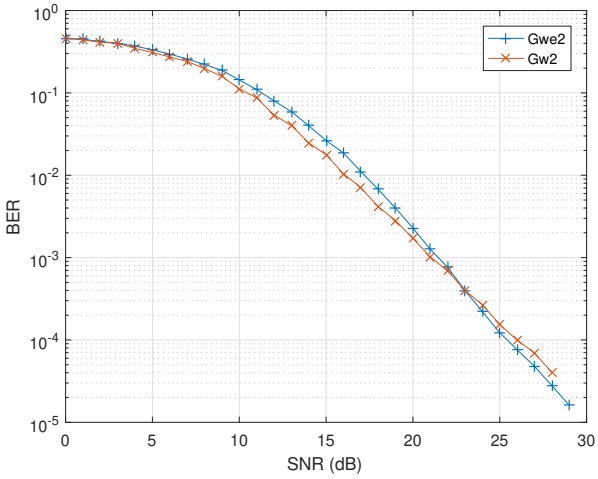

(d) $\chi = 30\,dB$

Figure 5.3 – Comparison between $\mathcal{G}_{w2}$ and $\mathcal{G}_{we2}$ for $\chi = 10, 12, 15$ and $30\,dB$

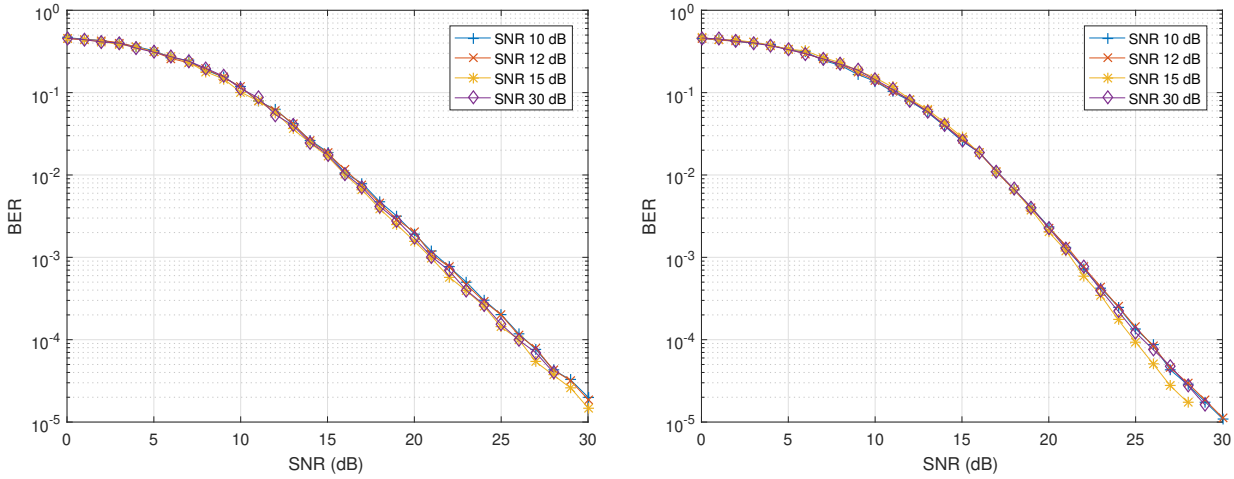

(a) $\mathcal{G}_{w2}$ (b) $\mathcal{G}_{we2}$

Figure 5.4 – $\mathcal{G}_{w2}$ and $\mathcal{G}_{we2}$ for $\chi = 10, 12, 15$ and $30\,dB$

that for $\mathcal{G}_{w2}$ the performance at 3.5 bps/Hz are similar for different χ, whereas in the case of $\mathcal{G}_{we2}$, $\chi = 15dB$ perform slightly better at high SNR. This is why this value is adopted in the generation of the PEPs for different scenarios.

5.7 Comparing the distance and PEP metrics

Here, we compare in Fig. 5.5 the PEP metric in the selection of the optimal information matrices with the selection using the distance metric for $\mathcal{G}_{w2}$.

For the low spectral efficiencies of 1 and 2 bps/Hz, a large difference is observed between the performances using the PEP metric and the distance metric. Indeed, for the 1 bps/Hz case in Fig. 5.5a, the system using the PEP metric reaches BER 10^{-5} for 16 dB whereas the one using the distance metric reaches it for 25 dB. In the case of 2 bps/Hz in Fig. 5.5b the performance with the PEP metric reaches 10^{-5} for 20 dB, which is explained by the fact that with the increase of the spectral efficiency, fewer optimal choices are available and the performance using the PEP metric begins to approach that of the distance metric until the performances match for the spectral efficiency of 3.5 bps/Hz in 5.5d. As shown in previous section, there are cases where couple of matrices share the same distance but different PEP values, which explains the out-performance of the PEP metric.

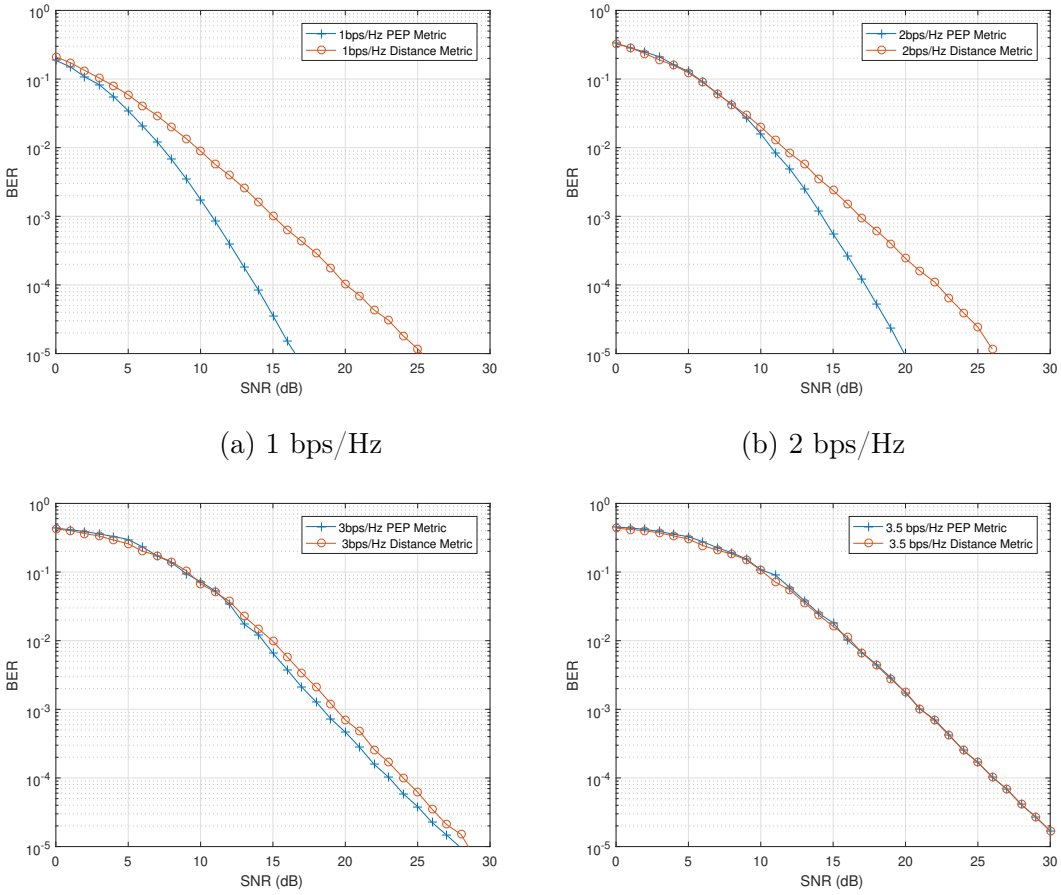

(a) 1 bps/Hz

(b) 2 bps/Hz

(c) 3 bps/Hz

(d) 3.5 bps/Hz

Figure 5.5 – Comparison between distance metric and PEP metric for different spectral efficiencies in $\mathcal{G}_{w2}$

5.8 Conclusion

In this chapter, we presented a different metric for the performance study of the DSTM systems, which is the PEP, rather than the distance metric. The derivation of the exact and upper bound closed forms of the PEP are presented for different channel fading scenarios, and a special case closed form expression of the PEP is presented for the Weyl group and its extensions. The theoretical results are validated through simulation, leading to the conception of a new optimal information matrix search algorithm which employs a tree search for optimal results. The performance results of the DSTM scheme using the PEP metric are better than that of the distance metric for low spectral efficiencies.

Conclusions and perspectives

Conclusion

Today, MIMO and massive MIMO techniques are very present in the different wireless communication systems. However, these schemes require at the receiver an estimate of the response of the propagation channel between each transmit and receive antenna, which in many cases can greatly reduce the final data rate of these systems. The aim of this thesis is to explore an alternative solution based on the use of DSTM schemes for these non-coherent MIMO systems that do not require an estimate of the channel response in reception.

In our work, sets of the multiplicative Weyl group of 2×2 unitary matrices $\mathcal{G}_{w2}$ is used as the space-time coded constellation of the DSTM scheme. As a first step, $\mathcal{G}_{w2}$ is extended in size through an optimal rotation, thus producing the new multiplicative group of unitary matrices $\mathcal{G}_{we2}$, having the elements of its matrices belonging to 16PSK constellation. This is done in the aim of increasing the maximum achievable spectral efficiency of the DSTM system from 3.5 bps/Hz with the matrices of $\mathcal{G}_{w2}$, to 4 bps/Hz obtained with the matrices of $\mathcal{G}_{we2}$. Similarly, and with the same aim, the first extended group $\mathcal{G}_{we2}$ is further extended through another optimal rotation to the multiplicative group of unitary matrices $\mathcal{G}_{wee2}$, with the elements of its matrices belonging to 32PSK constellation, thus further increasing the maximum achievable spectral efficiency to 4.5 bps/Hz. In this part, we used the distance among couple of matrices as a performance metric, thus the distance spectrum of $\mathcal{G}_{w2}$, $\mathcal{G}_{we2}$ and $\mathcal{G}_{wee2}$ are studied thoroughly. Then an information matrices selection algorithm and optimal mapping are produced with the purpose of enhancing the error performance of the system which is analyzed through simulation results.

As a second step, $\mathcal{G}_{w2}$ is expanded through the use of the Kronecker product operator, producing the multiplicative group $\mathcal{G}_{w4}$ of 4×4 unitary matrices. This group, as before, is extended to $\mathcal{G}_{we4}$ and $\mathcal{G}_{wee4}$, thus increasing the maximum achievable spectral efficiency from 3 bps/Hz to 3.25 bps/Hz and 3.5 bps/Hz respectively. The distance spectrum of the generated groups are studied and the same search algorithm and optimal mapping are applied, then simulation results are analyzed. Furthermore, the group $\mathcal{G}_{w8}$ of 8×8 unitary matrices is produced through the use of the Kronecker product similarly, which is followed by the generation of its extensions $\mathcal{G}_{we8}$ and $\mathcal{G}_{wee8}$ which further increase the maximum achievable spectral efficiency from 2 bps/Hz to 2.125 bps/Hz and 2.25 bps/Hz respectively.

Afterwards, the DSTM MIMO scheme is studied under a continuously fading channel model which is based on the Nyquist sampling theorem. More explicitly, each column of the transmission matrix is multiplied by an interpolated channel matrix from randomly generated channel matrices. This model has been previously adopted, we add new improvements to it through adding an initialization process. The extensions of the Weyl group have been used for 2, 4 and 8 transmit antennas and the performance results under the new channel model are compared to the results under the step channel model. This shows a degradation of the results under the new model in high SNR region due to the continuous variation of the channel, depicting a real case scenario. Simulation results also show how the fast variation of the channel degrades the performance of the DSTM schemes.

This thesis work ends with studying the performance of the proposed DSTM schemes using PEP expressions inspired from the work in [1]. Previous work involving the derivation of closed forms expressions of the exact and upper bound of PEP in multiple fading scenarios are described. This is followed by a derivation of a special case closed form expression of the PEP which suits the structure of the Weyl group and its extensions. Furthermore, a new optimal algorithm for selecting information matrices, having as a performance measure the exact value of the PEP between pairs of matrices, is proposed. The optimality of the selected matrices for a given spectral efficiency is guaranteed by the use of a tree search method in the selection process. In particular, it is shown that the BER performance of the MIMO

DSTM systems thus obtained is superior to the results obtained with the previous schemes that use the distance between couple of matrices as a metric of performance, and thus offers interesting perspectives.

Perspectives

As it was shown in Chapter 1, the domain of non-coherent communication is wide and provides numerous opportunities for research. Based on this thesis, many interesting areas and prospects can be further investigated.

First, theoretically speaking, the optimal rotations applied on the Weyl group can further be extended to higher order modulations, leading to a greater increase in the achievable spectral efficiency. For performance enhancement purposes, the system employing these extensions could make use of suitable channel correcting code that would compensate the performance loss due to the employment of a larger amount of matrices. Furthermore, the use of the PEP metric and optimal search algorithm could be extended for DSTM MIMO systems employing 4 and 8 transmit antennas. This would enhance the performance of the mentioned systems, under the same argument that the PEP is a far more suitable performance metric than the distance between couple of matrices.

Moreover, as was seen in Chapter 1, spatial modulation (SM) schemes are being widely used in recent research. The Weyl group suits this type of systems, and could be integrated along with its proposed extensions in the aim of achieving higher rate than the commonly used SM-STBC and with lower complexity.

Also, regarding the work achieved in chapter 4, a perspective is using a simpler method for the interpolation of the channel matrices. The natural class C2 cubic splines could be used instead of using the Nyquist sampling theorem. It would be also interesting to study the channel coefficients as correlated random variable. Since the antennas at transmit or receive side could be close to each other, this would present a more realistic performance.

In addition to this, non-coherent schemes could have contributions in contemporary systems as 5G-NR. More specifically, in the inherent broadcast of channels for

initial access, also in blind detection in the broadcast and control channels as well as the benefit of non-coherent detection in high mobility scenarios [48]. In light of this, DSTM schemes based on the Weyl group and its extensions could play role.

Bibliography

[1] Van Khanh Nguyen. « Performance analysis of differential space–time modulation ». In: *IEEE Transactions on Information Theory* 58.5 (2012), pp. 2620–2632.

[2] Andrea Goldsmith. *Wireless communications*. Cambridge university press, 2005.

[3] Fourth Edition, Athanasios Papoulis, and S Unnikrishna Pillai. « Probability, Random Variables, and Stochastic Processes ». In: (2002).

[4] Michel Mouly, Marie-Bernadette Pautet, and Thomas Foreword By-Haug. *The GSM system for mobile communications*. Telecom publishing, 1992.

[5] Theodore S Rappaport et al. *Wireless communications: principles and practice*. Vol. 2. prentice hall PTR New Jersey, 1996.

[6] J. G. Proakis. *Digital Communications*. Vol. 2. McGraw-Hill, 1995.

[7] Claude E Shannon. « A mathematical theory of communication ». In: *The Bell system technical journal* 27.3 (1948), pp. 379–423.

[8] Gerard J Foschini. « Layered space-time architecture for wireless communication in a fading environment when using multi-element antennas ». In: *Bell labs technical journal* 1.2 (1996), pp. 41–59.

[9] Hesham El Gamal and A Roger Hammons. « A new approach to layered space-time coding and signal processing ». In: *IEEE Transactions on Information Theory* 47.6 (2001), pp. 2321–2334.

[10] Peter W Wolniansky, Gerard J Foschini, Glen D Golden, and Reinaldo A Valenzuela. « V-BLAST: An architecture for realizing very high data rates over the rich-scattering wireless channel ». In: *1998 URSI international symposium on signals, systems, and electronics. Conference proceedings (Cat. No. 98EX167)*. IEEE. 1998, pp. 295–300.

[11] Lajos Hanzo, Osamah Alamri, Mohammed El-Hajjar, and Nan Wu. *Near-capacity multi-functional MIMO systems: sphere-packing, iterative detection and cooperation*. Vol. 4. John Wiley & Sons, 2009.

[12] Stephan Ten Brink. « Convergence of iterative decoding ». In: *Electronics letters* 35.10 (1999), pp. 806–808.

[13] Oussama Damen, Ammar Chkeif, and J-C Belfiore. « Lattice code decoder for space-time codes ». In: *IEEE Communications letters* 4.5 (2000), pp. 161–163.

[14] Christoph Studer and Helmut Bölcskei. « Soft–input soft–output single tree-search sphere decoding ». In: *IEEE Transactions on Information Theory* 56.10 (2010), pp. 4827–4842.

[15] Chao Xu et al. « Two decades of MIMO design tradeoffs and reduced-complexity MIMO detection in near-capacity systems ». In: *IEEE Access* 5 (2017), pp. 18564–18632.

[16] Mathini Sellathurai and Simon Haykin. « Turbo-BLAST for wireless communications: theory and experiments ». In: *IEEE Transactions on Signal Processing* 50.10 (2002), pp. 2538–2546.

[17] Chao Xu, Dandan Liang, Shinya Sugiura, Soon Xin Ng, and Lajos Hanzo. « Reduced-complexity approx-log-MAP and max-log-MAP soft PSK/QAM detection algorithms ». In: *IEEE transactions on communications* 61.4 (2013), pp. 1415–1425.

[18] Carlos A Belfiore and John H Park. « Decision feedback equalization ». In: *Proceedings of the IEEE* 67.8 (1979), pp. 1143–1156.

[19] David D Falconer and Gerard J Foschini. « Theory of minimum mean-square-error QAM systems employing decision feedback equalization ». In: *Bell System Technical Journal* 52.10 (1973), pp. 1821–1849.

[20] Siavash M Alamouti. « A simple transmit diversity technique for wireless communications ». In: *IEEE Journal on selected areas in communications* 16.8 (1998), pp. 1451–1458.

[21] Vahid Tarokh, Hamid Jafarkhani, and A Robert Calderbank. « Space-time block codes from orthogonal designs ». In: *IEEE Transactions on Information theory* 45.5 (1999), pp. 1456–1467.

[22] Girish Ganesan and Petre Stoica. « Space-time diversity using orthogonal and amicable orthogonal designs ». In: *Wireless Personal Communications* 18.2 (2001), pp. 165–178.

[23] Girish Ganesan and Petre Stoica. « Space-time block codes: A maximum SNR approach ». In: *IEEE Transactions on Information Theory* 47.4 (2001), pp. 1650–1656.

[24] Girish Ganesan and Petre Stoica. « Differential modulation using space-time block codes ». In: *Conference Record of Thirty-Fifth Asilomar Conference on Signals, Systems and Computers (Cat. No. 01CH37256)*. Vol. 1. IEEE. 2001, pp. 236–240.

[25] Hamid Jafarkhani. « A quasi-orthogonal space-time block code ». In: *IEEE Transactions on Communications* 49.1 (2001), pp. 1–4.

[26] Constantinos B Papadias and Gerard J Foschini. « A space-time coding approach for systems employing four transmit antennas ». In: *2001 IEEE International Conference on Acoustics, Speech, and Signal Processing. Proceedings (Cat. No. 01CH37221)*. Vol. 4. IEEE. 2001, pp. 2481–2484.

[27] Constantinos B Papadias and Gerard J Foschini. « Capacity-approaching space-time codes for systems employing four transmitter antennas ». In: *IEEE Transactions on Information Theory* 49.3 (2003), pp. 726–732.

[28] Naresh Sharma and Constantinos B Papadias. « Improved quasi-orthogonal codes through constellation rotation ». In: *IEEE Transactions on Communications* 51.3 (2003), pp. 332–335.

[29] Weifeng Su and Xiang-Gen Xia. « Signal constellations for quasi-orthogonal space-time block codes with full diversity ». In: *IEEE Transactions on Information Theory* 50.10 (2004), pp. 2331–2347.

[30] Hsiao-feng Lu and P Vijay Kumar. « A unified construction of space-time codes with optimal rate-diversity tradeoff ». In: *IEEE Transactions on Information Theory* 51.5 (2005), pp. 1709–1730.

[31] Chau Yuen, Yong Liang Guan, and Tjeng Thiang Tjhung. « Quasi-orthogonal STBC with minimum decoding complexity ». In: *IEEE Transactions on Wireless Communications* 4.5 (2005), pp. 2089–2094.

[32] Lizhong Zheng and David N. C. Tse. « Diversity and multiplexing: A fundamental tradeoff in multiple-antenna channels ». In: *IEEE Transactions on information theory* 49.5 (2003), pp. 1073–1096.

[33] Babak Hassibi and Bertrand M Hochwald. « High-rate codes that are linear in space and time ». In: *IEEE Transactions on Information theory* 48.7 (2002), pp. 1804–1824.

[34] Robert W Heath and Arogyaswami J Paulraj. « Linear dispersion codes for MIMO systems based on frame theory ». In: *IEEE Transactions on Signal Processing* 50.10 (2002), pp. 2429–2441.

[35] Marco Di Renzo, Harald Haas, Ali Ghrayeb, Shinya Sugiura, and Lajos Hanzo. « Spatial modulation for generalized MIMO: Challenges, opportunities, and implementation ». In: *Proceedings of the IEEE* 102.1 (2013), pp. 56–103.

[36] Ping Yang et al. « Single-carrier SM-MIMO: A promising design for broadband large-scale antenna systems ». In: *IEEE Communications Surveys & Tutorials* 18.3 (2016), pp. 1687–1716.

[37] Shumei Song et al. « A channel hopping technique I: Theoretical studies on band efficiency and capacity ». In: *2004 International Conference on Communications, Circuits and Systems (IEEE Cat. No. 04EX914)*. Vol. 1. IEEE. 2004, pp. 229–233.

[38] Yawgeng A Chau and Shi-Hong Yu. « Space modulation on wireless fading channels ». In: *IEEE 54th Vehicular Technology Conference. VTC Fall 2001. Proceedings (Cat. No. 01CH37211)*. Vol. 3. IEEE. 2001, pp. 1668–1671.

[39] Harald Haas, S Sinanovic, CW Ahn, and S Yun. « Spatial modulation ». In: *IEEE Trans. Veh. Technol.* 57.4 (2008), pp. 2228–2241.

[40] Ertugrul Başar, Umit Aygölü, Erdal Panayirci, and H Vincent Poor. « Space-time block coded spatial modulation ». In: *IEEE transactions on communications* 59.3 (2010), pp. 823–832.

[41] Jeyadeepan Jeganathan, Ali Ghrayeb, and Leszek Szczecinski. « Generalized space shift keying modulation for MIMO channels ». In: *2008 IEEE 19th International Symposium on Personal, Indoor and Mobile Radio Communications*. IEEE. 2008, pp. 1–5.

[42] Jintao Wang, Shuyun Jia, and Jian Song. « Generalised spatial modulation system with multiple active transmit antennas and low complexity detection scheme ». In: *IEEE Transactions on Wireless Communications* 11.4 (2012), pp. 1605–1615.

[43] Yue Xiao et al. « Low-complexity signal detection for generalized spatial modulation ». In: *IEEE Communications Letters* 18.3 (2014), pp. 403–406.

[44] Shinya Sugiura, Takumi Ishihara, and Miyu Nakao. « State-of-the-art design of index modulation in the space, time, and frequency domains: Benefits and fundamental limitations ». In: *IEEE Access* 5 (2017), pp. 21774–21790.

[45] Ertugrul Basar et al. « Index modulation techniques for next-generation wireless networks ». In: *IEEE access* 5 (2017), pp. 16693–16746.

[46] Naoki Ishikawa, Shinya Sugiura, and Lajos Hanzo. « 50 years of permutation, spatial and index modulation: From classic RF to visible light communications and data storage ». In: *IEEE Communications Surveys & Tutorials* 20.3 (2018), pp. 1905–1938.

[47] Shinya Sugiura, Sheng Chen, and Lajos Hanzo. « Coherent and differential space-time shift keying: A dispersion matrix approach ». In: *IEEE Transactions on Communications* 58.11 (2010), pp. 3219–3230.

[48] Chao Xu et al. « Sixty years of coherent versus non-coherent tradeoffs and the road from 5G to wireless futures ». In: *IEEE Access* 7 (2019), pp. 178246–178299.

[49] Jinlin Fu, Chunping Hou, Wei Xiang, Lei Yan, and Yonghong Hou. « Generalised spatial modulation with multiple active transmit antennas ». In: *2010 IEEE Globecom Workshops*. IEEE. 2010, pp. 839–844.

[50] Abdelhamid Younis, Nikola Serafimovski, Raed Mesleh, and Harald Haas. « Generalised spatial modulation ». In: *2010 conference record of the forty fourth Asilomar conference on signals, systems and computers*. IEEE. 2010, pp. 1498–1502.

[51] Shinya Sugiura, Sheng Chen, and Lajos Hanzo. « Generalized space-time shift keying designed for flexible diversity-, multiplexing-and complexity-tradeoffs ». In: *IEEE Transactions on Wireless Communications* 10.4 (2011), pp. 1144–1153.

[52] Shinya Sugiura, Chao Xu, Soon Xin Ng, and Lajos Hanzo. « Reduced-complexity iterative-detection-aided generalized space-time shift keying ». In: *IEEE Transactions on Vehicular Technology* 61.8 (2012), pp. 3656–3664.

[53] R Thomas Derryberry, Steven D Gray, D Mihai Ionescu, Giridhar Mandyam, and Balaji Raghothaman. « Transmit diversity in 3G CDMA systems ». In: *IEEE communications magazine* 40.4 (2002), pp. 68–75.

[54] Yang Xiao. « IEEE 802.11 n: enhancements for higher throughput in wireless LANs ». In: *IEEE Wireless Communications* 12.6 (2005), pp. 82–91.

[55] Hannes Ekstrom et al. « Technical solutions for the 3G long-term evolution ». In: *IEEE Communications Magazine* 44.3 (2006), pp. 38–45.

[56] Thomas L. Marzetta and Bertrand M. Hochwald. « Capacity of a mobile multiple-antenna communication link in Rayleigh flat fading ». In: *IEEE transactions on Information Theory* 45.1 (1999), pp. 139–157.

[57] Peter J Smith and Mansoor Shafi. « On a Gaussian approximation to the capacity of wireless MIMO systems ». In: *2002 IEEE International Conference on Communications. Conference Proceedings. ICC 2002 (Cat. No. 02CH37333)*. Vol. 1. IEEE. 2002, pp. 406–410.

[58] Lajos Hanzo, Yosef Akhtman, Jos Akhtman, Li Wang, and Ming Jiang. *MIMO-OFDM for LTE, WiFi and WiMAX: Coherent versus non-coherent and cooperative turbo transceivers*. John Wiley & Sons, 2011.

[59] Lajos Hanzo, Soon Xin Ng, WT Webb, and T Keller. *Quadrature amplitude modulation: From basics to adaptive trellis-coded, turbo-equalised and space-time coded OFDM, CDMA and MC-CDMA systems*. IEEE Press-John Wiley, 2004.

[60] Babak Hassibi and Bertrand M Hochwald. « How much training is needed in multiple-antenna wireless links? » In: *IEEE Transactions on Information Theory* 49.4 (2003), pp. 951–963.

[61] Thomas Kailath. « Correlation detection of signals perturbed by a random channel ». In: *IRE Transactions on Information Theory* 6.3 (1960), pp. 361–366.

[62] GDJR Forney. « Maximum-likelihood sequence estimation of digital sequences in the presence of intersymbol interference ». In: *IEEE Transactions on Information theory* 18.3 (1972), pp. 363–378.

[63] R Morley and D Snyder. « Maximum likelihood sequence estimation for randomly dispersive channels ». In: *IEEE Transactions on Communications* 27.6 (1979), pp. 833–839.

[64] John G Lawton. « Theoretical error rates of" Differentially Coherent" binary and" Kineplex" data transmission systems ». In: *Proc. IRE.* 47.2 (1959), pp. 333–334.

[65] JOHN G LAWTON. *INVESTIGATION OF DIGITAL DATA COMMUNICATION SYSTEMS*. Tech. rep. CORNELL AERONAUTICAL LAB INC BUFFALO NY, 1961.

[66] Charles Cahn. « Performance of digital phase-modulation communication systems ». In: *IRE Transactions on Communications Systems* 7.1 (1959), pp. 3–6.

[67] P Bello and B Nelin. « The influence of fading spectrum on the binary error probabilites of incoherent and differentially coherent matched filter recievers ». In: *IRE Transactions on Communications Systems* 10.2 (1962), pp. 160–168.

[68] Stephen G Wilson, James Freebersyser, and Christopher Marshall. « Multisymbol detection of M-DPSK ». In: *1989 IEEE Global Telecommunications Conference and Exhibition'Communications Technology for the 1990s and Beyond'*. IEEE. 1989, pp. 1692–1697.

[69] Paul Ho and Dominic Fung. « Error performance of multiple-symbol differential detection of PSK signals transmitted over correlated Rayleigh fading channels ». In: *IEEE Transactions on Communications* 40.10 (1992), pp. 1566–1569.

[70] Dariush Divsalar and Marvin K Simon. « Maximum-likelihood differential detection of uncoded and trellis coded amplitude phase modulation over AWGN and fading channels/spl minus/metrics and performance ». In: *IEEE Transactions on Communications* 42.1 (1994), pp. 76–89.

[71] KM Mackenthun. « A fast algorithm for multiple-symbol differential detection of MPSK ». In: *IEEE Transactions on Communications* 42.234 (1994), pp. 1471–1474.

[72] Harry Leib and Subbarayan Pasupathy. « The phase of a vector perturbed by Gaussian noise and differentially coherent receivers ». In: *IEEE Transactions on Information Theory* 34.6 (1988), pp. 1491–1501.

[73] Franz Edbauer. « Bit error rate of binary and quaternary DPSK signals with multiple differential feedback detection ». In: *IEEE Transactions on Communications* 40.3 (1992), pp. 457–460.

[74] Lutz Lampe, Robert Schober, Volker Pauli, and Christoph Windpassinger. « Multiple-symbol differential sphere decoding ». In: *2004 IEEE International Conference on Communications (IEEE Cat. No. 04CH37577)*. Vol. 2. IEEE. 2004, pp. 787–791.

[75] Volker Pauli, Lutz Lampe, and Robert Schober. « " Turbo DPSK" using soft multiple-symbol differential sphere decoding ». In: *IEEE Transactions on Information Theory* 52.4 (2006), pp. 1385–1398.

[76] Chao Xu, Soon Xin Ng, and Lajos Hanzo. « Multiple-symbol differential sphere detection and decision-feedback differential detection conceived for differential QAM ». In: *IEEE Transactions on Vehicular Technology* 65.10 (2015), pp. 8345–8360.

[77] Chao Xu, Li Wang, Soon Xin Ng, and Lajos Hanzo. « Soft-decision multiple-symbol differential sphere detection and decision-feedback differential detection for differential QAM dispensing with channel estimation in the face of rapidly fading channels ». In: *IEEE Transactions on Wireless Communications* 15.6 (2016), pp. 4408–4425.

[78] Vahid Tarokh and Hamid Jafarkhani. « A differential detection scheme for transmit diversity ». In: *IEEE journal on selected areas in communications* 18.7 (2000), pp. 1169–1174.

[79] Hamid Jafarkhani and Vahid Tarokh. « Multiple transmit antenna differential detection from generalized orthogonal designs ». In: *IEEE Transactions on Information Theory* 47.6 (2001), pp. 2626–2631.

[80] Xiang-Gen Xia. « Differentially en/decoded orthogonal space-time block codes with APSK signals ». In: *IEEE Communications Letters* 6.4 (2002), pp. 150–152.

[81] Meixia Tao and Roger S Cheng. « Differential space-time block codes ». In: *GLOBECOM'01. IEEE Global Telecommunications Conference (Cat. No. 01CH37270)*. Vol. 2. IEEE. 2001, pp. 1098–1102.

[82] Chan-Soo Hwang, Seung Hoon Nam, Jaehak Chung, and Vahid Tarokh. « Differential space time block codes using nonconstant modulus constellations ». In: *IEEE Transactions on Signal Processing* 51.11 (2003), pp. 2955–2964.

[83] Bertrand M Hochwald and Thomas L Marzetta. « Unitary space-time modulation for multiple-antenna communications in Rayleigh flat fading ». In: *IEEE transactions on Information Theory* 46.2 (2000), pp. 543–564.

[84] Brian L Hughes. « Differential space-time modulation ». In: *IEEE transactions on Information Theory* 46.7 (2000), pp. 2567–2578.

[85] L-H Zetterberg. « A class of codes for polyphase signals on a bandlimited Gaussian channel ». In: *IEEE Transactions on Information Theory* 11.3 (1965), pp. 385–395.

[86] David Slepian. « Permutation modulation ». In: *Proceedings of the IEEE* 53.3 (1965), pp. 228–236.

[87] Bertrand M Hochwald, Thomas L Marzetta, Thomas J Richardson, Wim Sweldens, and Rüdiger Urbanke. « Systematic design of unitary space-time constellations ». In: *IEEE transactions on Information Theory* 46.6 (2000), pp. 1962–1973.

[88] G David Forney. « Geometrically uniform codes ». In: *IEEE Transactions on Information Theory* 37.5 (1991), pp. 1241–1260.

[89] David Slepian. « A class of binary signaling alphabets ». In: *Bell System Technical Journal* 35.1 (1956), pp. 203–234.

[90] Shinya Sugiura, Chao Xu, Soon Xin Ng, and Lajos Hanzo. « Reduced-complexity coherent versus non-coherent QAM-aided space-time shift keying ». In: *IEEE Transactions on communications* 59.11 (2011), pp. 3090–3101.

[91] Chao Xu, Shinya Sugiura, Soon Xin Ng, and Lajos Hanzo. « Reduced-complexity noncoherently detected differential space-time shift keying ». In: *2011 IEEE Wireless Communications and Networking Conference*. IEEE. 2011, pp. 1505–1510.

[92] Yuyang Bian, Miaowen Wen, Xiang Cheng, H Vincent Poor, and Bingli Jiao. « A differential scheme for spatial modulation ». In: *2013 IEEE Global Communications Conference (GLOBECOM)*. IEEE. 2013, pp. 3925–3930.

[93] Yuyang Bian et al. « Differential spatial modulation ». In: *IEEE Transactions on Vehicular Technology* 64.7 (2014), pp. 3262–3268.

[94] Philippa A Martin. « Differential spatial modulation for APSK in time-varying fading channels ». In: *IEEE Communications Letters* 19.7 (2015), pp. 1261–1264.

[95] Jiang Liu et al. « High-rate APSK-aided differential spatial modulation: Design method and performance analysis ». In: *IEEE Communications Letters* 21.1 (2016), pp. 168–171.

[96] Naoki Ishikawa and Shinya Sugiura. « Unified differential spatial modulation ». In: *IEEE Wireless Communications Letters* 3.4 (2014), pp. 337–340.

[97] Rakshith Rajashekar, Naoki Ishikawa, Shinya Sugiura, KVS Hari, and Lajos Hanzo. « Full-diversity dispersion matrices from algebraic field extensions for differential spatial modulation ». In: *IEEE Transactions on Vehicular Technology* 66.1 (2016), pp. 385–394.

[98] Naoki Ishikawa and Shinya Sugiura. « Rectangular differential spatial modulation for open-loop noncoherent massive-MIMO downlink ». In: *IEEE Transactions on Wireless Communications* 16.3 (2017), pp. 1908–1920.

[99] Naoki Ishikawa, Rakshith Rajashekar, Chao Xu, Shinya Sugiura, and Lajos Hanzo. « Differential space-time coding dispensing with channel estimation approaches the performance of its coherent counterpart in the open-loop massive MIMO-OFDM downlink ». In: *IEEE Transactions on Communications* 66.12 (2018), pp. 6190–6204.

[100] Florence Jessie MacWilliams and Neil James Alexander Sloane. *The theory of error correcting codes*. Vol. 16. Elsevier, 1977.

[101] Hui Ji. « Study and optimization of new differential space-time modulation schemes based on the Weyl group for the second generation of MIMO systems ». 2015ISAR0021. PhD thesis. 2015. URL: `http://www.theses.fr/2015ISAR0021/document`.

[102] Bertrand M Hochwald and Wim Sweldens. « Differential unitary space-time modulation ». In: *IEEE Transactions on Communications* 48.12 (2000), pp. 2041–2052.

[103] William C Jakes and Donald C Cox. *Microwave mobile communications*. Wiley-IEEE Press, 1994.

[104] Richard Hedley Clarke. « A statistical theory of mobile-radio reception ». In: *Bell system technical journal* 47.6 (1968), pp. 957–1000.

[105] Hui Ji, Gheorghe Zaharia, and Jean-François Hélard. « Performance of DSTM MIMO systems in continuously changing Rayleigh channel ». In: *2015 International Symposium on Signals, Circuits and Systems (ISSCS)*. IEEE. 2015, pp. 1–4.

[106] Hong Shen Wang and Nader Moayeri. « Finite-state Markov channel-a useful model for radio communication channels ». In: *IEEE Transactions on Vehicular Technology* 44.1 (1995), pp. 163–171.

[107] Qingyuan Dai and ED Shwedyk. « Detection of bandlimited signals over frequency selective Rayleigh fading channels ». In: *IEEE Transactions on Communications* 42.234 (1994), pp. 941–950.

[108] Michail K Tsatsanis, Georgios B Giannakis, and Guotong Zhou. « Estimation and equalization of fading channels with random coefficients ». In: *Signal Processing* 53.2-3 (1996), pp. 211–229.

[109] John W Craig. « A new, simple and exact result for calculating the probability of error for two-dimensional signal constellations ». In: *MILCOM 91-Conference record*. IEEE. 1991, pp. 571–575.

[110] Marvin K Simon. « Evaluation of average bit error probability for space-time coding based on a simpler exact evaluation of pairwise error probability ». In: *Journal of Communications and Networks* 3.3 (2001), pp. 1–8.

[111] George L Turin. « The characteristic function of Hermitian quadratic forms in complex normal variables ». In: *Biometrika* 47.1/2 (1960), pp. 199–201.

[112] W-H Sheen and Gordon L Stuber. « MLSE equalization and decoding for multipath-fading channels ». In: *IEEE Transactions on Communications* 39.10 (1991), pp. 1455–1464.

INSA de RENNES
Service des Formations

AVIS DU JURY SUR LA REPRODUCTION DE LA THESE SOUTENUE

Titre de la thèse:
Design, Optimization and Performance Evaluation of Non-Coherent MIMO Schemes for Future Wireless Systems

Nom Prénom de l'auteur : DAWI IBRAHIM

Membres du jury :
- Madame BERBINEAU Marion
- Monsieur MEGHDADI Vahid
- Monsieur KHALIL Ayman
- Monsieur ROS Laurent
- Monsieur HELARD Jean-François
- Monsieur ZAHARIA Gheorghe

Président du jury : ROS Laurent

Date de la soutenance : 01 Juin 2021

Reproduction de la these soutenue

☒ Thèse pouvant être reproduite en l'état
☐ Thèse pouvant être reproduite après corrections suggérées

Fait à Rennes, le 01 Juin 2021

Signature du président de jury

Le Directeur,

Abdellatif MIRAOUI

Titre : Conception, optimisation et évaluation des performances de schémas MIMO non cohérents pour les futurs systèmes sans fil

Mots clés :
MIMO, DSTM, group Weyl, CSI

Résumé : Aujourd'hui les techniques multi-antennaires MIMO (Multiple Input Multiple Output) et Massive MIMO sont très présentes dans les différents systèmes de communications sans fils. Cependant, ces schémas nécessitent de disposer en réception d'une estimation de la réponse de chaque canal entre chaque antenne d'émission et de réception, ce qui, dans beaucoup de cas, peut diminuer fortement l'efficacité spectrale finale de ces systèmes. Cette thèse a pour but d'explorer une solution alternative reposant sur l'utilisation de schémas de modulation différentielle espace-temps (DSTM) pour ces systèmes MIMO non cohérents ne nécessitant pas de disposer d'une estimation de la réponse du canal en réception.

Dans un premier temps, des schémas reposant sur l'utilisation du groupe multiplicatif de Weyl de matrices unitaires 2×2 sont étudiés dans le but de construire des systèmes MIMO de type DSTM à 2 antennes d'émission. Puis en utilisant le produit Kronecker, étendu aux matrices 4×4et 8×8.Afin d'améliorer l'efficacité spectrale de ces schémas, des extensions simples et doubles du groupe de Weyl sont proposées. Un algorithme de sélection des matrices d'information maximisant la distance entre les matrices sélectionnées ainsi qu'un mapping optimisé sont ensuite développés. Enfin, une étude analytique des performances des schémas DSTM proposés par des expressions de la probabilité d'erreur par paire (PEP)est menée. En particulier, un nouvel algorithme optimal de sélection des matrices d'information, ayant comme mesure de performance la valeur exacte de la PEP entre les couples de matrices, est optimisé.

Title : Conception, optimization and evaluation of the performance of non-coherent MIMO systems for future wireless systems.

Keywords : MIMO, DSTM, group Weyl, CSI

Abstract: Today the multi-antenna techniques MIMO (Multiple Input Multiple Output) and Massive MIMO are very present in the various wireless communication systems. However, these diagrams make it possible to have in reception an estimate of the response of each channel between each transmit and receive antenna, which, in many cases, can greatly reduce the final spectral efficiency of these systems. The purpose of this thesis is to explore an alternative solution based on the use of differential space-time modulation (DSTM) schemes for these non-coherent MIMO systems that does not require an estimate of the response of the receiving channel. First, schemes based on the use of the Weyl multiplicative group of 2 × 2 unit matrices are studied in the process of building DSTM type MIMO building DSTM type MIMO systems with 2 transmitting antennas.

Then using the Kronecker product, extended to 4 × 4 and 8 × 8 matrices. In order to improve the spectral efficiency of these schemes, single and double extensions of the Weyl group are proposed. An information matrix selection algorithm maximizing the distance between the improved matrices as well as an optimized mapping are then developed. Finally, an analytical study of the performance of DSTM schemes proposed by expressions of the pairwise error conversation (PEP) is continued. In particular, a new optimal algorithm for selecting the information matrices, having as a performance measure the exact value of the PEP between the pairs of matrices, is optimized.